

THESIS

EFFECT OF PHASE CHANGE MATERIAL ON DYNAMIC THERMAL MANAGEMENT
PERFORMANCE FOR POWER ELECTRONICS PACKAGES

Submitted by

Justin Ralph Hollis

Department of Mechanical Engineering

In partial fulfillment of the requirements

For the Degree of Master of Science

Colorado State University

Fort Collins, Colorado

Fall 2021

Master's Committee:

Advisor: Todd M. Bandhauer

Anthony Marchese
Peter Young

Copyright Justin Ralph Hollis 2021

All Rights Reserved

ABSTRACT

EFFECT OF PHASE CHANGE MATERIAL ON DYNAMIC THERMAL MANAGEMENT PERFORMANCE FOR POWER ELECTRONICS PACKAGES

High temperature silicon carbide (SiC) die are the most critical and expensive component in electric vehicle (EV) power electronic packages and require both active and passive methods to dissipate heat during transient operation. The use of phase change materials (PCMs) to control the peak junction temperature of the SiC die and to buffer the temperature fluctuations in the package during simulated operation is modeled here. The latent heat storage potential of multiple PCM and PCM composites are explored in both single-sided and dual-sided package configurations. The results of this study show that the addition of phase change material (PCM) into two different styles of power electronics (PE) packages is an effective method for controlling the transient junction temperatures experienced during two different drive cycles. The addition of PCM in a single-sided package also serves to decrease temperature fluctuations experienced by the package as a whole and may be used to reduce the necessary number of SiC die required to divide the heat load, lowering the overall material cost and volume of the package by over 50%. PCM in a single-sided package may be nearly as effective as the double-sided cooling approach of a dual-sided package in the reduction of both peak junction temperature of SiC as well as controlling temperature variations between package layers.

ACKNOWLEDGEMENTS

First and foremost, I would like to thank Dr. Todd Bandhauer for his guidance, patience, and support (both personally and professionally) throughout my undergraduate and graduate career. His positive attitude and enthusiasm for thermal sciences and engineering in general are both unending and infectious.

I would also like to thank the Army Research Laboratory for their contributions to this project and their financial support. Specifically, thank you to Mike Fish for answering numerous questions and sharing his knowledge with all things ParaPower and to Darin Sharar for his guidance and support throughout.

I must also thank all the members of the REACH CoLab. It is inspiring to work with such a talented and diverse group of individuals. I would specifically like to thank Ethan Markey and Brandi Grauberger for their constant support, and Caleb Anderson for his help and advice throughout this project.

Finally, thank you to my family. Without your love and support I would not be the person I am today.

TABLE OF CONTENTS

ABSTRACT.....	ii
ACKNOWLEDGEMENTS.....	iii
LIST OF TABLES.....	vii
LIST OF FIGURES.....	viii
NOMENCLATURE.....	xvi
CHAPTER 1 INTRODUCTION.....	1
1.1. Background and Motivation.....	1
1.2. Research Objectives.....	2
1.3. Thesis Organization.....	3
CHAPTER 2 LITERATURE REVIEW.....	4
2.1. Power Electronic Packaging.....	4
2.2. Phase Change Materials.....	10
2.3. Research Needs.....	14
2.4. Focus of Current Study.....	14
CHAPTER 3 MODELING APPROACH.....	16
3.1. Package Geometry.....	16
3.2. Dynamic Power and Heat Load.....	19
3.3. Heat Transfer Coefficient.....	21

3.4.	PCM Selection.....	23
3.5.	PCM Thickness	25
3.6.	Package Modeling with PCM	25
3.7.	Simulation Matrix	26
CHAPTER 4 RESULTS AND DISCUSSION.....		29
4.1.	Impact of PCM Selection and Placement.....	29
4.1.1	Single-Sided Package	30
4.1.2	Dual-Sided Package.....	36
4.2.	US06 Drive Cycle Results with Erythritol-Copper PCM	39
4.3.	Urban Drive Cycle Results with Erythritol-Copper PCM	43
4.4.	Relative Impact of Drive Cycle with Erythritol-Copper PCM	47
4.5.	System Level Considerations.....	50
CHAPTER 5 CONCLUSIONS AND RECOMMENDATIONS OF FURTHER WORK.....		56
5.1.	Recommendations for Future Work.....	58
REFERENCES		59
APPENDIX A RESULTS.....		66
A.1.	Single-Sided Package US06 Results: Sections 4.1.1 and 4.2.....	66
APPENDIX B HAND CALCULATIONS.....		87
APPENDIX C PARAPOWER		91
C.1.	ParaPower.....	91

C.1.1	Opening ParaPower	91
C.1.2	ParaPower GUI.....	91
APPENDIX D MATLAB CODE		98
D.1.	US06 Power Function	98
D.2.	Urban Power Function	99

LIST OF TABLES

Table 3-1.	Selected PCMs in present study.....	24
Table 3-2.	Simulations performed.....	28
Table 4-1.	Comparison of PCM effect on maximum junction temperature in single-sided package during US06.....	35
Table 4-2.	Cost comparison of PE package materials.....	51
Table 4- 3.	Comparison of Single and Dual-Sided package performance, material cost, and size	52
Table B-1.	Churchill correlation and overall heat transfer coefficient hand calculations...	88
Table B-2.	Representative Power Calculation	90

LIST OF FIGURES

Figure 2-1.	Functional block diagram of EV propulsion system. Adapted from [12].....	4
Figure 2-2.	Conventional PE package with single-sided cooling [17]	5
Figure 2-3.	Dual-sided package using flip chip technology [18]	6
Figure 2- 4.	Dual-sided package using power overlay technology [19].....	6
Figure 2-5.	Dual-sided package using EPCM [20].....	7
Figure 2-6.	PE packages in recent all-electric and hybrid-electric vehicles adapted from [5]	8
Figure 2-7.	Photos of porous nickel before (a) and after (b) the vacuum impregnation of erythritol [27].....	11
Figure 2-8.	Thermal conductivity and volumetric density of latent heat of each erythritol- nickel composite tested [27]	12
Figure 2-9.	Endmember composites with fins parallel (a) and perpendicular (b) to heat flow [28].....	12
Figure 2-10.	Package with PCM modeled by Nafis et. al. [7].....	13
Figure 3-1.	Single-sided power electronic package based on 2014 Honda Accord modeled in SolidWorks (top) and ParaPower (bottom).....	17
Figure 3-2.	Dual-sided power electronic package based on 2016 Chevrolet Volt modeled in SolidWorks (top) and ParaPower (bottom).....	18
Figure 3-3.	ParaPower GUI with single-sided package modeled.....	19
Figure 3-4.	Additional forces acting on vehicle	20
Figure 3-5.	Speed and modeled power derived from the US06 (top) and Urban (bottom)	

	drive cycles	21
Figure 3-6.	Maximum temperature in package with varying erythritol (a) and erythritol-copper composite (b) PCM thicknesses.....	25
Figure 3-7.	Single-sided power electronic package with PCM	26
Figure 3-8.	Dual-sided power electronic package with PCM in periphery (a), emitter/collector (b), and DBC (c).....	26
Figure 4-1.	Die temperatures in single-sided package containing 10, 12, 14, 16, 18, 20, and 24 die during full US06 drive cycle.....	30
Figure 4-2.	Junction temperature of SiC die in packages with 10 die with all PCMs modeled during US06 drive cycle	30
Figure 4-3.	Temperature profile of PE package layers of single-sided package with 24 die and no PCM for complete US06 drive cycle	32
Figure 4-4.	Temperature profile of die, cold plate, and erythritol in single-sided package with 24 die during portion of US06 drive cycle	32
Figure 4-5.	Temperature profile of die, cold plate, and erythritol-nickel in single-sided package with 20 die during portion of US06 drive cycle	33
Figure 4-6.	Temperature profile of die, cold plate, and indium in single-sided package with 12 die during portion of US06 drive cycle.....	34
Figure 4-7.	Temperature profile of die, cold plate, and erythritol-copper in single-sided package with 12 die (top) and 10 die (bottom) during portion of US06 drive cycle	35
Figure 4-8.	Temperature profile of dual-sided PE package with 24 SiC and no PCM (top left) and dual-sided PE package with erythritol in periphery (top right), emitter	

	and collector (bottom left), and DBC (bottom right) during portion of US06 Drive Cycle	36
Figure 4-9.	Junction temperature of SiC die in dual-sided PE package with 10 SiC and erythritol in different package configurations during portion of US06 drive cycle	37
Figure 4-10.	Erythritol-copper melt fraction according to placement location in dual-sided package with 10 die throughout US06 cycle	38
Figure 4-11.	Erythritol melt fraction according to placement location in dual-sided package with 10 die throughout US06 cycle	39
Figure 4-12.	Temperature profile of single-sided PE package with no PCM and 24 SiC (top), single-sided PE package with erythritol-copper and 24 SiC (middle) and single-sided PE package with erythritol-copper and 10 SiC (bottom) during portion of US06 drive cycle.....	40
Figure 4-13.	Erythritol-copper melt fraction in single-sided package with 10 and 24 die throughout US06 cycle	41
Figure 4-14.	Temperature profile of dual-sided PE package with 10 SiC, no PCM (top) and erythritol-copper composite PCM in the DBC (bottom) during a portion of the US06 drive cycle.....	43
Figure 4-15.	Temperature profile of single-sided PE package with no PCM and 24 SiC (top), single-sided PE package with erythritol-copper and 24 SiC (middle) and single-sided PE package with erythritol-copper and 10 SiC (bottom) during portion of Urban Drive Cycle	44
Figure 4-16.	Erythritol-copper melt fraction in single-sided package with 10 throughout	

	urban cycle.....	46
Figure 4-17.	Temperature profile of dual-sided PE package with no PCM and 10 SiC (top) and dual-sided PE package with erythritol-copper in DBC and 10 SiC (bottom) during portion of urban drive cycle	47
Figure 4-18.	Histogram of SiC die time at temperature in single-sided (a) and dual-sided package (b) throughout US06 Drive Cycle.....	49
Figure 4-19.	Histogram of SiC die time at temperature in single-sided (a) and dual-sided package (b) throughout Urban Drive Cycle.....	50
Figure 4-20.	Temperature profile of single-sided PE package with erythritol-copper and 10 SiC (top) and dual-sided PE package with 10 SiC no PCM (bottom) during portion of US06 cycle	53
Figure 4-21.	Temperature profile to steady-state of single-sided PE package with copper thermal mass and 10 SiC (top) and single-sided PE package with PCM and 10 SiC PCM (bottom) during extended maximum power of US06 cycle	55
Figure A-1.	Temperature profile in single-sided package with 24 die and no PCM over full US06 cycle.....	66
Figure A-2.	Temperature profile in single-sided package with 24 die and erythritol	67
Figure A-3.	Erythritol melt fraction in single-sided package with 24 die over full US06 cycle	67
Figure A-4.	Temperature profile in single-sided package with 20 die and erythritol-nickel	68
Figure A-5.	Erythritol-nickel melt fraction in single-sided package with 20 die over full US06 cycle	68
Figure A-6.	Temperature profile in single-sided package with 12 die and indium.....	69

Figure A-7.	Indium melt fraction in single-sided package with 12 die over full US06 cycle	69
Figure A-8.	Temperature profile in single-sided package with 12 die and erythritol-copper	70
Figure A-9.	Erythritol-copper melt fraction in single-sided package with 12 die over full US06 cycle	70
Figure A-10.	Temperature profile in single-sided package with 10 die and erythritol-copper	71
Figure A-11.	Erythritol-copper melt fraction in single-sided package with 10 die over full US06 cycle	71
Figure A-12.	Temperature profile in single-sided package with 24 die and erythritol-copper	72
Figure A-13.	Erythritol-copper melt fraction in single-sided package with 24 die over full US06 cycle	72
Figure A-14.	Temperature profile in dual-sided package with 24 die and no PCM	73
Figure A-15.	Temperature profile in dual-sided package with 10 die and no PCM	73
Figure A-16.	Temperature profile in dual-sided package with 24 die and erythritol in the periphery over full US06 cycle	74
Figure A-17.	Erythritol melt fraction in periphery of dual-sided package with 24 die over full US06 cycle	74
Figure A-18.	Temperature profile in dual-sided package with 24 die and erythritol in the emitter and collector over full US06 cycle.....	75
Figure A-19.	Erythritol melt fraction in emitter and collector of dual-sided package with 24 die over full US06 cycle	75
Figure A-20.	Temperature profile in dual-sided package with 24 die and erythritol in the DBC over full US06 cycle	76
Figure A-21.	Erythritol melt fraction in DBC of dual-sided package with 24 die over full US06	

	cycle	76
Figure A-22.	Temperature profile in dual-sided package with 24 die and erythritol-copper in the periphery over full US06 cycle	77
Figure A-23.	Erythritol-copper melt fraction in periphery of dual-sided package with 24 die over full US06 cycle	77
Figure A-24.	Temperature profile in dual-sided package with 24 die and erythritol-copper in the emitter and collector over full US06 cycle	78
Figure A-25.	Erythritol-copper melt fraction in emitter and collector of dual-sided package with 24 die over full US06 cycle	78
Figure A-26.	Temperature profile in dual-sided package with 24 die and erythritol-copper in the DBC over full US06 cycle	79
Figure A-27.	Erythritol-copper melt fraction in DBC of dual-sided package with 24 die over full US06 cycle	79
Figure A-28.	Temperature profile in dual-sided package with 10 die and erythritol-copper in the periphery over full US06 cycle	80
Figure A-29.	Erythritol-copper melt fraction in periphery of dual-sided package with 10 die over full US06 cycle	80
Figure A-30.	Temperature profile in dual-sided package with 10 die and erythritol-copper in the emitter and collector over full US06 cycle	81
Figure A-31.	Erythritol-copper melt fraction in emitter and collector of dual-sided package with 10 die over full US06 cycle	81
Figure A-32.	Temperature profile in dual-sided package with 10 die and erythritol-copper in the DBC over full US06 cycle	82

Figure A-33.	Erythritol-copper melt fraction in DBC of dual-sided package with 10 die over full US06 cycle	82
Figure A-34.	Temperature profile in single-sided package with 24 die and no PCM over full urban cycle.....	83
Figure A- 35.	Temperature profile in single-sided package with 24 die and erythritol-copper	83
Figure A-36.	Erythritol-copper melt fraction in single-sided package with 24 die over full urban cycle	84
Figure A-37.	Temperature profile in single-sided package with 10 die and erythritol-copper	84
Figure A-38.	Erythritol-copper melt fraction in single-sided package with 10 die over full urban cycle	85
Figure A-39.	Temperature profile in dual-sided package with 10 die and no PCM	85
Figure A-40.	Temperature profile in dual-sided package with 10 die and erythritol-copper in the DBC over full urban cycle	86
Figure A-41.	Erythritol-copper melt fraction in DBC of dual-sided package with 10 die over full urban cycle	86
Figure C-1.	MATLAB home screen with ParaPower folder and subfolders added to MATLAB path and command to open GUI in Command Window.....	91
Figure C-2.	Blank ParaPower GUI with 7 user interface sections boxed in red.....	92
Figure C-3.	Features define for use in current study.....	93
Figure C-4.	Analysis section of GUI.....	93
Figure C-5.	Parameters used to construct single-sided package	94
Figure C-6.	Materials list with library of materials (and their properties) with option for users to insert materials.....	94

Figure C-7.	Geometry visualization including materials assigned to geometry layers (single-sided package shown)	95
Figure C-8.	Environmental Parameters used in current study.....	95
Figure C-9.	Initial conditions, time steps, and length of analysis used in current study.....	96
Figure C- 10.	Run Solver and Detailed Visual Results sections of the GUI.....	97

NOMENCLATURE

<i>Symbol</i>	<i>Description</i>	<i>Units</i>
<i>Symbols</i>		
<i>A</i>	Area	m^2
<i>a</i>	acceleration	m s^{-2}
<i>c_D</i>	Coefficient of drag resistance	-
<i>c_R</i>	Coefficient of rolling resistance	-
<i>D_h</i>	Hydraulic diameter	m
<i>F</i>	Force	N
<i>FOM</i>	Figure of merit	$\text{kJ m}^{-4} \text{s}^{-1} \text{K}^{-1}$
<i>f</i>	Friction factor	-
<i>g</i>	Gravity	m s^{-2}
<i>H_f</i>	Latent heat of fusion	kJ kg^{-1}
<i>h_f</i>	Heat transfer coefficient	$\text{W m}^{-2} \text{K}^{-1}$
<i>k</i>	Thermal conductivity	$\text{W m}^{-1} \text{K}^{-1}$
<i>m</i>	Mass	kg
<i>\dot{m}</i>	Mass flow rate	kg s^{-1}
Nu	Nusselt number	-
<i>P</i>	Power	W
Pr	Prandtl number	-
Re	Reynolds number	-
<i>T</i>	Temperature	C
t	Time	s
<i>U</i>	Overall heat transfer coefficient	$\text{W m}^{-2} \text{K}^{-1}$
u	Flow speed	m s^{-1}
<i>V</i>	Velocity	m s^{-1}

<i>Greek Symbols</i>		
ρ	Density	kg m ⁻³
η	Efficiency	-
μ	Dynamic viscosity	kg m ⁻¹ s ⁻¹
<i>Subscripts</i>		
b	Fin prime surface	-
m	Melt	-
o	Overall	-
t	Total fin surface	-

CHAPTER 1 INTRODUCTION

1.1. Background and Motivation

As the market for more fuel efficient and environmentally friendly vehicles grows, the demand for more versatile and capable all-electric and hybrid-electric vehicles increases. These vehicles will require more electrical power to accommodate a wide variety of uses, from commercial transportation of passengers and goods to military vehicles of varying size and capabilities. Power electronics are one of the most important components in the electric vehicle (EV) system. Power electronics are responsible for converting DC power from the traction batteries to AC power for the traction motor. Increasing the PE efficiency, durability and lifespan is crucial in developing more robust and cost-friendly EVs.

In the past, power electronic systems used a silicon insulated-gate bipolar transistor as the main working component [1]. The advent of silicon carbide (SiC) based power electronic devices has resulted in substantial performance improvements [2]. SiC devices are highly efficient, thinner than Si devices, have a higher thermal conductivity (and therefore a lower thermal resistance), and can operate reliably at much higher temperatures [2]. Si devices typically cannot withstand temperatures higher than 150°C, whereas SiC devices have been calculated, using first order simulations, to operate at temperatures up to 600°C [2, 3]. While operating at such high temperatures is theoretically possible, some SiC devices have shown unstable behavior at temperatures above 150°C, implying that high temperatures have the potential to reduce both device and package reliability [4]. The package is made up of a variety of substrate layers that act to both dissipate heat and add stability to the package. Due to the varying coefficients of thermal expansion (CTE) in the substrate layers, high temperature fluctuations can degrade package

stability over time [5]. Three of the most important factors in PE packaging are performance, reliability, and cost. Reliability of PE packages may be improved by decreasing both the maximum temperature and temperature fluctuations experienced by the package [5]. The cost of the packaging can be reduced by decreasing the number of SiC die that are necessary to divide the power load, and in turn, the heat load experienced by the devices.

Due to its thermal storage properties, utilizing PCM in PE packaging has the potential to aid in thermal management [6]. PCMs work by absorbing heat from the surrounding while rising to its transition temperature, then undergoing a constant temperature phase change while continuing to absorb heat [7]. PCM incorporated into PE packaging can effectively store heat dissipated by the devices during its transient operation via phase change from solid to liquid (or in some cases solid to solid) transformations, lowering the peak junction temperature in the device [8]. The latent heat absorption during phase change also reduces dramatic temperature fluctuations experienced by the package [9]. The reduction in temperature fluctuations in the package could help mitigate thermally accelerated failures in the substrate layers of the package, increasing the overall fatigue life of the package [5, 10].

1.2. Research Objectives

While there have been reviews of both PCMs [9] and packages [5] for automotive PE, there are limited studies on performance of PCMs under the transient conditions devices will be exposed to during operation. Power pulses have been used to evaluate the viability of PCM as a source of supplemental cooling in PE packages, but only model a single PCM (Xylitol) in the study [7]. This paper investigates the effects of incorporating PCM into both single-sided and dual-sided power electronics packages. PCMs with varying material properties are incorporated into the packages. The PCMs effect on the maximum junction temperature of the SiC die, temperature fluctuations

in the package, and the potential for die reduction are analyzed. This analysis used heat load models based off transient conditions PE packages would experience during both urban and interstate travel.

1.3. Thesis Organization

This thesis includes four additional chapters: Chapter 2 Literature Review, Chapter 3 Modeling Approach, Chapter 4 Results and Discussion, Chapter 5 Conclusions and Recommendations for Further Work and an Appendix. The literature review includes a detailed review of previous work on power electronics packaging, PCM studies and reviews, and studies incorporating PCM into power electronics packages. Chapter 3 will examine the approach used to create the package geometries, heat loads, heat transfer coefficient, and PCMs modeled in the simulations. Results and Discussion examines the results of the simulations and the significance of the findings. Chapter 5 will provide a summary of the work and offer recommendations for further work and studies. Finally, the Appendix provides the results of the full cycle simulations, hand calculations performed to validate the heat transfer coefficient used throughout this study as well as hand calculations for representative power calculations, a description of the use of ParaPower, and the MATLAB functions used by ParaPower to apply transient heat loads to the modeled packages.

CHAPTER 2 LITERATURE REVIEW

The previous chapter discussed the importance of PE and their use in electric and hybrid-electric vehicles. As detailed above, PE are responsible for the energy conversion from the traction batteries to the traction motor, making them an integral component in electric and hybrid electric vehicles. Effective thermal management is crucial to ensure both reliability and durability of the devices. The thermal storage properties of PCM offer a unique means of passively cooling transient devices. The purpose of this chapter is to provide a detailed literature review on both packaging techniques and the use of PCM to improve the thermal performance of the power electronics found in electric vehicles.

2.1. Power Electronic Packaging

Power electronics control the flow of power between the battery and the traction motor, and account for 7-15% of the overall cost of an electric vehicle [11]. Figure 2-1 shows a functional block diagram of an EV propulsion system. The thick lines represent power flow, the thin lines represent signal flow, and the arrowheads denote directionality. Based on user input from the brake

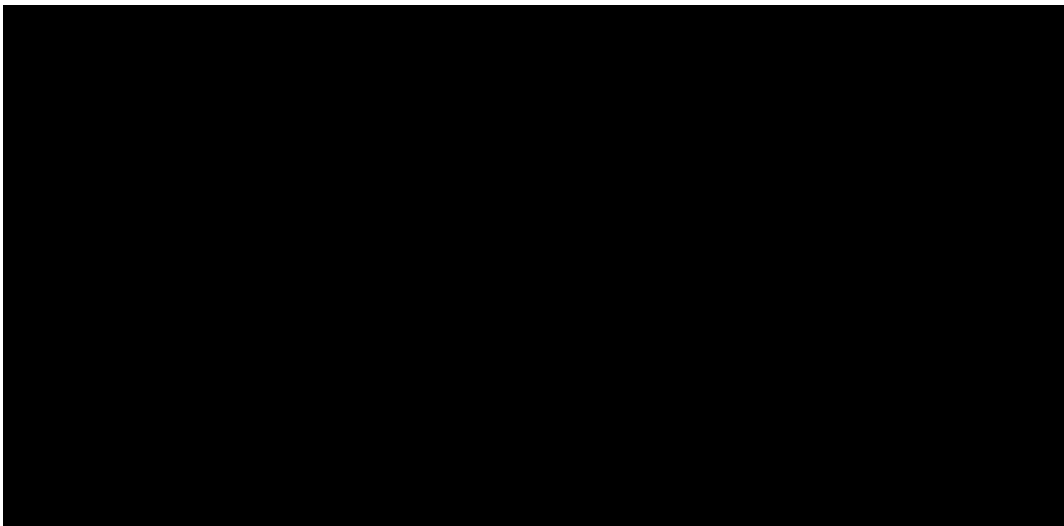


Figure 2-1. Functional block diagram of EV propulsion system. Adapted from [12].

or accelerator pedals, the electronic controller sends control signals to the power electronics, which regulates the power flow and converts DC power from the batteries to AC power for the motor [12]. The backward flow of power from the motor to the batteries is due to regenerative braking, where power is transferred back to the batteries during active deceleration.

Experimental studies have shown SiC devices achieving a peak efficiency of 99.5% in EV propulsion applications [13]. While these devices are highly efficient, they generate a significant amount of waste heat during operation that must be dissipated to ensure reliable operation. Although the SiC PE devices offer significant performance improvements when compared to Si devices, their performance is only as good as the package design. While numerous studies and reviews of PE packaging techniques have been conducted, packaging methods employed for SiC devices have not changed much from the traditional Si modules [14]. Many current packages are still designed using a conventional approach to the module architecture. Figure 2-2 shows a conventional PE package, with the PE soldered onto a direct bonded copper (DBC) substrate, which is then attached with either solder or a thermal material interface (TIM) directly to a heat spreader and/or a cold plate [15, 16]. This architecture only allows for single sided cooling, and

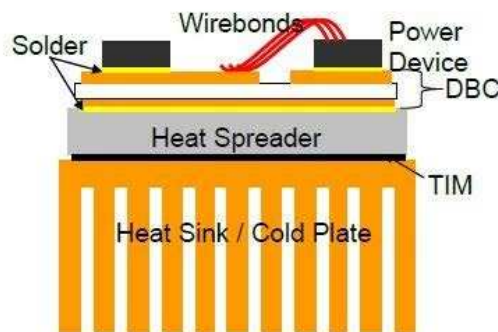


Figure 2-2. Conventional PE package with single-sided cooling [17]

precautions must be taken when designing substrate layers to match materials with similar coefficients of thermal expansion (CTE) to reduce the risk of mechanical failure. The lower

thermal resistance advantages of the SiC devices are also reduced with each layer added to the module.

Wire-bondless technologies have led to several novel packaging designs, the most notable of which create a dual-sided package architecture. Figure 2-3 shows a package designed using flip chip technology, which allows for the wire-bonds to be replaced with solder bumps, allowing for

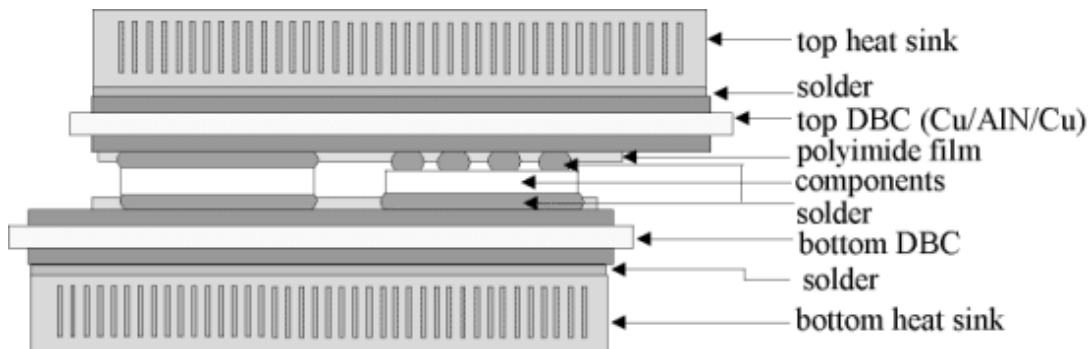


Figure 2-3. Dual-sided package using flip chip technology [18]

a dual-sided package [17]. Power overly technology (Figure 2-4) eliminates the wire-bonds by curing the devices in resin, securing device interconnections with metalized through holes, and

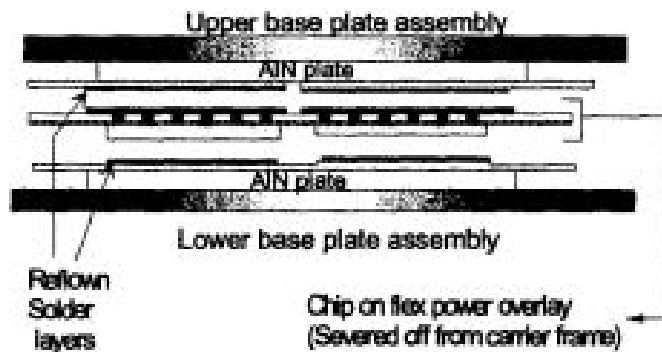


Figure 2- 4. Dual-sided package using power overlay technology [19]

applying base plates to both sides to aid in stability [18]. Figure 2-5 shows a single chip that is incorporated into an Embedded Power Chip Module (EPCM), which replaces the conventional wire-bonds with a metallization layer and provides a heat path for topside cooling [19]. The use of

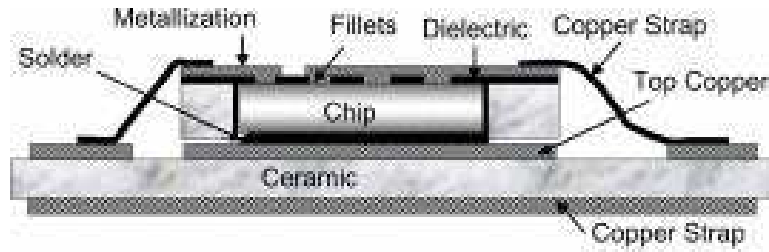


Figure 2-5. Dual-sided package using EPCM [20]

a dual-sided package architecture introduces the possibility of double-sided cooling, which significantly improves the thermal performance of the package. Multiple papers have been written exploring different the dual-sided configurations, potential packaging materials, and working fluids to test the benefits of double-sided cooling [12-23]. Schletz et. al. highlighted the benefits of utilizing the topside of the device as an additional heat removal path: thermal resistance is lowered, and the active elements can operate more efficiently [15]. Kelley et. al. noted that double sided cooling may allow for air to be used as a working fluid, eliminating the need for a dedicated coolant loop, dramatically reducing the size and weight of the system [20]. Despite the numerous benefits of dual-sided packaging, it has not been universally adopted commercially due to the lack of design methodology, the high cost of production, unsolved thermo-mechanical models, and a lack of understanding of the package lifespan [11, 21]. High temperature packaging, as well as novel approaches to packaging architecture, have both been recognized as areas that need to be further developed, so that the benefits of SiC devices can be fully realized [22].

Broughton et. al. conducted a thorough review of PE packaging materials as well as a review of various power modules deployed in recent all-electric and hybrid-electric vehicles and included packages with both the conventional single-sided and the newer dual-sided architectures [5]. The authors note that package substrate layers typically of the die, which are connected to either an aluminum or copper substrate layer, which acts as both an electrical interconnection and

a thermal path, with lead-free solder. The next layer of the substrate acts as an electrical insulator. This substrate layer is typically a ceramic, such as silicon nitride (Si_3N_4), chosen for its excellent electrical insulation and high thermal conductivity. The ceramic is sandwiched between two metal layers to provide an electrical ground on the top and additional heat spreading and stress reduction on the bottom. The bottom metal layer is connected to a copper or aluminum heat spreader and/or cold plate with either solder or TIM. Figure 2-6 shows the incremental advances in both package design and material selection of the various PE packages reviewed by the authors.

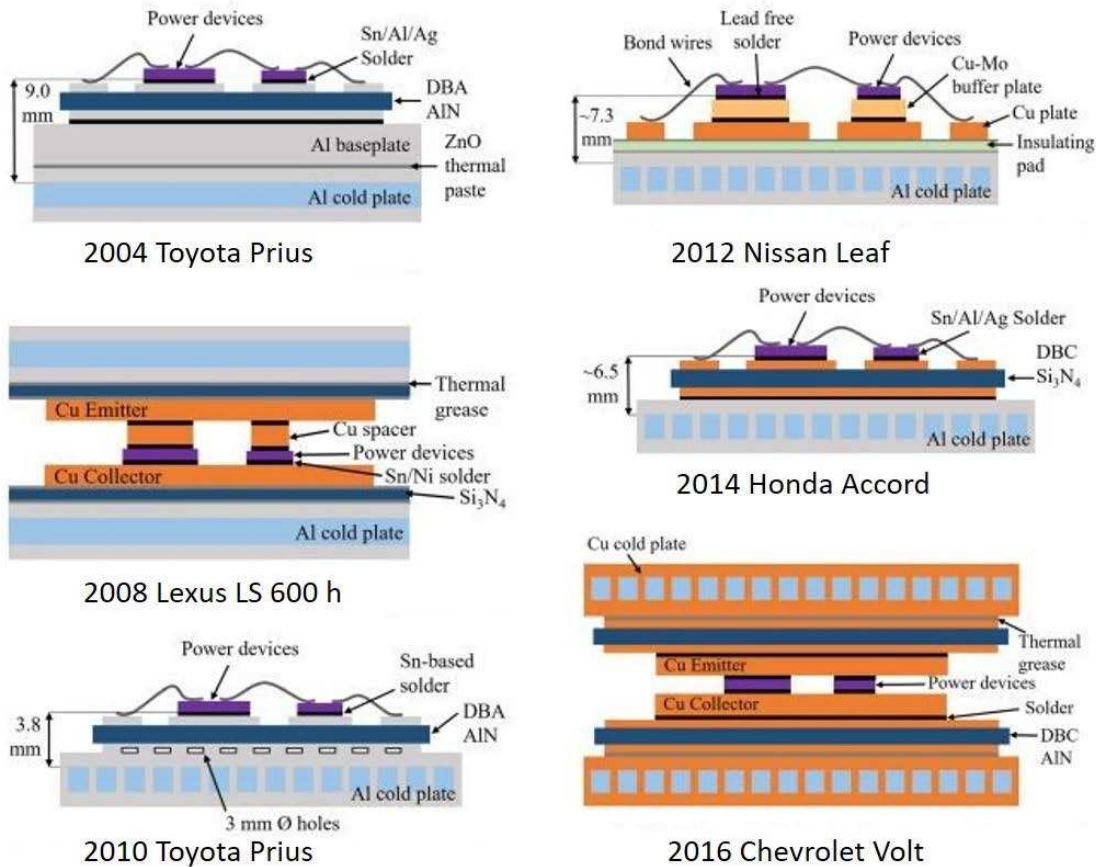


Figure 2-6. PE packages in recent all-electric and hybrid-electric vehicles adapted from [5]

The 2004 Toyota Prius (Figure 2-6, top left) uses a conventional packaging architecture similar to that shown in Figure 2-2 [5, 23]. The authors note the design engineer’s preference of

aluminum in the substrate layers, possibly due to aluminum's low density, offering weight saving when compared to copper. The large base plate used in the package to aid in heat spreading places the die 9mm from the active cooling provided by the working fluid.

The 2008 Lexus LS 600 h (Figure 2-6, middle left) utilizes a dual-sided package, allowing for active cooling of both sides of the die [5, 24]. Authors note the package uses copper spacers, along with copper emitter and collectors to serve as device interconnects and allow for heat spreading. A layer of Si_3N_4 is used for electrical isolation, and is connected to the aluminum cold plate with thermal grease as the TIM.

The 2010 Toyota Prius (Figure 2-6, bottom left) altered the design from 2004 by significantly reducing the distance between the die and the coolant (from 9mm to 3.8mm). This distance was decrease through the removal of the base plate, reducing the total package thickness. The 3mm hole shown in the figure where also added to relax stresses caused by the CTE mismatch between the aluminum and AlN ceramic used for electrical isolation [23].

Nissan's 2012 Leaf (Figure 2-6, top right) uses copper-molybdenum buffer plate under the die to ease the thermal transitions and relax CTE stresses [25]. The package also uses an insulating pad with thermal grease as the TIM instead of ceramic DBC for electrical isolation. While this reduces both the weight and cost of the package, this method incurs an increase in thermal resistance when compared to the use of ceramic [5].

The 2014 Honda Accord uses a conventional package similar to that of the 2010 Toyota Prius but used copper instead of aluminum near the PE devices [5, 26]. Authors note that copper was likely chosen to increase heat spreading near the device. The package also uses solder in place of thermal grease between the BDC and cold plate, reducing the overall thermal resistance in the package.

Chevrolet's 2016 volt utilizes a double-sided package architecture with the emitter and collector in direct contact with the die, serving as the device interconnects [5, 27]. This package also uses copper for the heat sink, where the packages previously discussed all used aluminum. Authors note that the channel geometry may differ from the straight channels used in the aluminum cold plates, possibly reducing the increase in weight from the use of copper.

2.2. Phase Change Materials

The latent heat thermal storage properties of PCMs offer a unique potential to aid in PE package thermal performance. Gong and Mujumdar carried out a series of numerical studies and found that the efficiency of thermal storage systems could theoretically be doubled using PCMs [8, 28, 29, 30]. Studies have also shown incorporating PCM into heat sink cavities can increase cooling performance of small transient electronic devices. Kandasamy et. al. conducted experimental and numerical investigations and found that incorporating PCM benefitted thermal performance of heat sinks when power levels were greater than 2 W, successfully lowering the peak junction temperature of the Si die and increasing the time necessary to reach steady state [8].

Multiple reviews of PCMs have been conducted discussing their potential use in a variety of thermal applications. Perhaps the most comprehensive review of PCM for vehicle applications was written by Jankowski and McCluskey [9]. The authors reviewed over 700 PCMs from many material classes, focusing on use in vehicle component thermal buffering. Of the PCMs reviewed, erythritol was rated as a top candidate to buffer the transient temperatures experienced by PE due to its appropriate melting temperature ($T_m = 117.7^\circ\text{C}$) and its high latent heat. The authors also note that erythritol is both non-toxic and non-corrosive.

While PCMs have been widely investigated as a means of passive cooling for transient electronics operation, the low thermal conductivity (k) of most pure PCMs presents significant

design challenges. Pure erythritol has a thermal conductivity of $0.733 \text{ W/m}\cdot\text{K}$ in its solid state which significantly hinders its thermal storage potential. To overcome this drawback, researchers have attempted to enhance thermal conductivity with high- k fins or impregnating erythritol in porous metals.

Oya et al. developed a PCM composite of erythritol and porous nickel using vacuum impregnation [31]. Figure 2-7 shows both macroscopic and microscopic views of the porous nickel

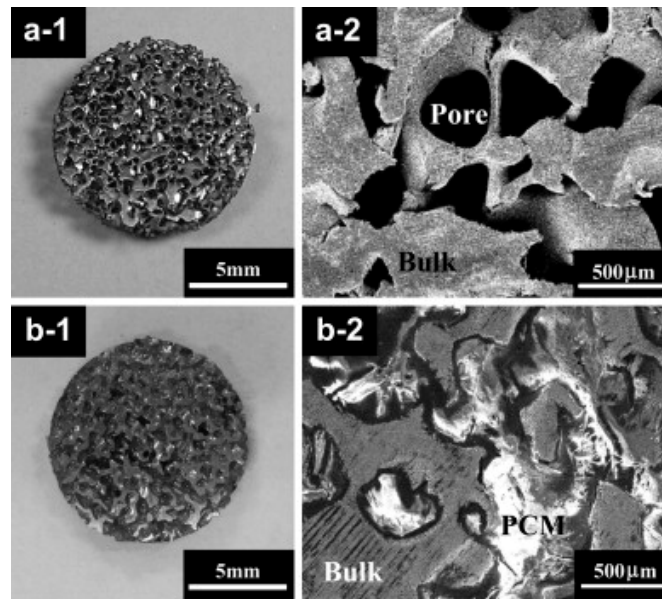


Figure 2-7. Photos of porous nickel before (a) and after (b) the vacuum impregnation of erythritol [27]

before and after the vacuum impregnation of erythritol. The authors experimentally tested samples with pore sizes of 100 , 300 , and $500\mu\text{m}$ and measured both thermal conductivity and volumetric density of latent heat (Figure 2-8). Best results were shown using a pore size of $500\mu\text{m}$, where thermal conductivity of the composite was improved to $11.6 \text{ W/m}\cdot\text{K}$, 15x greater than that of pure erythritol.

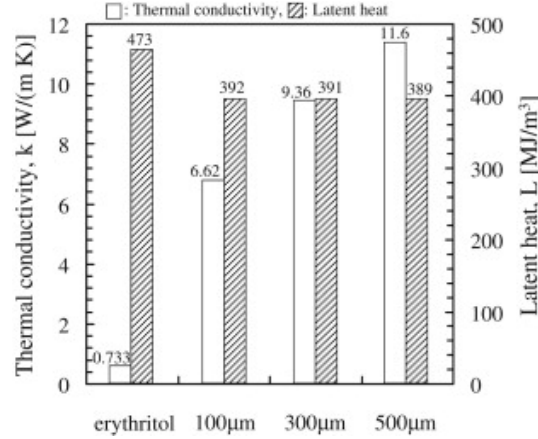


Figure 2-8. Thermal conductivity and volumetric density of latent heat of each erythritol-nickel composite tested [27]

Shamberger and Fisher developed a method for approximating the thermophysical properties of low- k PCMs with the addition of high- k fins [32]. The authors found that with the proper ratio of high and low- k materials and the appropriate fin design, PCMs with high- k fins could be viewed as composites. Upper and lower bounds of the composite’s effective thermal conductivity, referred to as “endmembers”, were calculated according to fins’ placement in relation to the thermal path:

$$k_{comp}^{\parallel} = \phi_{PCM} k_{PCM} + \phi_{high-k} k_{high-k} \quad (1)$$

$$(k_{comp}^{\perp})^{-1} = \phi_{PCM} (k_{PCM})^{-1} + \phi_{high-k} (k_{high-k})^{-1} \quad (2)$$

where ϕ_i and k_i are the volume fraction and thermal conductivity, respectively, of component i . The upper bound was set with fins parallel to the heat flow (Figure 2-9a) and the lower bound with

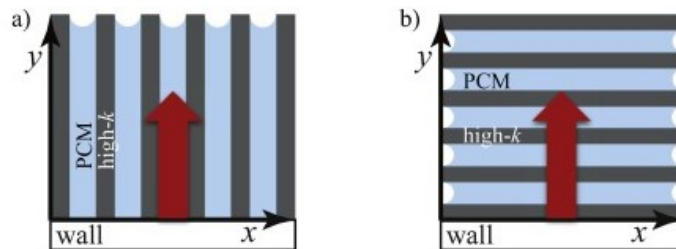


Figure 2-9. Endmember composites with fins parallel (a) and perpendicular (b) to heat flow [28]

fins perpendicular to the heat flow (Figure 2-9b). The composite's intrinsic properties of interest (density, heat capacity, and heat of fusion) could be estimated using the law of mixtures:

$$X_{comp} = \sum_i \phi_i X_i \quad (3)$$

where ϕ_i is the volume fraction of a component, and X_{comp} and X_i are the intrinsic property of interest. They also found that while the addition of randomly dispersed high- k particles can improve the thermal performance of PCMs, this method will not approach the upper bounds of composite behavior.

Of the literature reviewed, only one study has investigated the use of PCM in PE thermal management. Nafis et. al. conducted numerical studies on the effect of incorporating PCM in the heat sink of a simplified single-sided PE package [7]. Their study used small power pulses with a maximum of 4W, convection coefficients ranging from 5-80 W/m²K, indicating air as the working fluid, and focused on a single PCM (Xylitol). While the results of this study showed that the PCM was helpful at mitigating peak temperature and allowed for a more consistent temperature profile, both the package (Figure 2-10) and the power loads modeled were simple and generic, making it difficult to accurately judge the impact of PCM in an operational environment.

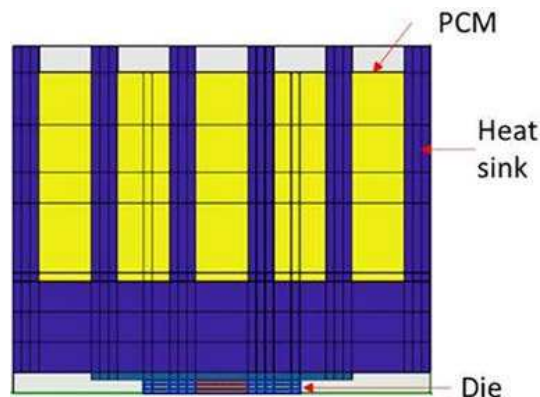


Figure 2-10. Package with PCM modeled by Nafis et. al. [7]

2.3. Research Needs

Research on the use of PCM has largely focused on mobile, intermittent use consumer electronics. While there have been numerous reviews on both PE package design and PCMs for thermal buffering of vehicle components, there have been limited studies on the actual impact of PCM on PE package thermal performance. The current gaps in literature that this study hopes to address are:

- The modeling of PE packages representative of those found in commercial use. While simplified PE package models can approximate the impact of PCM on the package's thermal performance, overly simplified models do not account for heat spreading or the thermal resistance of the various materials throughout the substrate layers.
- The modeling of realistic, transient operating conditions. Heat loads experienced by the PE devices are transient in nature and can vary significantly depending on the operational environment (highway, city, etc.). Simulating a variety of use cases is necessary to understand PCMs effect on PE package's thermal performance.
- The only study found in literature studying the impact of PCM on PE package thermal performance modeled a single PCM. Modeling multiple PCMs and PCM composites is necessary to truly quantify the impact of PCMs on PE package thermal performance and determine the material properties of the PCM that are necessary to have the maximum impact.

2.4 Focus of Current Study

The current study seeks to investigate the impact of PCM on the dynamic thermal management performance of PE packages. Two PE packages (single-sided and dual-sided), representative of those found in commercial use, were modeled with multiple PCMs/PCM

composites and their thermal performance was simulated using ParaPower, a thermal modeling platform created by the Army Research Lab (ARL). To test the packages thermal performance, transient heat loads were created using two EPA driving schedules. These drive cycles served to simulate real world driving conditions in both an urban and highway environment.

CHAPTER 3 MODELING APPROACH

The previous chapter discussed the lack of published data on the impact of incorporating PCM into PE packages. The current study seeks to quantify the impact of PCM addition in two different packages that are representative of packages found in recent all-electric vehicles. To quantify this impact, two package geometries were modeled in ParaPower. Two dynamic power and heat load models were created using published EPA drive cycles. These models were applied to the SiC die in the package model and used to simulate the transient operating conditions of the PE. A heat transfer coefficient was also calculated and applied to the package cold plate, simulating flow from the vehicle's cooling loop. The following section details the approach used to create these models.

3.1. Package Geometry

Two PE packages, without PCM, were modeled using ParaPower, an open-source tool developed by the Army Research Lab. ParaPower uses a MATLAB based code that solves a resistor network model of the system using implicit Euler formulation that offers a fast analysis of thermomechanical systems and medium fidelity modeling of PCMs [33, 34]. The single-sided model was based on packaging used in the 2014 Honda Accord [5, 26]. The package is comprised of an aluminum base plate, solder, direct bonded copper (DBC) on silicon nitride (Si_3N_4) with the power devices (2 SiC die) located 6.5 mm from the coolant. Figure 3-1 shows a SolidWorks model of the package (top) as well as the ParaPower model (bottom) with the applied boundary conditions. The second model was based on package geometry used in the 2016 Chevrolet Volt [5, 27]. This package is comprised of the same materials, but with two layers to take advantage of double-sided cooling. Figure 3-2 shows a SolidWorks model of the package (top) as well as the

ParaPower model (bottom) with the applied boundary conditions.

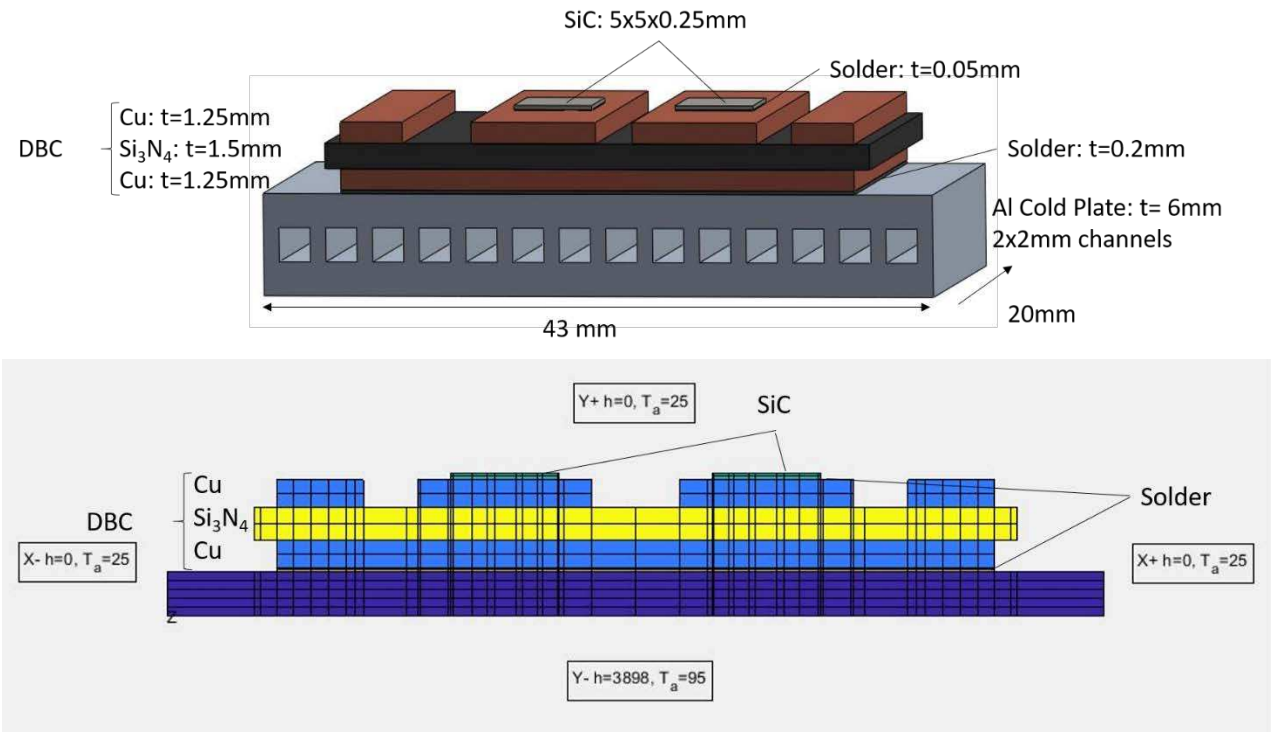


Figure 3-1. Single-sided power electronic package based on 2014 Honda Accord modeled in SolidWorks (top) and ParaPower (bottom)

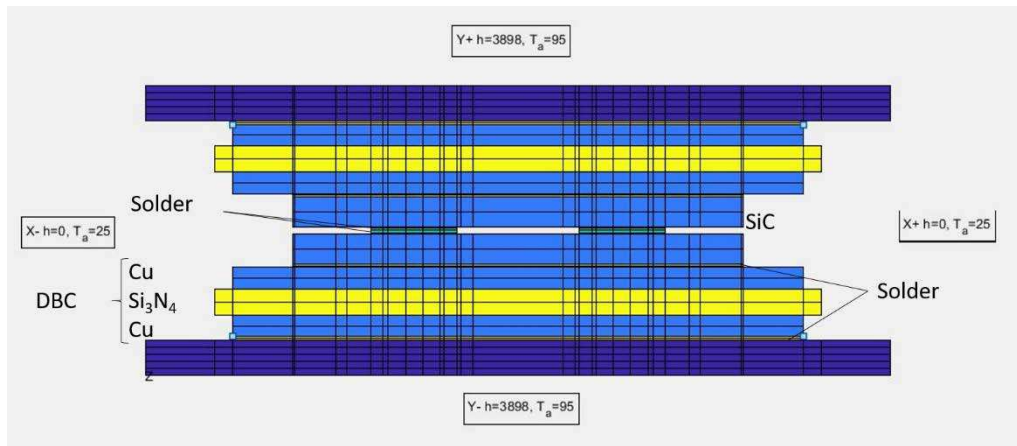
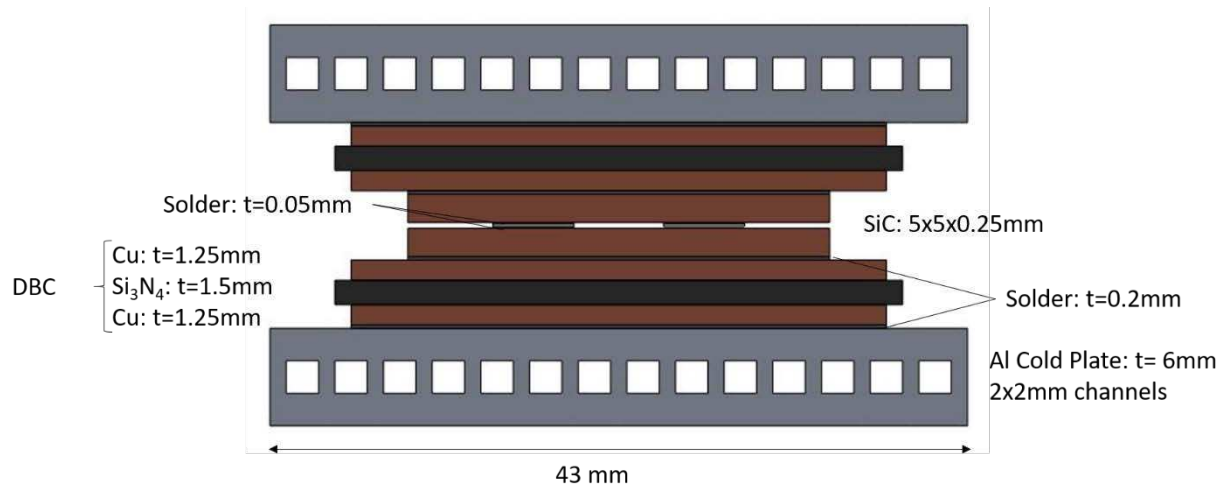


Figure 3-2. Dual-sided power electronic package based on 2016 Chevrolet Volt modeled in SolidWorks (top) and ParaPower (bottom)

ParaPower offers a graphical user interface (GUI) that allows users to define features, model 3D geometries, and assign materials and material properties to different model layers (Figure 3-3). The GUI also allows the user to assign boundary conditions, such as a heat transfer coefficient, to the geometrical faces of the model and to assign power scalar values or functions to any feature modeled. ParaPower then uses a 3D resistance network based on a mesh assigned by the user to solve the heat equation. Parapower has shown to have good accuracy with fairly large time steps and grid sizes, and the reduced order phase-change thermal model has accuracy comparable to

high-fidelity commercial software [35]. A detailed description on the use of ParaPower (creating geometries, assigning materials, applying boundary conditions, etc.) can be found in Appendix C.

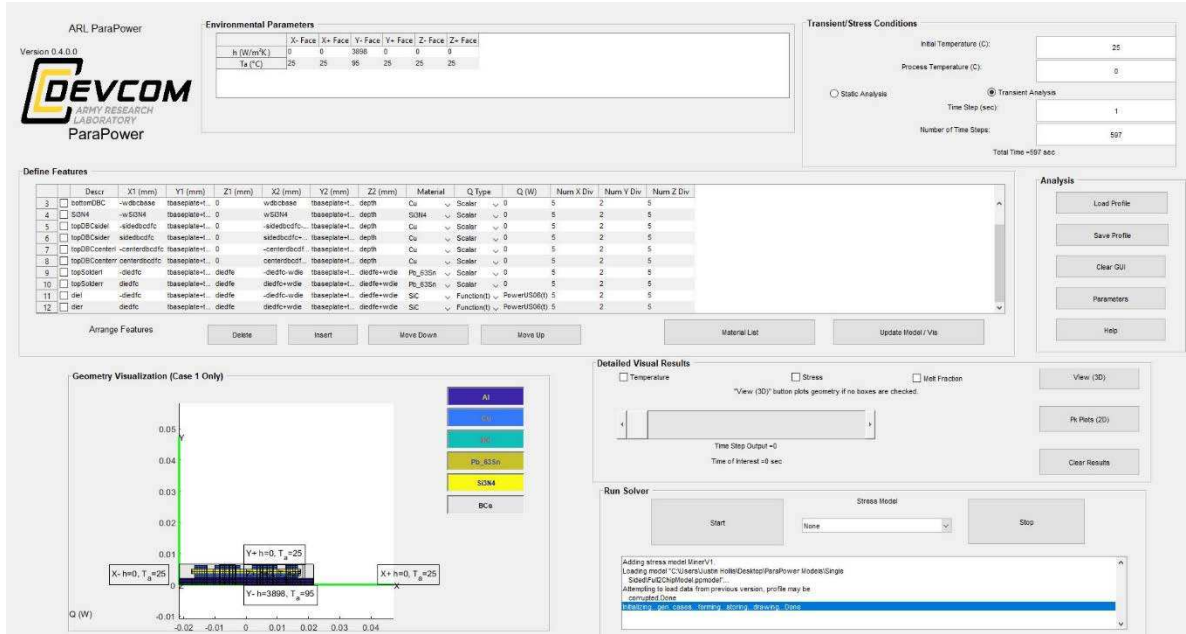


Figure 3-3. ParaPower GUI with single-sided package modeled

3.2. Dynamic Power and Heat Load

A transient heat load model was created using both the US06 and EPA Urban Dynamometer Driving Schedule [36], which were designed to simulate a vehicle’s speed during interstate and city travel respectively. To simulate the heat load experienced by the PE during these drive cycles, the derivative of each velocity profile was calculated through interpolation to determine the vehicle’s acceleration. This acceleration, combined with the drag force and the rolling resistance experienced by the vehicle during travel, were used to create a simple model approximating the forces acting on a moving vehicle (Figure 3-4). Equation 4 shows the force equation used:

$$F = ma + c_R mg + \frac{1}{2} \rho c_D A V^2 \quad (4)$$

where m is the mass of the vehicle (1600 kg), a is the vehicle's acceleration, c_R is the coefficient of rolling resistance (0.015), g is gravity, ρ is air density (1.225 kg/m³), c_D is the coefficient of drag

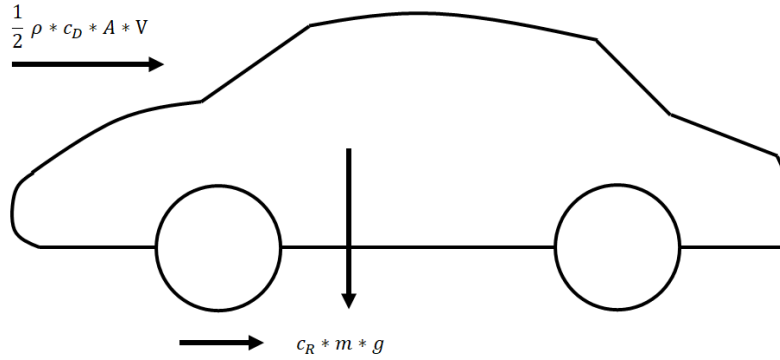


Figure 3-4. Additional forces acting on vehicle

resistance (0.3), A is the frontal area of the car (0.58 m²), and V is the velocity [37, 38]. Equation 5 describes the traction power necessary to propel the vehicle:

$$P=VF \tag{5}$$

where P is the traction power need to propel the vehicle forward, V is the velocity from the specific drive cycle, and F is the force calculated in Equation 4. Equation 6 describes the heat load equation that was applied to the SiC die in ParaPower:

$$Heat\ Load = (1 - \eta)|P| \tag{6}$$

where the maximum efficiency, η , is 98% and assumed constant [39]. The absolute value of the power is taken to maintain power even during deceleration, to simulate regenerative braking. Figure 3-5 shows the power and speed used to create the heat load model. This transient heat load was divided by the number of die in the package (N), with the assumption that the heat rate was divided evenly among the die in the package (Equation 7). The US06 drive cycle (top) was the more aggressive cycle, with power spikes reaching over 80kW and average power stretches up to

20kW. The Urban drive cycle (bottom) had lower power levels, but longer periods of moderate power levels up to 10kW.

$$Q(\text{die}) = \text{Heat Load} / N \tag{7}$$

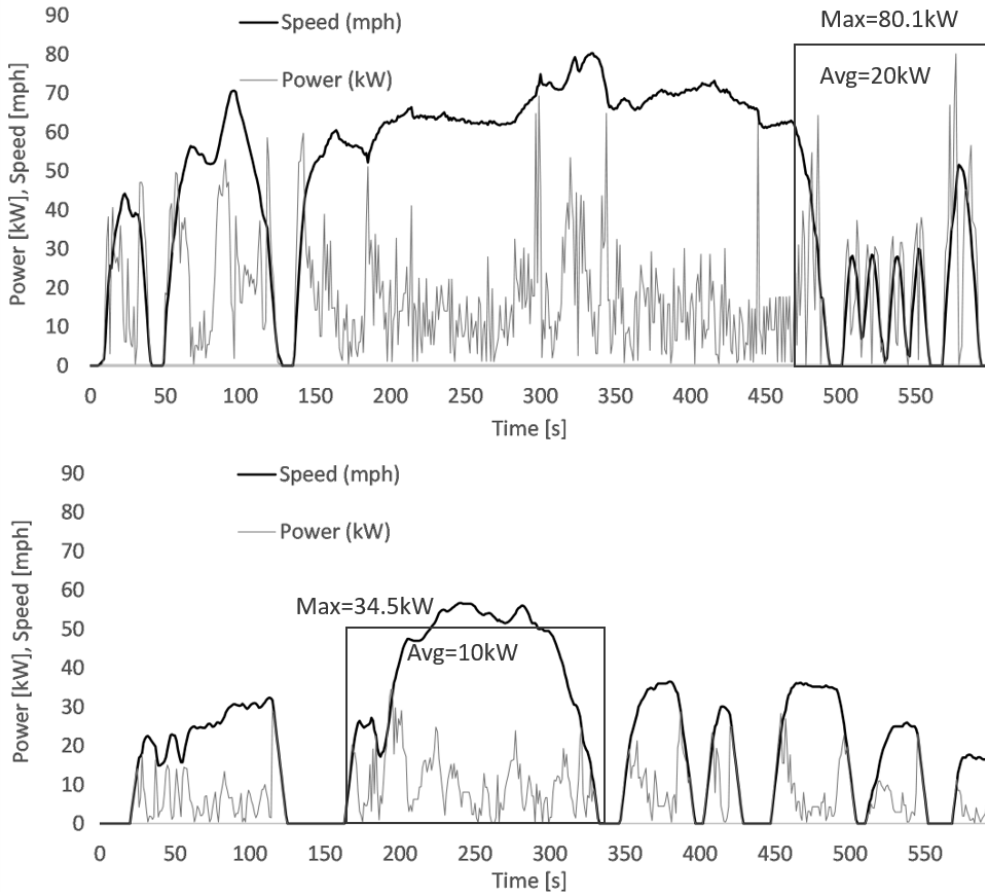


Figure 3-5. Speed and modeled power derived from the US06 (top) and Urban (bottom) drive cycles

3.3. Heat Transfer Coefficient

A typical vehicle engine coolant loop consists of a 50/50 mixture of water and ethylene glycol that is pumped to a radiator to reject heat and maintain an operating temperature between 80°C and 100°C [8]. EVs typically have a cooling loop that operates at lower temperatures (60-70°C) to cool electrical components. The higher operating temperatures of SiC devices are

prompting new vehicle designs that target a single vehicle coolant loop for electrical and mechanical components. For this reason, an average working fluid temperature of 95°C (higher than average for an ICE vehicle) was chosen for this model for simplicity. An overall heat transfer coefficient of 3898 W/m²K was calculated using the flow through and geometry inside the cold plate and applied to the bottom of the package. The overall heat transfer coefficient (U) was calculated from the heat transfer coefficient, fin efficiencies, and the cold plate geometry (Equation 8):

$$U = \frac{\eta_o h A_t}{A_b} \quad (8)$$

where η_o is the overall fin efficiency, A_t is the total surface area of the fins, and A_b is the area of the prime surface [18]. The heat transfer coefficient (h) was solved for using the Nusselt number (Equation 9):

$$Nu = \frac{h D_h}{k} \quad (9)$$

where Nu is the Nusselt number, D_h is the hydraulic diameter of the cold plate channels, and k is the thermal conductivity of the working fluid. Churchill correlations [20] were used to solve for the friction factor, and Nusselt number, and are described in Equations (10-14). Equation (10) describes the overall Nusselt number:

$$Nu = \left[Nu_t^{10} + \left[\frac{\exp\left[\frac{2200 - Re D_h}{365}\right]}{Nu_l} + \left[\frac{1}{Nu_t} \right]^2 \right]^{-5} \right]^{0.1} \quad (10)$$

where Nu_t describes the Nusselt number through the turbulent regime with Nu_l and Nu_o describing the Nusselt number through the laminar and transition regimes (Equations 11-13). Nusselt numbers for the laminar and transition regimes were fixed under the assumption of uniform heat flux [19].

$$Nu_t = Nu_o + \frac{0.079Re_{D_h}\sqrt{f}Pr}{(1+Pr^{0.8})^{\frac{5}{6}}} \quad (11)$$

$$Nu_i = 5.33 \quad (12)$$

$$Nu_o = 6.3 \quad (13)$$

Equation (10) describes the empirical relationship between the friction factor (f) and the Reynolds number.

$$\frac{1}{f} = \left[\frac{1}{\left[\left(\frac{8}{Re_{D_h}} \right)^{10} + \left(\frac{Re_{D_h}}{36500} \right)^{20} \right]^{\frac{1}{2}}} + \left(2.21 \ln \frac{Re_{D_h}}{7} \right)^{10} \right]^{\frac{1}{5}} \quad (14)$$

The Reynolds number from the coolant is described by Equation (15):

$$Re_{D_h} = \frac{\rho u D_h}{\mu} \quad (15)$$

where ρ is the density, u is the flow speed, and μ is the dynamic viscosity of the fluid. During the simulations, the total mass flow through the channels was 1.14E-3 kg/s and yielded a Reynolds number of 754 for the 24-module design, indicating a laminar flow, even if the same amount of flow was directed through 10 modules (the minimum number modeled). Thus, the variation in the overall heat transfer coefficient was insignificant and assumed constant throughout during all simulations.

3.4. PCM Selection

Multiple PCM and PCM composites were selected for modeling in both the single-sided and dual-sided packages. PCMs were selected from their melt temperature (T_m) and figure of merit (FOM), which is defined as:

$$FOM = \rho H_f k \quad (16)$$

where ρ is the density, H_f is the latent heat of fusion, and k is the thermal conductivity of the high temperature phase [40]. Erythritol was chosen due to its melting temperature and high heat of fusion, though pure erythritol has the disadvantage of poor thermal conductivity (Table 3-1). A PCM consisting of erythritol impregnated with nickel was also simulated. This PCM was developed and tested by Oya et. al., and retained the high heat of fusion of pure erythritol, while increasing its thermal conductivity by a factor of 15 [31]. An erythritol-copper composite was modeled using methods developed by Shamberger et. al. to simulate the performance and material characteristics of low- k and high- k composite materials [32]. As previously mentioned, the authors found that when high- k material fins were appropriately designed and embedded in low- k PCMs, the materials could be considered a composite. The effective thermal conductivity of the composite was calculated using their formula for the upper-bound value (fins parallel to heat flow), and the general linear rule of mixtures was used to determine the intrinsic properties of interest. Finally, indium was selected for modeling for its relatively high thermal conductivity during liquid phase and the ongoing interest in metallic PCMs. Due to indiums high melt temperature, a maximum junction temperature of 175°C had to be considered for this case alone.

Table 3-1. Selected PCMs in present study

PCM	T_{melt} [°C]	k [W/mC]	H_f [kJ/kg]	ρ [kg/m ³]	FOM [kJ ² /m ⁴ sC]	Optimum thickness [mm]
Erythritol [9]	117	0.33	340	1480	166	7
Erythritol and Nickel [31]	117	11.4	315	1453	5218	9
Erythritol-Copper Composite	117	250.5	254	5833	397096	25
Indium [9]	156	36	28.4	7310	7474	25

3.5. PCM Thickness

The amount of each PCM that was incorporated into the packages was determined from parametric simulations. Care must be taken when selecting the PCM thickness as there can be negative returns when considering low- k PCMs and diminishing returns in PCM thickness with higher- k composite PCMs (Figure 3-6). Figure 3-6a shows the negative returns experienced by a package with 24 die and erythritol during the US06 drive cycle. Due to the low- k of erythritol, increasing the PCM thickness beyond the optimum 7mm increases the maximum temperature experienced by the die as the lower conductivity of the liquid phase begins to have an insulative effect. Figure 3-6b shows the diminishing returns experienced by a package with 24 die and erythritol-copper composite during the US06 drive cycle. Even with a higher- k composite, increasing the thickness of the PCM show diminishing returns due to the melt temperature and the transient nature of the heat load. Table 3-1 shows the optimum thickness for each PCM modeled.

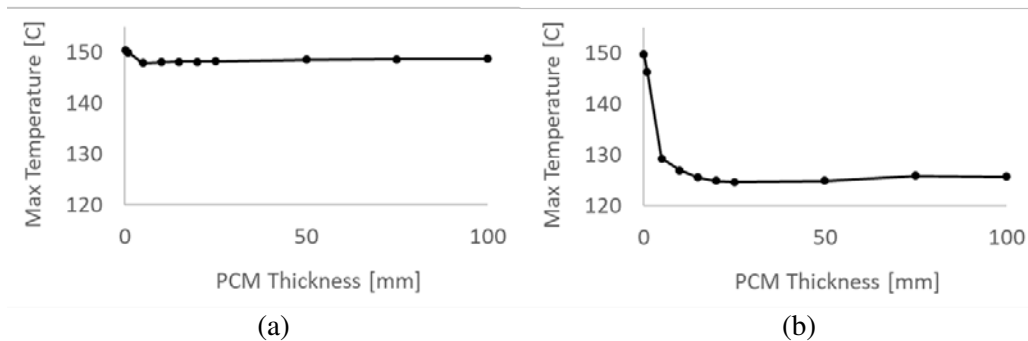


Figure 3-6. Maximum temperature in package with varying erythritol (a) and erythritol-copper composite (b) PCM thicknesses

3.6. Package Modeling with PCM

Once the PCMs were selected, the packages were modeled with various PCM placement. A single-sided package with phase change material was designed with the PCM in direct contact

with the top surface (Figure 3-7). Any potential electrical complications due to the introduction of metallic PCMs or PCM-metal composites was ignored for simplicity. Three different dual-sided packages were investigated with PCM incorporated into different layers of the package (Figure 3-8 a-c). Multiple configurations of dual-sided packages were modeled to observe the effects of heat spreading on PCM effectiveness. Figure 3-8a shows the PCM inserted into the periphery of the package. Figure 3-8b shows the PCM embedded into the emitter and collector of the package, closest to the SiC die. Figure 3-8c shows the PCM embedded in the layer of DBC nearest to the SiC die.

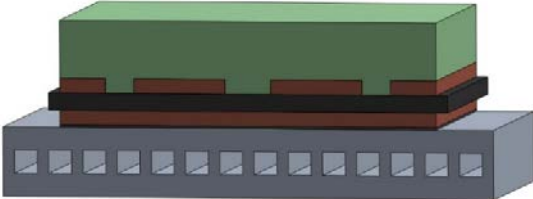


Figure 3-7. Single-sided power electronic package with PCM

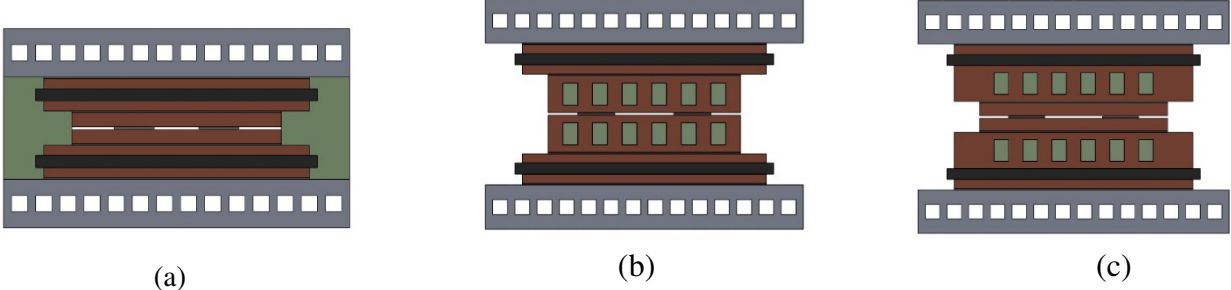


Figure 3-8. Dual-sided power electronic package with PCM in periphery (a), emitter/collector (b), and DBC (c)

3.7. Simulation Matrix

The purpose of this study is to quantify the impact of PCM on the dynamic thermal performance of PE packages. Simulations were run in ParaPower using the PE packages described above with the calculated overall heat transfer coefficient applied to base of the package and the

calculated power/heat load applied to the die. First, base lines were determined for each package without PCM, for both the urban and US06 drive cycles, with package configurations containing 10, 12, 14, 16, 18, 20, and 24 die. Once these base lines were established, the PCMs detailed in Table 3-1 were incorporated into the packages as shown above. Table 3-2 outlines the simulations performed in this study, with the key results discussed in Chapter 4.

Table 3-2. Simulations performed

Package	Die [#]	PCM	PCM Location	Drive Cycle
Single-Sided	10, 12, 14, 16, 18, 20 ,24	None	N/A	US06
Single-Sided	10, 12, 14, 16, 18, 20, 24	Erythritol	Top	US06
Single-Sided	10, 12, 14, 16, 18, 20, 24	Erythritol-Nickel	Top	US06
Single-Sided	10, 12, 14, 16, 18, 20, 24	Erythritol-Copper	Top	US06
Single-Sided	10, 12, 14, 16, 18, 20, 24	Indium	Top	US06
Single-Sided	10, 12, 14, 16, 18, 20, 24	None	N/A	Urban
Single-Sided	10, 12, 14, 16, 18, 20, 24	Erythritol	Top	Urban
Single-Sided	10, 12, 14, 16, 18, 20, 24	Erythritol-Nickel	Top	Urban
Single-Sided	10, 12, 14, 16, 18, 20, 24	Erythritol-Copper	Top	Urban
Single-Sided	10, 12, 14, 16, 18, 20, 24	Indium	Top	Urban
Dual-Sided	10, 12, 14, 16, 18, 20, 24	None	N/A	US06
Dual-Sided	10, 24	Erythritol	periphery, emitter/collector, DBC	US06
Dual-Sided	10, 24	Erythritol-Nickel	periphery, emitter/collector, DBC	US06
Dual-Sided	10, 24	Erythritol-Copper	periphery, emitter/collector, DBC	US06
Dual-Sided	10, 24	Indium	periphery, emitter/collector, DBC	US06
Dual-Sided	10, 24	None	N/A	Urban
Dual-Sided	10, 24	Erythritol	periphery, emitter/collector, DBC	Urban
Dual-Sided	10, 24	Erythritol-Nickel	periphery, emitter/collector, DBC	Urban
Dual-Sided	10, 24	Erythritol-Copper	periphery, emitter/collector, DBC	Urban
Dual-Sided	10, 24	Indium	periphery, emitter/collector, DBC	Urban

CHAPTER 4 RESULTS AND DISCUSSION

The preceding chapter outlined the approaches used to model the two PE packages, the power and heat load models, and the overall heat transfer coefficient of the simulated working fluid. The current chapter will present the key results of the simulations described at the end of the previous chapter. First the impact of the PCM selection and placement is presented. Since multiple PCM were being investigated it was imperative to understand the impact of each. PCM placement in the dual-sided package is also discussed. Next, the impact of the PCM is discussed under two different operational heat loads. These heat loads were modeled using transient power/heat loads derived from EPA drive cycles as described in the previous chapter. Finally, the impact of incorporating PCM into PE packaging is discussed in terms of system level considerations.

4.1. Impact of PCM Selection and Placement

Base line simulations were run with both the single-sided containing 10, 12, 14, 16, 18, 20, and 24 die and dual-sided packages containing 10 and 24 die. Figure 4-1 shows how temperatures experienced by the die during the full US06 drive cycle (with peak temperature at 575s) can be reduced by incorporating more die into the module to divide the power load. While this strategy is effective at reducing peak temperatures, it can dramatically increase the overall cost of the package. Simulations were run with all four PCMs in both packages to determine the impact of each and to determine the placement that is most effective in the dual-sided package.

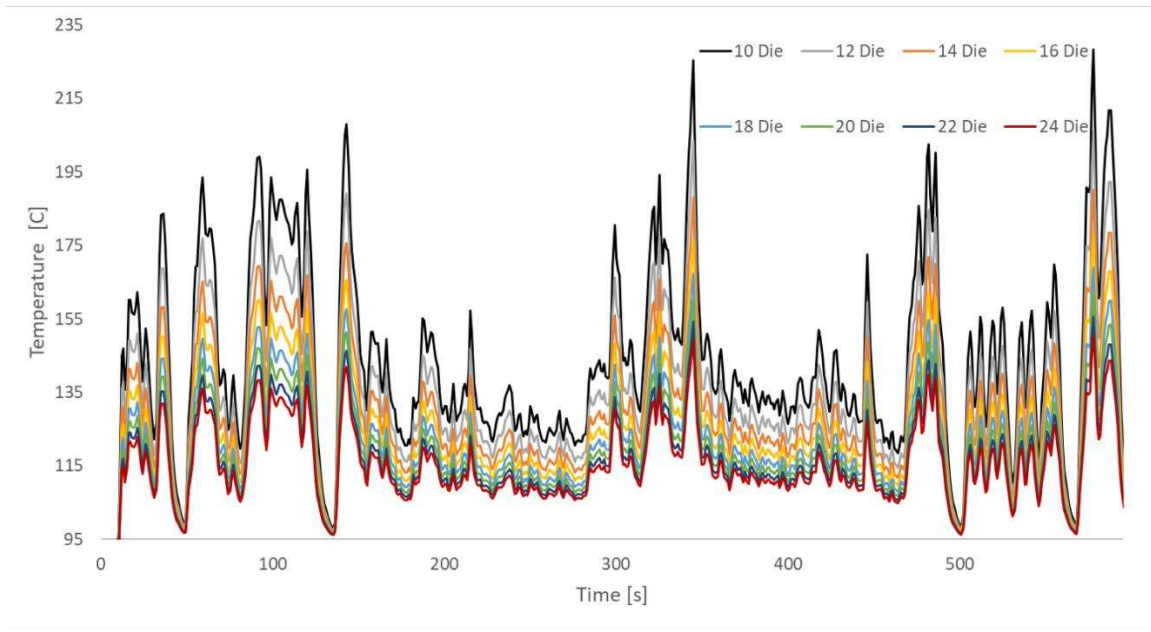


Figure 4-1. Die temperatures in single-sided package containing 10, 12, 14, 16, 18, 20, and 24 die during full US06 drive cycle

4.1.1 Single-Sided Package

Of the PCMs modeled the erythritol-copper composite allowed for the greatest reduction in the number of die in the single-sided package. Figure 4-2 shows the junction temperature in the

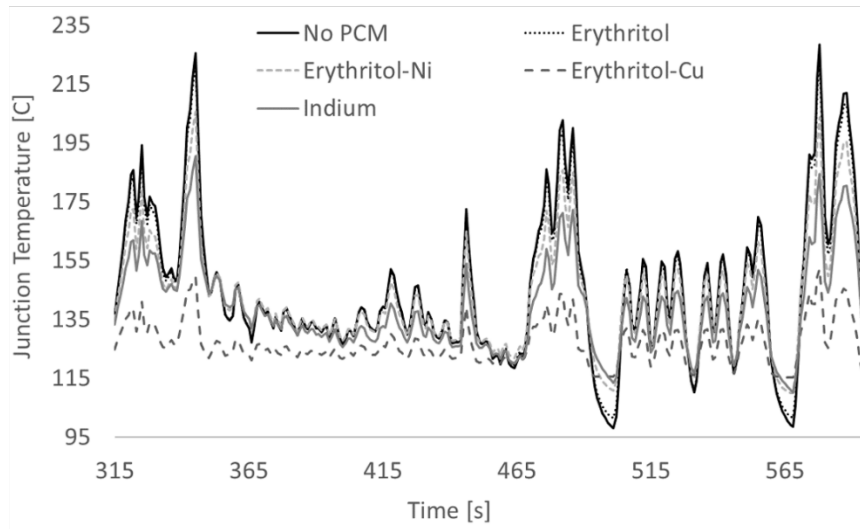


Figure 4-2. Junction temperature of SiC die in packages with 10 die with all PCMs modeled during US06 drive cycle

single-sided packages with 10 die for each PCM in the most aggressive drive cycle. The portion of the US06 drive cycle shown contains two of the highest power spikes of the cycle, at 350 and 575s, which is consistent with the two highest die temperatures experienced in the cycle. All cases show a reduction in the maximum temperature experienced. However, only the erythritol-copper composite was able to keep the peak temperature near 150°C with 10 die. For example, at 575s, the peak temperature was 228°C with no PCM, and the addition of the erythritol-copper composite reduced the peak temperature to 152°C. Indium also performed well, reducing the temperature at 575s to 184°C, but its higher transition temperature and lower enthalpy of melting were a disadvantage. Pure erythritol and erythritol-nickel had the highest enthalpy of melting, but the performance of both PCMs was hindered by their poor thermal conductivity. In all cases, the ΔT experienced in the package was also reduced, with the results varying as expected with the PCMs' FOM.

While the best results were shown with the erythritol-copper composite, the addition of PCM to the single-sided package improved its thermal performance in all cases. The single-sided package with no PCM required 24 SiC die to keep the maximum temperature near 150°C during the drive cycle, which was assumed to be the target junction temperature in this study (an exception was made for the use of indium). Figure 4-3 shows temperature in each substrate layer of the package over the complete US06 drive cycle, with the peak die temperature of 150.5°C at 575s. While the entire package is modeled for all results shown in this chapter, only the portion of the drive cycle with the highest peak powers (producing the highest die temperatures) will be detailed, along with temperature profiles of the cold plate, die, and PCM when applicable. All other substrate layers will not be shown for figure clarity, and full results of the simulations discussed below can be found in Appendix A.

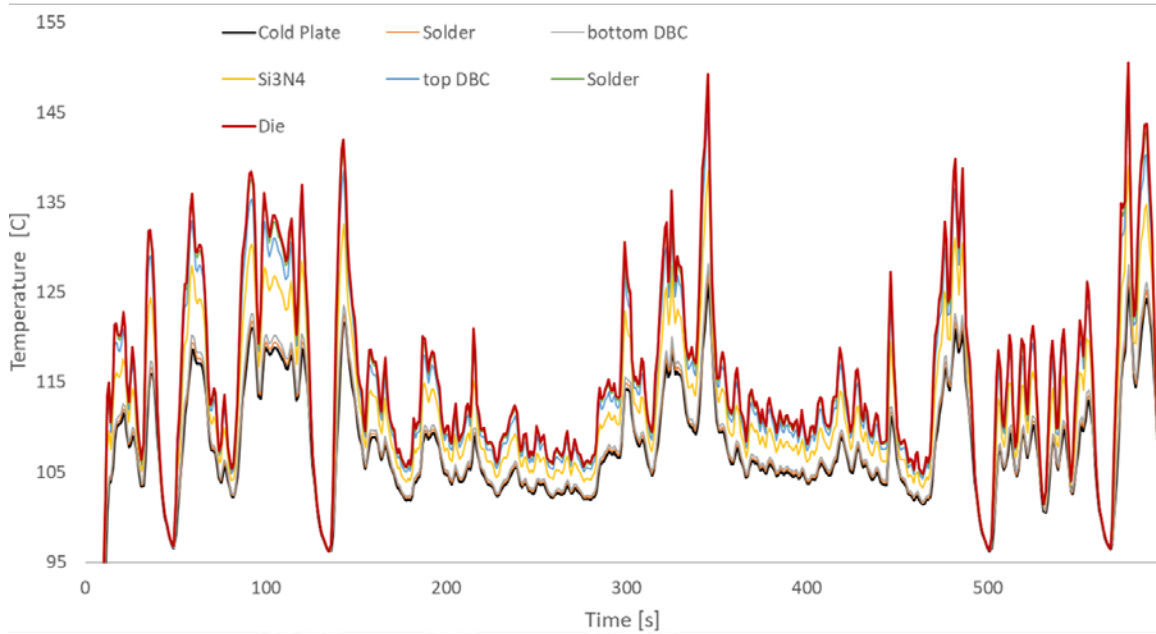


Figure 4-3. Temperature profile of PE package layers of single-sided package with 24 die and no PCM for complete US06 drive cycle

With the addition of pure erythritol to the package, the maximum temperature was reduced to 147.9°C, again at 575s, but 24 die were still required to achieve this temperature (Figure 4-4). While the peak temperature of the die was slightly reduced, temperature variability throughout the

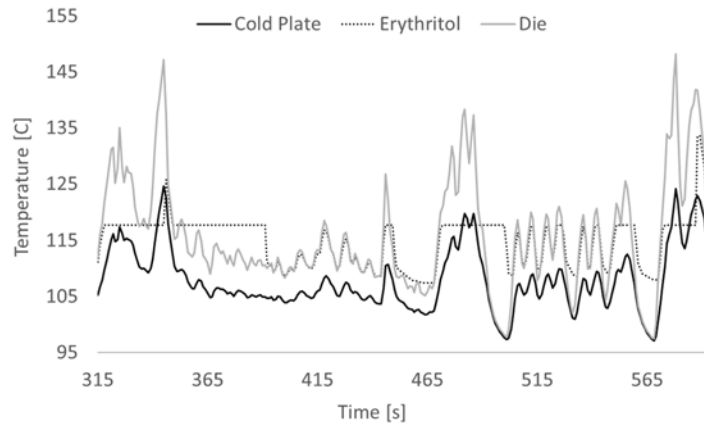


Figure 4-4. Temperature profile of die, cold plate, and erythritol in single-sided package with 24 die during portion of US06 drive cycle

package remains roughly the same. Peak temperatures could be reduced further to 142°C with 24 die by incorporating the erythritol-nickel composite. The temperature could also be kept below the

target temperature while reducing the number of die to 22. Reducing the number of die to 20 with the erythritol-nickel PCM kept temperatures slightly below those experience by the package with 24 die and no PCM at 575s (Figure 4-5). While use of erythritol-nickel is more effective at reducing the peak temperatures when compared to pure erythritol, it too shows little effect in dampening the transient temperature fluctuations throughout the cycle or decreasing temperature variability throughout the package.

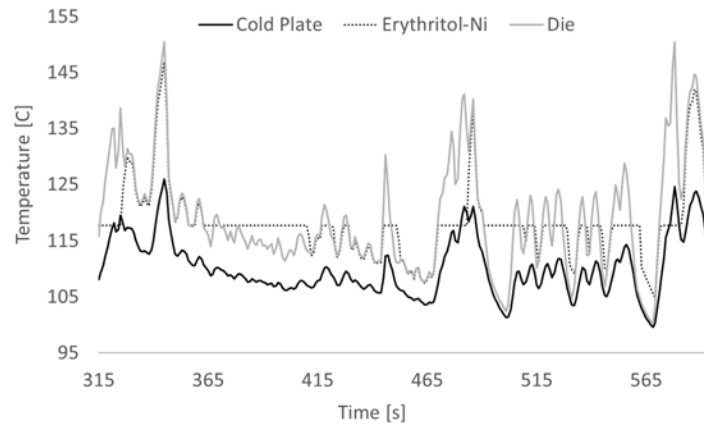


Figure 4-5. Temperature profile of die, cold plate, and erythritol-nickel in single-sided package with 20 die during portion of US06 drive cycle

To utilize the thermal storage potential of indium, the maximum allowable junction temperature was increased to 175°C due to the higher melting point of indium. The single-sided package without PCM required 18 die to keep the temperature below that point, while the addition of indium reduced to necessary number of die to 12. While the die temperature reaches above the targeted 150°C throughout the cycle, with peak value approaching 175°C at 345s, significant reductions in temperature variations throughout the package can be seen in Figure 4-6, indicating a possible reduction in thermomechanical stress in the package throughout the cycle.

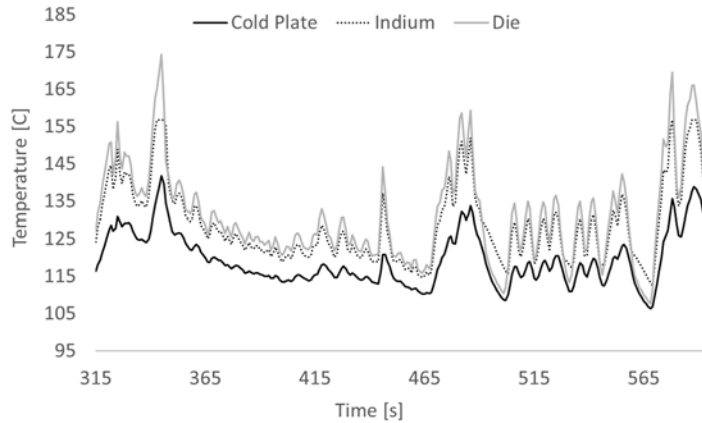


Figure 4-6. Temperature profile of die, cold plate, and indium in single-sided package with 12 die during portion of US06 drive cycle

Figure 4-7 shows the temperature profile of the cold plate, die, and erythritol-copper PCM in a package containing 12 die (top) and 10 die (bottom). In addition to allowing for a significant reduction in the number of die necessary to keep temperature around 150°C, the erythritol-copper also show the potential to dampen the transient temperature fluctuations experienced by the package throughout the cycle, as well as decrease temperature variability throughout the package layers.

Table 4-1 shows a summary of the results discussed above. Results from the full US06 cycle simulations, including temperature profiles for each substrate layer in the package can be found in Appendix A.

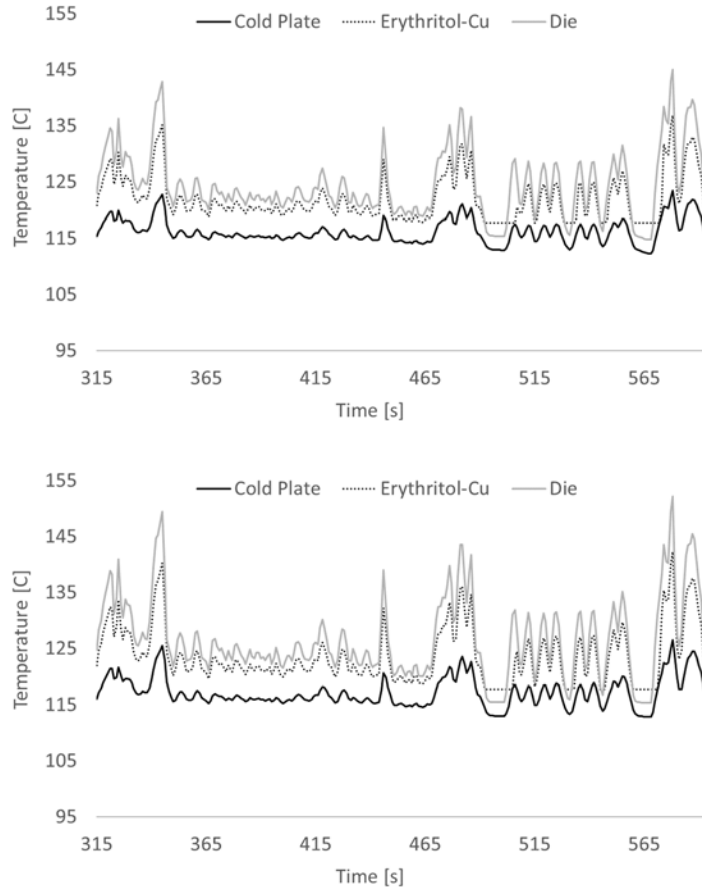


Figure 4-7. Temperature profile of die, cold plate, and erythritol-copper in single-sided package with 12 die (top) and 10 die (bottom) during portion of US06 drive cycle

Table 4-1. Comparison of PCM effect on maximum junction temperature in single-sided package during US06

PCM	Number of Die	Maximum Junction Temperature [°C]
None	24	150.5
Erythritol	24	147.9
Erythritol and Nickel	20	150.4
Indium	12	174.2
Erythritol-Copper Composite	12	145
Erythritol-Copper Composite	10	152.1

4.1.2 Dual-Sided Package

In simulations of a dual-sided package modeled with 24 die, the addition of PCM was less effective at reducing peak temperatures and can increase the maximum temperatures experienced throughout the package in many configurations. For example, Figure 4-8 shows the temperatures experienced in a dual-sided package with 24 die and erythritol in the different configurations shown in Figure 3-8 during the portion of the US06 drive cycle with the highest average power (20kW). The package temperatures never reach the transition temperature of the PCM, and as a

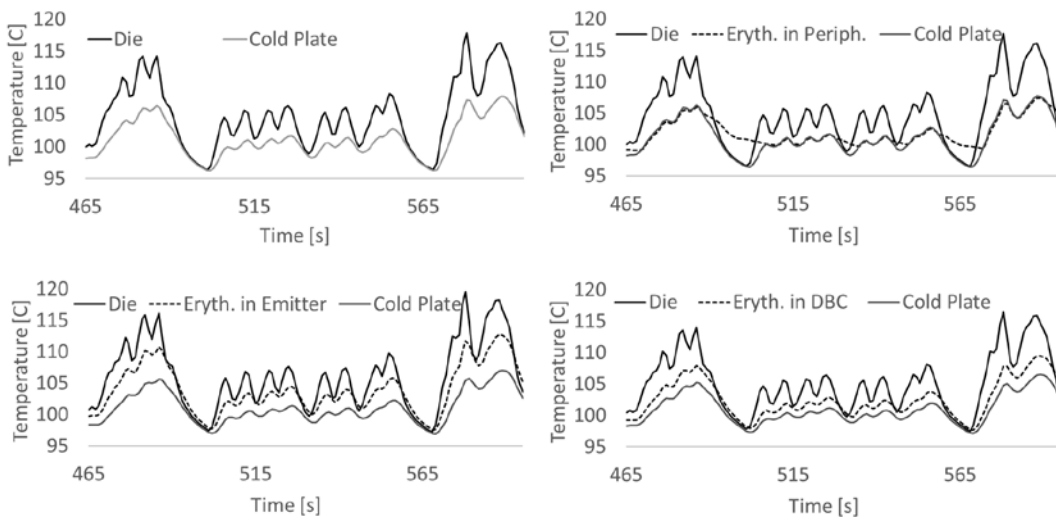


Figure 4-8. Temperature profile of dual-sided PE package with 24 SiC and no PCM (top left) and dual-sided PE package with erythritol in periphery (top right), emitter and collector (bottom left), and DBC (bottom right) during portion of US06 Drive Cycle

result, the thermal storage potential of the PCM is not utilized. The addition of PCM to the periphery of the package (top right) has little to no effect on package thermal performance. Adding PCM into the emitter/collector (bottom left) provided additional thermal resistance to the respective package layer, limiting heat spreading and increasing the maximum die temperature by over 3°C. A noticeable increase in temperature variation between the cold plate and die is visible between 575-585s. Incorporating erythritol into the DBC showed a slight decrease in the maximum die temperature. For example, Figure 4-8 (bottom right) show the maximum temperature reduced from 115 to 113°C at 485s and from 118 to 116°C at 575s. This suggests that placing PCM directly

in the thermal path, but far enough away from the die to allow for heat spreading is the most suitable placement. These results also suggest that care must be taken when adding PCM to a dual sided package to ensure that the transition temperature is reached, otherwise the thermal storage potential is not utilized, and the lower thermal conductivity can negatively impact the packages thermal management properties.

Due to the advantage of dual-sided cooling, the dual-sided package without PCM was able to maintain a peak junction temperature of 150°C during the drive cycle with only 10 SiC die. The erythritol-copper composite was incorporated into different layers of the dual-sided package models to test the effectiveness of the best performing PCM in improving package thermal management performance. The maximum temperature reached during the cycle occurs at 575s. The addition of the composite PCM to the periphery of the package reduced the maximum temperature from 149.9 to 145.1°C (Figure 4-9). While successful, the indirect placement of the PCM in relation to the thermal path allowed less the 10% of the PCM to melt throughout the cycle.

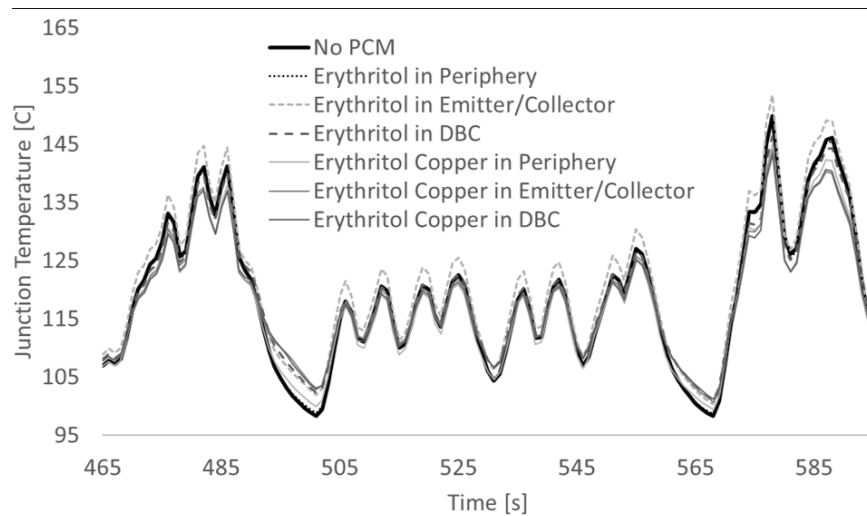


Figure 4-9. Junction temperature of SiC die in dual-sided PE package with 10 SiC and erythritol in different package configurations during portion of US06 drive cycle

Figure 4-10 show the melt fraction of the erythritol-copper when placed into the periphery, emitter/collector, and DBC as detailed in Figure 3-8. The composite was the most successful when placed directly in the thermal path. When placed in substrate layers of the package, either the emitter and collector or the top layer of DBC, the peak temperature was reduced to below 145°C. When placed closest to the die, in the emitter and collector, the PCM reached nearly 70% melting at 120s and reduced the peak temperature to 144°C at 575s. The peak temperature was further

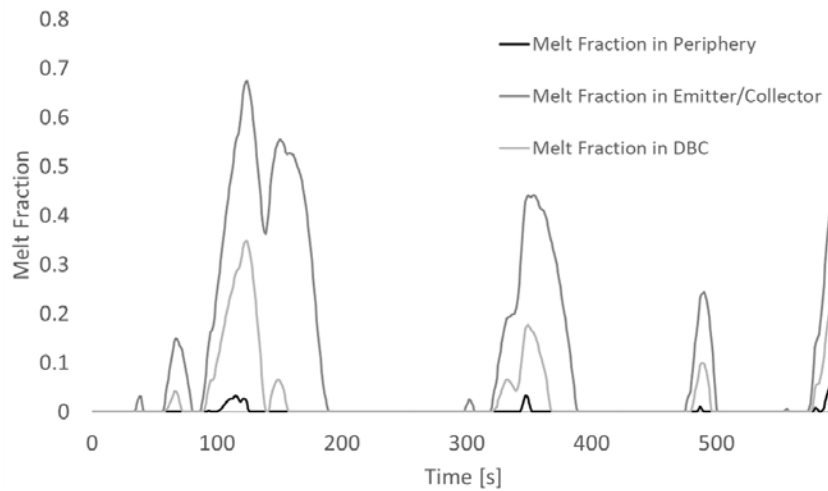


Figure 4-10. Erythritol-copper melt fraction according to placement location in dual-sided package with 10 die throughout US06 cycle

reduced to 143.1°C at 575s with placement in the top layers of the DBC. While a maximum 35% of the PCM melted at 125s while in this location, the placement allowed for more heat spreading and less thermal resistance in the substrate layers closest to the die, reducing the temperature slightly when compared to placement in the emitter/collector.

Other materials modeled showed different results according to where they were placed in the package. Figure 4-9 also shows the temperatures experienced by the die in a dual-sided PE package with erythritol placed in the same configurations. The addition of the lower-*k* erythritol to the periphery of the package reduced the maximum temperature at 575s from 149.9 to 149.3°C, but less than 25% of the PCM melted during the cycle due to the indirect placement relative to the

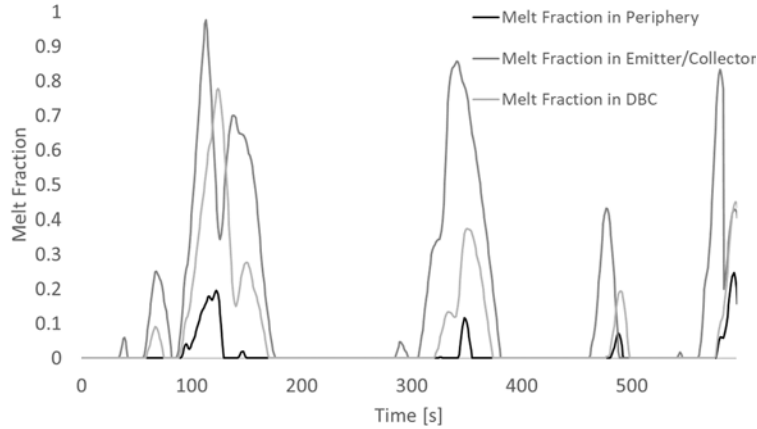


Figure 4-11. Erythritol melt fraction according to placement location in dual-sided package with 10 die throughout US06 cycle

thermal path (Figure 4-11). Placing erythritol directly in the thermal path had mixed results. The lower- k erythritol showed the ability to disrupt the thermal path when placed in layers closest to the SiC die, resulting in an increase in maximum temperature to 153.5°C. The PCM melted completely during the cycle, as shown at 120s, but the lower- k of erythritol increased thermal resistance of the substrate layer. Placement in the DBC allowed for more heat spreading closer to the die and a reduction of peak temperature to 146.4°C, though only 25% of the PCM transitioned during the cycle. These results again suggest care must be taken when incorporating PCM into the dual-sided package so as not to negatively impact its thermal performance.

4.2. US06 Drive Cycle Results with Erythritol-Copper PCM

While all PCMs chosen for this study showed the ability to reduce temperatures in the packages modeled, erythritol-copper composite showed the best results. Therefore, a detailed discussion on the impact of the drive cycle will be given here with this PCM only. Again, the full drive cycle results presented here can be seen in Appendix A. The US06 is an aggressive drive cycle and was chosen to evaluate PCM performance under extreme conditions, with speeds reaching over 80 miles per hour and rapid decelerations, creating transient power spikes of over

80 kW. Figure 4-12 shows the temperatures experienced in the single-sided package during the portion of US06 drive cycle with the greatest power spike (80.1 kW) and the highest sustained

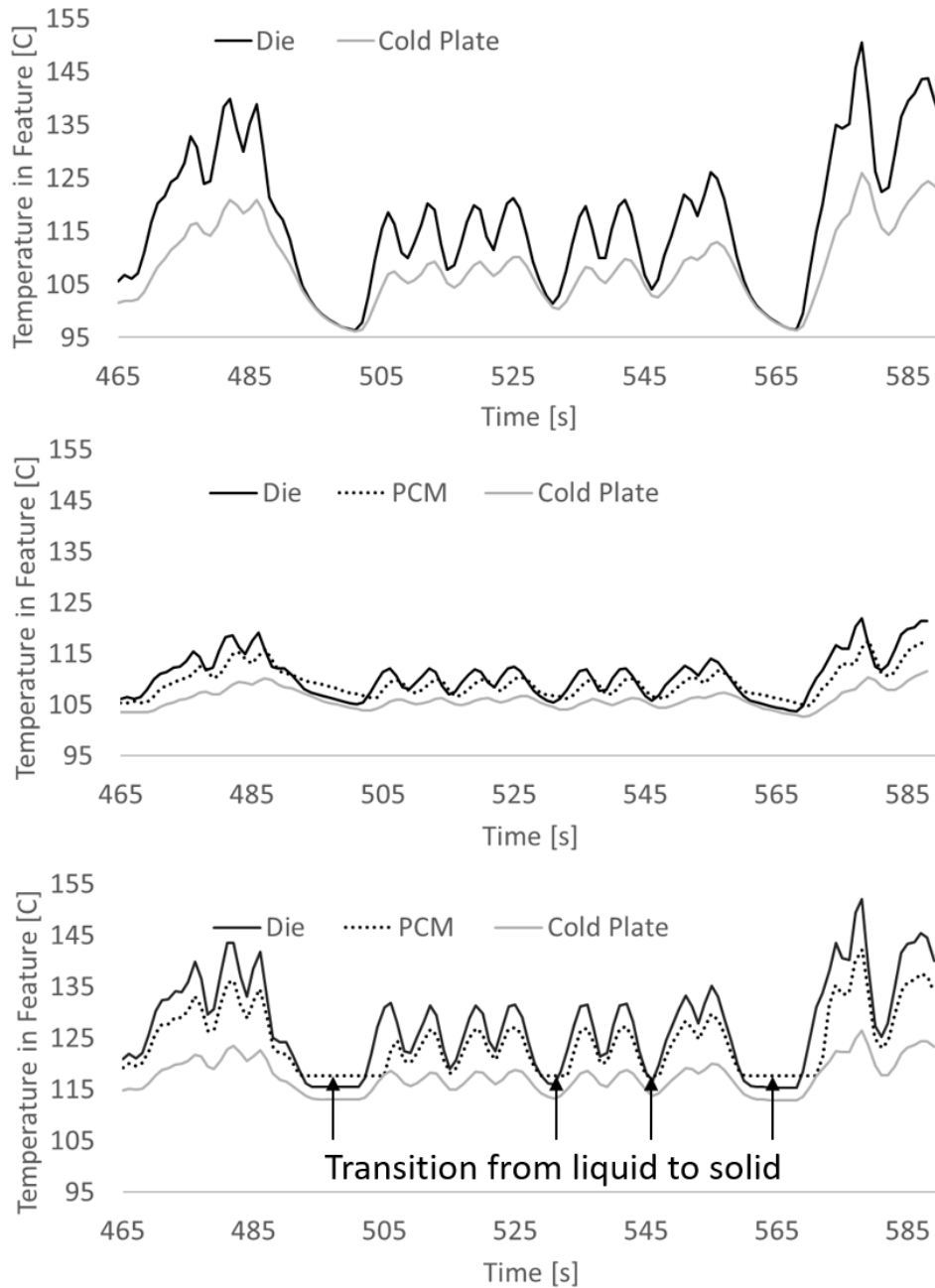


Figure 4-12. Temperature profile of single-sided PE package with no PCM and 24 SiC (top), single-sided PE package with erythritol-copper and 24 SiC (middle) and single-sided PE package with erythritol-copper and 10 SiC (bottom) during portion of US06 drive cycle

average power (20 kW). The top figure shows the package with 24 die and no PCM. The most significant temperature increase can be seen between 565 and 575s, where the junction temperature

jumps from 96°C to 150°C and creates a temperature difference between package layers of over 20°C. These large temperature variations in the package create thermomechanical stress in substrate layers that can reduce both performance and reliability throughout its life.

To mitigate these temperature fluctuations, an addition of 2.5cm of erythritol-copper composite PCM was added to the single-side package. Figure 4-12 (middle) shows that the maximum junction temperature is reduced to below 125°C, and temperature variation throughout the package is significantly reduced. The PCM is effective at reducing both the transient temperature spikes as well as the temperature variation in the package, therefore likely reducing the thermomechanical stress in the package. In this case, the PCM temperature rarely goes above the melting temperature and acts mostly as a thermal mass, with less than 2% of the PCM undergoes phase change throughout the drive cycle (Figure 4-13). Though it does not impede the thermal pathway, the latent heat storage potential of the PCM is not being thoroughly utilized in this case.

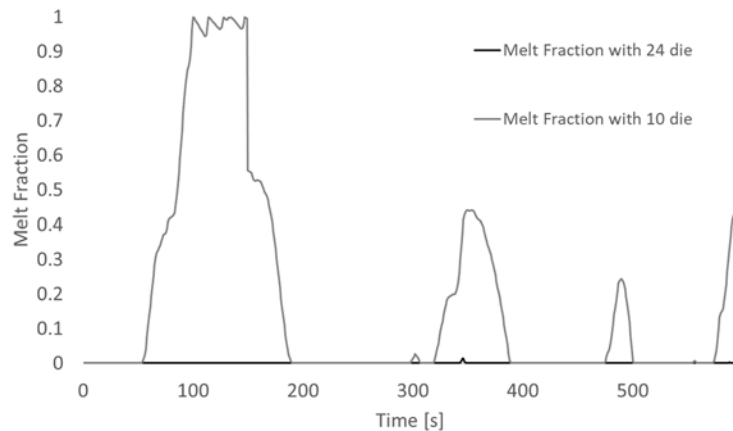


Figure 4-13. Erythritol-copper melt fraction in single-sided package with 10 and 24 die throughout US06 cycle

To increase PCM utilization, the number of die were reduced to increase the amount of heat dissipated. The bottom of Figure 4-12 shows the temperatures experienced in a single-sided

package with 10 die and the addition of 2.5cm of erythritol-copper composite PCM. The maximum junction temperature of the die reaches 150°C, but the number of die necessary to achieve this temperature was reduced by over 50%. For reference, the same package without PCM reached a peak junction temperature of 228°C, with temperature fluctuations approaching 130°C during the cycle. The latent heat is fully utilized in this case as 100% of PCM melts earlier in the cycle, as shown in Figure 4-13. The transition back from liquid to solid can be seen near 500, 535, 545, and 565s. The reduction of temperature variation in the package during these times is shown due to the heat release during this transition. As previously mentioned, device reliability may be improved by decreasing temperature fluctuations in the package, mitigating thermally accelerated failures in substrate layers, increasing its overall fatigue life [5, 10]. The reduction in temperature variation throughout substrate layers provided by the PCM may increase in package reliability and lifespan due to the likely reduction of thermomechanical stresses in the package.

In addition to the single-sided package, the impact of erythritol-copper composite was determined using the best performing configuration of a dual-sided package: in the DBC (Figure 3-8c). Figure 4-14 shows the temperatures experienced in the dual-sided package with and without PCM during the same portion of US06 drive cycle. The top figure shows a package with 10 die and no PCM. The most significant temperature increase can be seen between 565 and 575s, where the junction temperature jumps from 98°C to 150°C and creates a temperature difference between package layers of over 25°C. The bottom figure shows the same package with erythritol-copper placed in the DBC. The addition of the PCM is effective at increasing package thermal management performance, reducing the peak temperature from 150 to 144°C at 575s. While PCM is effective at reducing the transient temperature spikes during the aggressive drive cycle, there is little effect on the temperature variation throughout the package. While the die temperature is

reduced to 6°C at 575s, the temperature variation between the package layers remains at 25°C. This is likely due to the PCM adding additional thermal resistance to its substrate layer, as well as its limited time at transition temperature.

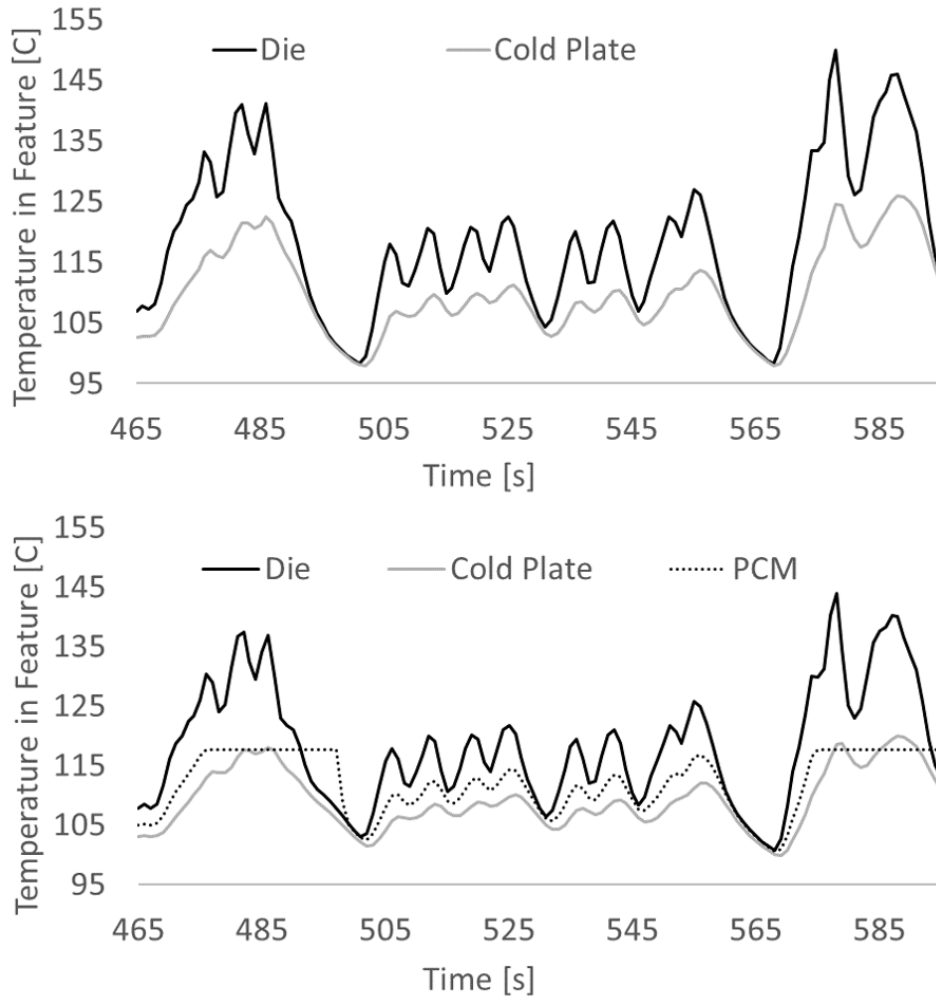


Figure 4-14. Temperature profile of dual-sided PE package with 10 SiC, no PCM (top) and erythritol-copper composite PCM in the DBC (bottom) during a portion of the US06 drive cycle

4.3. Urban Drive Cycle Results with Erythritol-Copper PCM

The EPA Urban Dynamometer Driving Schedule (UDDS) is a less aggressive drive cycle and was used to simulate PCM performance during the to stop and go conditions of city driving. Figure 4-15 shows the temperatures experienced in the single-sided package during the portion of

the drive cycle with the highest average power (10 kW). Figure 4-15 (top) shows the package with 24 die and no PCM. The maximum temperature experienced by the SiC die is approximately 122°C at 190s. The largest temperature increase can be seen between 190-200s, where the junction

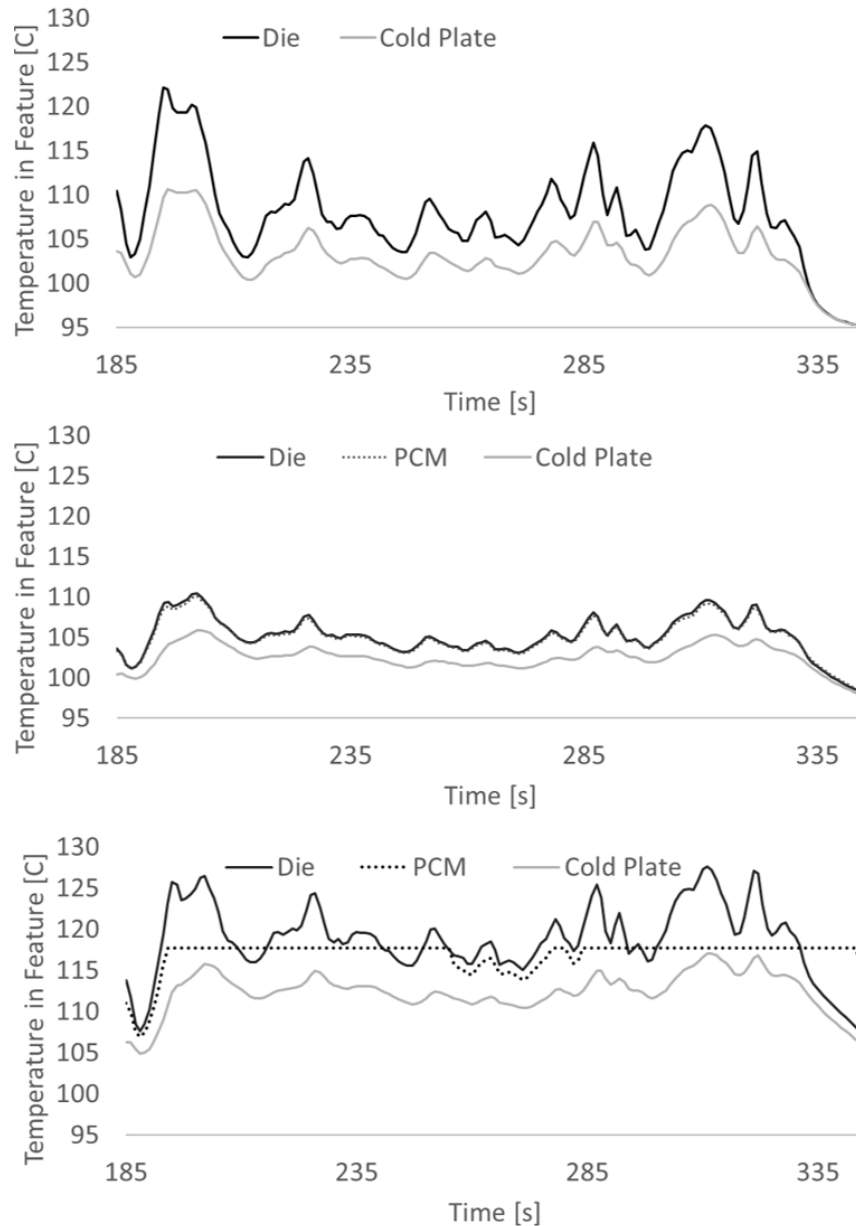


Figure 4-15. Temperature profile of single-sided PE package with no PCM and 24 SiC (top), single-sided PE package with erythritol-copper and 24 SiC (middle) and single-sided PE package with erythritol-copper and 10 SiC (bottom) during portion of Urban Drive Cycle

temperature increases by 20°C and the temperature variation in the package increases from 2°C to 12°C. Incorporation of a PCM mitigates these fluctuations. The middle figure shows the

temperatures experienced in a single-sided package with 24 die and the addition of 2.5cm of erythritol-copper composite PCM. The maximum junction temperature was reduced to approximately 110°C, and temperature variations experienced in the package was reduced by 50% relative to the baseline case without PCM. The PCM is effective at reducing both the transient temperature spikes as well as the temperature variation in the package, therefore likely reducing the thermomechanical stress in the package. In this case, the PCM temperature never rises above the melting temperature and acts solely as a thermal mass. Again, it does not impede the thermal pathway but the latent heat storage potential of the PCM is not utilized in this case.

To increase the amount of melting, a single-sided package with 10 die and the addition of 2.5cm of erythritol-copper composite PCM was simulated (Figure 4-15, bottom). In this case, the maximum junction temperature of the die is increased to 127°C, but the number of die necessary to achieve this temperature was reduced by over 50%. For comparison, the same package without PCM reached a peak junction temperature of 160°C, with temperature fluctuations of 65°C during the cycle. Due to the lower power levels and corresponding lower temperature in this drive cycle, the latent heat storage potential is only partially utilized as only 25% of PCM melts during the cycle (Figure 4-16). Under less extreme conditions, the PCM is still effective at smoothing the transient temperatures by also acting as a thermal mass. The addition of PCM allows for both a reduction of the cost of the package, as well as possible increase in the package lifespan due to the reduction of thermomechanical stress in the package.

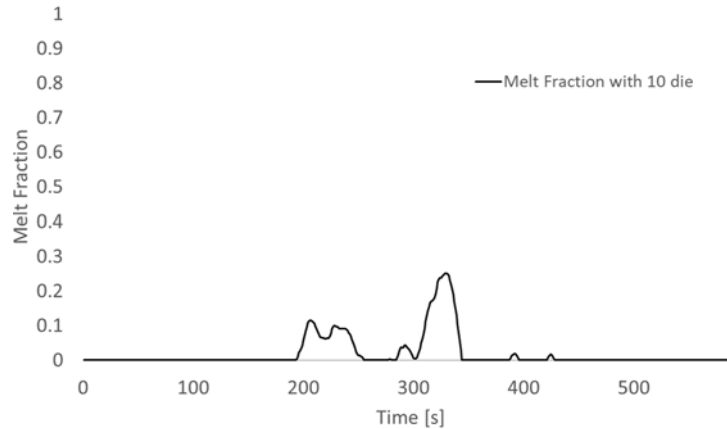


Figure 4-16. Erythritol-copper melt fraction in single-sided package with 10 throughout urban cycle

Figure 4-17 shows the temperatures experienced in the dual-sided package with and without PCM during the same portion of Urban drive cycle. While the PCM is also effective at reducing the transient temperature spikes during this less aggressive drive cycle, there is again little effect on the temperature variation throughout the package due to the addition of a lower- k material into the thermal path. For example, without PCM, the maximum temperature experienced by the SiC die is 122°C at 190s. The largest temperature increase can be seen between 190-200s, where the junction temperature jumps by 17°C and the temperature variation in the package increases to 10°C . In contrast, Figure 4-17 (bottom) shows the same package with erythritol-copper placed in the DBC. The addition of the PCM is effective at increasing the package's thermal management performance, reducing the peak temperature by 3°C . Unlike the single-sided package there is little effect on the temperature variation throughout the package in this cycle. While the placement of the lower- k material does not impede the thermal path, the PCMs distance from the die does not allow it to reach transition temperature due to the lower power levels and corresponding lower temperatures in this drive cycle.

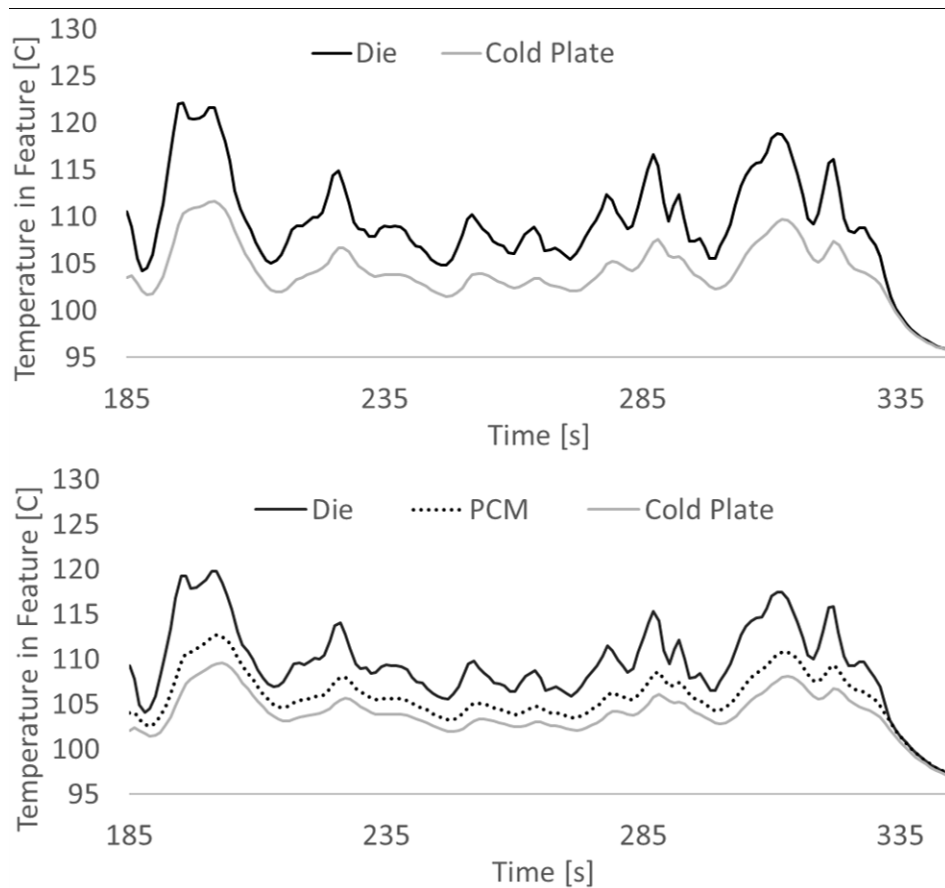


Figure 4-17. Temperature profile of dual-sided PE package with no PCM and 10 SiC (top) and dual-sided PE package with erythritol-copper in DBC and 10 SiC (bottom) during portion of urban drive cycle

4.4. Relative Impact of Drive Cycle with Erythritol-Copper PCM

While the temperature profiles of the die and substrate layers offer a dynamic visualization of the transient operating conditions experienced by the PE during the drive cycles, it can be difficult to quantify the impact of the PCM with the profiles alone. To better understand the impact of the PCM over the entirety of the drive cycles, histograms were created to compare the SiCs overall time at different temperatures in the package configurations of interest. Histograms of the SiC time at temperature highlight the composite PCMs ability to reduce the temperature variability experienced by the die during the two drive cycles. To observe a comprehensive picture of the

impact of PCM, both single-sided and dual-sided packages are compared. The single-sided package contains 24 die with no PCM, and well as 24 and 10 die with the erythritol-copper composite while the dual-side package contains 10 die without PCM and with PCM in the DBC. Figure 4-18a shows that the single-sided package with 24 die and no PCM spends 90% of the time during the drive cycle between 95-145°C, with peaks up to 150°C. The same package with the addition of PCM spends 91% of the same drive cycle between 95-125°C, and 75% between 105-115°C, with junction temperatures never rising above 125°C. Keeping the PCM and reducing the number of die to 10 still keeps the junction temperature within a 30°C window for 91% of the drive cycle, but shifts this window to 115-145°C, with a few peaks up to 150°C. One of the most common causes of failure in SiC devices is the repeated temperature fluctuation leading to temperature-induced degradation [41]. These results suggest that PCM addition to single-sided PE packages may increase the overall durability as well as allow for a reduction in the number of die necessary to control peak junction temperature.

As shown in the previous section, dual-side cooling improves the performance by reducing the thermal resistance from the junction to the cooling fluid. Improved performance allows the dual-sided package to spend the majority of the aggressive US06 drive cycle below the transition temperature of erythritol-copper, 117.7°C (Figure 4-18b). This limited time above transition temperature, along with PCM placement constraints of the dual-sided package, reduce the PCMs effectiveness at reducing temperature variations between package layers and fluctuations in junction temperature. However, PCM is still effective at reducing the maximum junction temperature during the US06 drive cycle. Figure 4-18b shows overall time at temperature of 10 SiC die in a dual-sided package without PCM and with erythritol-copper in the DBC. The dual-sided package without PCM spends 98% of time during the US06 drive cycle between 95-155°C.

The dual-sided package with the addition of PCM spends 98% of time during the same cycle between 95-145°C. As previously mentioned, some SiC devices have been found to exhibit unstable behavior above 150°C [4]. Incorporating PCM into a dual-sided package may provide a buffer to aid in the reduction of peak junction temperature and improve the packages overall thermal performance, but overall, the impact is minimal.

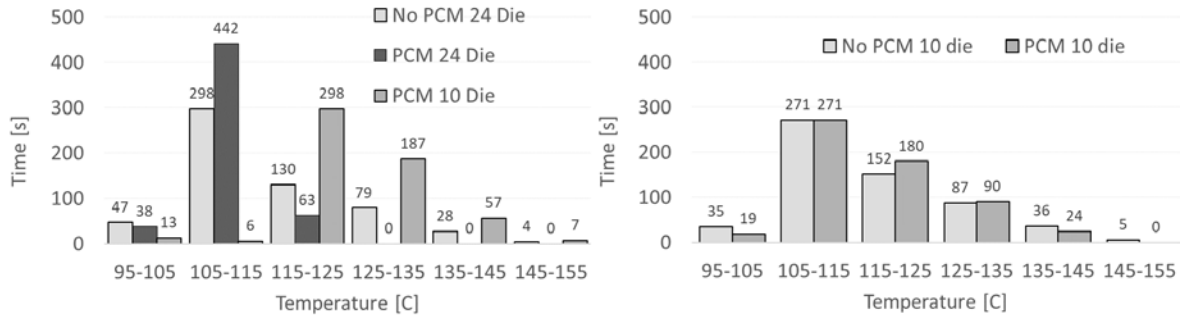


Figure 4-18. Histogram of SiC die time at temperature in single-sided (a) and dual-sided package (b) throughout US06 Drive Cycle

A histogram of the SiC time at temperature during the urban drive cycle is shown in Figure 4-19. Figure 4-19a shows the single-sided package with 24 die and no PCM spends 96% of the time during the less aggressive drive cycle between 95-125°C, with peaks up to 125°C. The same package with the addition of PCM spends 93% of the same drive cycle between 95-115°C, and 75% between 95-105°C, with junction temperatures never rising above 115°C. Keeping the PCM and reducing the number of die to 10 keeps the junction temperature within 30°C for 90% of the drive cycle, keeping the main temperature window from 95-125°C, similar to the package with 24 die and no PCM with the exception of a few transient spikes over 125°C. Again, the addition of PCM created a more even junction temperature distribution over the course of the drive cycle, reducing the transient spikes that can contribute to temperature-induced degradation of the device.

Figure 4-19b shows overall time at temperature of 10 SiC die in a dual-sided package without PCM and with erythritol-copper in the DBC. Improved performance allows the die in the

dual-sided package to spend the majority of the urban drive cycle below the transition temperature of erythritol-copper, 117.7°C. The PCMs distance from the die due to packaging constraints does not allow it to reach transition temperature, reducing the PCMs effectiveness at reducing temperature variations between package layers and fluctuations in junction temperature. However, PCM is again effective at reducing the maximum junction temperature during the Urban drive cycle, reducing the amount of time the die spends above 115°C by 41% by adding an additional thermal mass to the package.

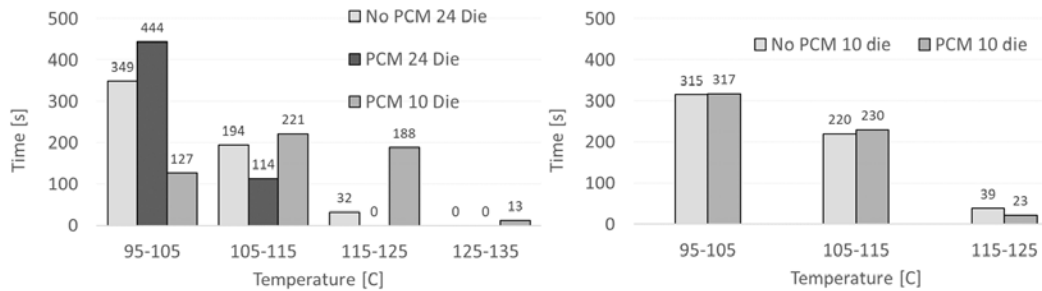


Figure 4-19. Histogram of SiC die time at temperature in single-sided (a) and dual-sided package (b) throughout Urban Drive Cycle

4.5. System Level Considerations

As shown above, using the same number of SiC die in a single-sided package and adding PCM reduces temperature fluctuations throughout the package during operation, potentially extending its operational life through the reduction of thermal fatigue. The addition of PCM could also be used to reduce the number of die in the package. Considering only raw materials, the SiC die are the most expensive portion of the package, and their reduction would serve to reduce the total material cost (Table 4-2) [42, 43, 44]. Due to the rapid transition from silicon-based power devices to SiC, both the cost and supply of SiC devices is extremely volatile, and demand is growing faster than supply [45].

Table 4-2. Cost comparison of PE package materials

Material	Price [\$/kg]
SiC Mosfet	\$32-82 per
Erythritol	\$2-42
Aluminum	\$1.77
Copper	\$6.58
Si ₃ N ₄	\$10-50

Incorporating PCM into PE packaging may help mitigate these challenges. Table 4-3 was created to compare thermal performance, estimated material cost, and size of the packages modeled, using data from the US06 simulations, package geometry, material properties, and material costs from Table 4-2. The addition of PCM to a single-sided package with 24 die reduced the maximum junction temperature by 26°C, while adding less than 20% to the volume and less than \$1 to material costs. Thermal performance of the package was increased significantly, with a negligible increase in material cost and an increase in package volume from 93.4 to 111.2 cm³. The addition of PCM into a single-sided package alternatively allowed for the reduction of die from 24 to 10, lowered the material cost of the package from \$1368 to \$570, reducing the package volume by almost 60%, and only slightly increasing the maximum junction temperature. All prices assumed the maximum cost for erythritol at \$42 per kilogram, and an average cost of \$57 per SiC die. While the addition of PCM to the single-sided package offered significant improvements in the packages overall thermal management performance, incorporating PCM into a dual-sided package showed mixed results. Adding PCM into a dual-sided package with 24 die had negligible results on package thermal performance, due to the low temperature experienced in the package and the addition of a lower-*k* material into the thermal path. When the number of die was reduced to 10, a dual-sided package had similar thermal performance when compared to a single-sided package with PCM, but with a greater volume. Incorporating PCM into a dual-sided package with

10 die reduced the peak junction temperature during the drive cycle but was less effective at reducing temperature variation in package layers due to placement constraints, increase in thermal resistance, and lower overall temperatures. The material cost of the dual-sided package is also comparable to the single-sided with the same number of die due the small size of the packages and the fact that the SiC devices are the cost driving factor with respect to materials.

Table 4-3. Comparison of Single and Dual-Sided package performance, material cost, and size

Pkg Type	# of Die	PCM	Max Junction Temp [°C]	Average Junction Temp [°C]	Standard Deviation [°C]	Material Cost [\$]	Volume [cm³]
Single	24	None	150.6	114.6	12.36	1368.20	93.4
Single	24	Erythritol Copper	124.4	106.3	13.54	1368.60	111.2
Single	10	None	228.3	142.8	26.54	570.20	38.9
Single	10	Erythritol Copper	152.1	122.6	15.43	570.50	46.3
Dual	24	None	106.3	98.16	6.399	1368.50	216.4
Dual	24	Erythritol Copper	116.8	103.2	8.371	1368.90	216.4
Dual	10	None	150.3	116.2	12.84	570.5	90.1
Dual	10	Erythritol Copper	144.7	116.1	12.36	570.8	90.1

The dual-sided package may be superior in terms of thermal performance, but it has yet to be universally adopted due to a lack of understanding of its thermo-mechanical lifetime and due to the high cost of manufacturing [21, 11]. Incorporating PCM into a single-sided package may be a viable alternative to improving PE reliability and thermal performance without incurring the high cost of manufacturing dual-sided packages. To better compare the performance of these two packaging approaches, Figure 4-20 shows the temperature profile of a single-sided package with PCM (top) and a dual-sided package without PCM (bottom), both with 10 die during the same

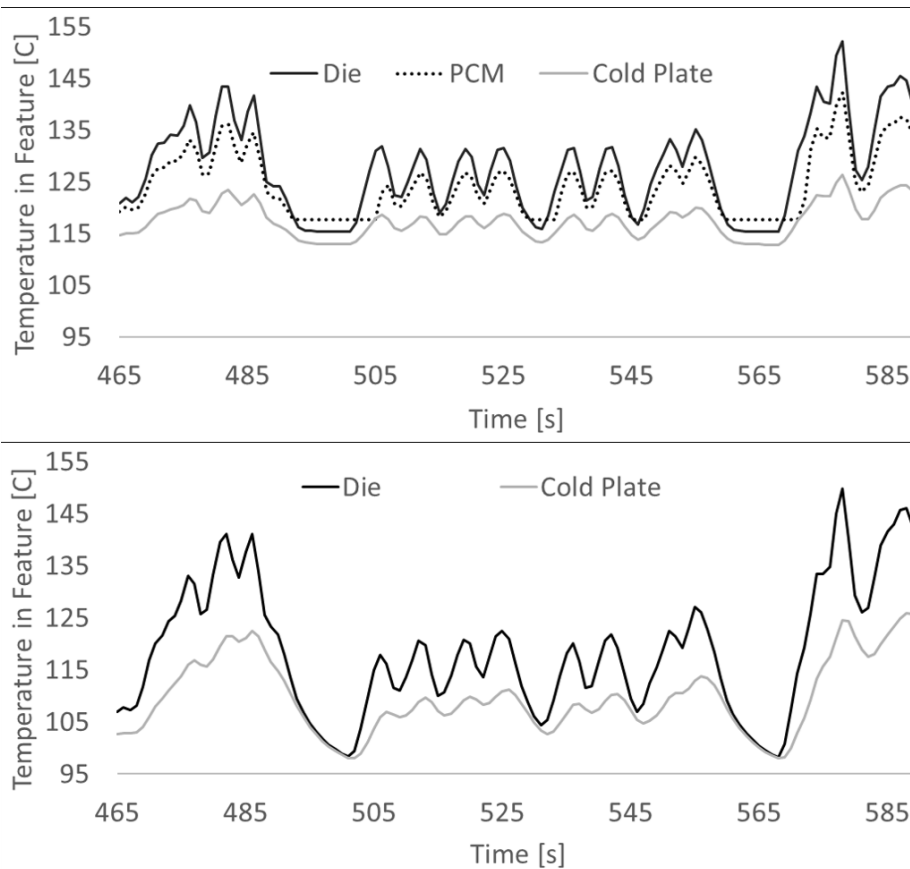


Figure 4-20. Temperature profile of single-sided PE package with erythritol-copper and 10 SiC (top) and dual-sided PE package with 10 SiC no PCM (bottom) during portion of US06 cycle portion of the US06 drive cycle. While the die temperature peaks are nearly identical at 575s, there is a noticeable buffering of the transient die temperatures in the single-sided package, especially between 500-560s. This suggests that the PCM is more effective at smoothing the transient

junction temperatures in the single-sided package. The latent heat storage of the PCM also smooths the low temperature valleys as shown at 490-505s and 560-570s, suggesting an overall reduction in temperature variation throughout the cycle and decreased temperature variation in the layers of the package. These reductions in the temperature fluctuation could create more temperature consistency between package layers and improve both the reliability and durability of the device.

To further emphasize the latent heat storage benefits of PCM, the thermal performance of a single-sided package (10 die) with erythritol-copper was compared to the same package with an equal volume of copper placed on top, acting solely as a thermal mass. While the volume of the materials was equal, the mass of copper modeled was 35% larger than that of the PCM. A steady-state heat load of 160.2W was applied to the die, simulating temperatures experienced by the die at a constant maximum power of 80.1kW (peak power of the US06 cycle). Figure 4-21 shows the time to steady-state temperature profiles for both packages. The SiC die reached a steady-state temperature of 239°C around 120s in the package with the copper thermal mass (Figure 4-21 top). Figure 4-21 (bottom) shows the same package with PCM. The die temperature remained around 150°C until the PCM was fully melted ($t=30s$). Once the PCM had fully transitioned and the thermal storage was exhausted, the die temperature rose to a steady-state of 245°C at around 210s. While the steady-state temperature was slightly higher ($\sim 7^\circ C$), due to the lower thermal conductivity of the PCM, the latent heat storage of the PCM delayed the steady state temperature by 90s.

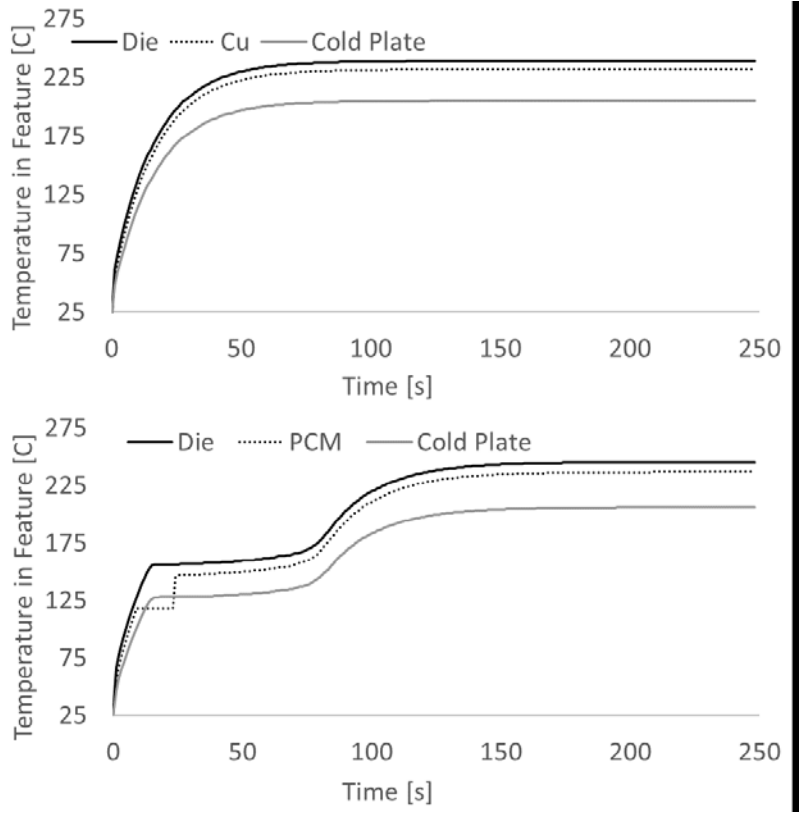


Figure 4-21. Temperature profile to steady-state of single-sided PE package with copper thermal mass and 10 SiC (top) and single-sided PE package with PCM and 10 SiC PCM (bottom) during extended maximum power of US06 cycle

CHAPTER 5 CONCLUSIONS AND RECOMMENDATIONS OF FURTHER WORK

The current study evaluated the effectiveness of PCM in improving a PE packages thermal performance. Chapter 3 described the modeling approach used in this investigation. Two different PE packages, representative of both single and dual-sided packages found commercially, were modeled in ParaPower. Dynamic power/heat load models were created to simulate the transient operating conditions of both highway and urban use. These heat loads were divided by the number of die in the package allowing for various package sizes to be simulated. Four different PCMs were modeled on top of the single-sided package and in three different locations within the dual-sided package. Chapter 4 presented the key results of the simulations performed. A summary of the key results is shown below:

- The addition of PCM to a single-sided package was shown to reduce the peak junction temperature experienced by the SiC die, as well as reduce the overall temperature fluctuations throughout the package during both the US06 and Urban drive cycles.
- The addition of PCM to a single-sided package with 24 die reduced the maximum junction temperature by 26°C, adding less than 20% to the package volume with a negligible addition the package material cost.
- The addition of PCM into a single-sided package alternatively allowed for the reduction in the number of die necessary to maintain a peak junction temperature at approximately 150°C from 24 to 10. This reduction in the number of SiC die resulted in a 58% reduction in the material cost of the package and a similar reduction in volume.

- A dual-sided package without PCM was also able to maintain a peak temperature below 150°C, but experienced greater temperature fluctuations in the package throughout both cycles when compared to the single-sided package with PCM.
- PCM placement in the dual-sided package was modeled in three different locations: the periphery, in the emitter/collector, and in the DBC. Results were mixed, depending on the properties of the PCM. The lowest performing PCM, erythritol, showed minimal effect on die temperature when placed in the periphery of the package. Placement in the emitter/collector had a negative effect, increasing the temperatures experienced by the die by adding thermal resistance to the layers and limiting heat spreading. Placement in the DBC lowered temperatures slightly (2°C) suggesting that placing PCM directly in the thermal path, but far enough from the die so as not to limit heat spreading, was the optimum location.
- The addition of the erythritol-copper PCM into the DBC layer of the dual-sided package served to suppress the peak junction temperature by 6°C but was not as successful in reducing the fluctuations when compared to the single-sided package. While the latent heat storage of the PCM successfully absorbs heat in the package, the additional thermal resistance added by the PCM to the substrate layer, along with lower overall temperatures in the cycle, reduced the PCMs effectiveness.
- PCM is most effective in the single-sided package, as it adds thermal mass to the top of the package, without adding additional thermal resistance to substrate layers between the die and working fluid.

5.1. Recommendations for Future Work

The current study has shown that incorporating PCM into PE packaging has the potential to increase the thermal performance of the package. Recommendations are future works are as follows:

- Experimental validation of the results of this study is a key step moving forward.
- Further work is needed to study and development different PCMs/PCM composites that should be explored as possible candidates for use in PE thermal management. The low thermal conductivity of most pure PCMs is a key hindrance to their use in thermal storage applications. The development and testing of high- k PCM composites will be necessary for this technology to move forward.
- A modeling of the thermo-mechanical stresses experienced by the packages during transient operation, and how these stresses affect package fatigue life, should also be developed in order to quantify the impact of reducing peak temperatures and temperature fluctuations within PE packages. These models could help quantify PCMs ability to improve PE package reliability.
- Future work should also quantify the potential system level impact these results have on the overall size, weight, and performance of a vehicles thermal management system. Trade-off analyses should be conducted comparing costs of incorporating PCM for die reduction purposes and incorporation of PCM to lower maximum temperatures, reducing the necessary size/weight of the thermal management system.

REFERENCES

- [1] K. Hamada, "Toyota's Activities on Power Electronics for Future Mobility," in *2011 14th European Conference on Power Electronics and Applications*, Birmingham, 2011.
- [2] L. M. Tolbet, B. Ozpineci, S. K. Islam and F. Z. Peng, "Impact of SiC Power Electronic Devices for Hybrid Electric Vehicles," SAE International, 2002.
- [3] K. Shenai, R. Scott and B. Baliga, "Optimum semiconductors for high-power electronics," *IEEE Transactions on Electron Devices*, vol. 36, no. 9, pp. 1811-1823, 1989.
- [4] W. Zhou, X. Zhong and K. Sheng, "High Temperature Stability and the Performance Degradation of SiC MOSFETS," *IEEE Transactions on Power Electronics*, vol. 29, no. 5, pp. 2329-2337, 2014.
- [5] J. Broughton, V. T. R. Smet and Y. Joshi, "Review of Thermal Packaging Technologies for Automotive Power Electronics for Traction Purposes," *Journal of Electronic Packaging*, vol. 140, no. 4, pp. 1-11, 2018.
- [6] D. J. Sharar, B. F. Donovan, R. J. Warzoha, A. A. Wilson, A. C. Leff and B. M. Hanrahan, "Solid-state thermal energy storage using reversible martensitic transformations," *Applied Physics Letters*, vol. 114, no. 143902, pp. 1-5, 2019.
- [7] B. M. Nafis, A.-C. Iradukunda and D. Huitink, "System-Level Thermal Management and Reliability of Automotive Electronics: Goals and Opportunities Using Phase-Change Materials," *Journal of Electronic Packaging*, vol. 142, pp. 1-6, 2020.
- [8] R. Kandasamy, X.-Q. Wang and A. S. Mujumdar, "Transient cooling of electronics using phase change material (PCM)-based heat sinks," *Applied Thermal Engineering*, vol. 28, pp.

1047-1057, 2008.

- [9] N. R. Jankowski and F. P. McCluskey, "A review of phase change materials for vehicle component thermal buffering," *Applied Energy*, vol. 113, pp. 1525-1561, 2014.
- [10] S. Pietranico, S. Pommier, S. Lefebvre and S. Pattofatto, "Thermal fatigue and failure of electronic power device substrates," *International Journal of Fatigue*, vol. 31, pp. 1911-1920, 2009.
- [11] Z. Zeng, K. Ou, L. Wang and Y. Yu, "Reliability-Oriented Automated Design of Double-Sided Cooling Power Module: A Thermo-Mechanical-Coordinated and Multi-Objective-Oriented Optimization Methodology," *IEEE Transactions on Device and Materials Reliability*, vol. 20, no. 3, 2020.
- [12] C. Chan and Y. Wong, "Electric vehicles charge forward," *IEEE Power and Energy Magazine*, vol. 2, no. 6, pp. 24-33, 2004.
- [13] J. Zhu, H. Kim, H. Chen, R. Erickson and D. Maksimovic, "High efficiency SiC traction inverter for electric vehicle applications," in *2018 IEEE Applied Power Electronics Conference and Exposition (APEC)*, San Antonio, 2018.
- [14] S. Seal and H. A. Mantooth, "High Performance Silicon Carbide Power Packaging- Past Trends, Present Practices, and Future Directions," *Energies*, vol. 10, no. 3, 2017.
- [15] A. Schletz, E. Schimanek and M. Marz, "Advanced Module Concepts," in *Advanced Technical Workshop Thermal Management*, San Jose, 2009.
- [16] L. Boteler, V. Niemann, D. Urciuoli and S. Miner, "Stacked power module with integrated thermal management," in *2017 IEEE International Workshop On Integrated Power Packaging (IWIPP)*, Delft, 2017.

- [17] C. Gillot, C. Schaeffer, C. Massit and M. Luc, "Double-Sided Cooling for High Power IGBT Modules Using Flip Chip Technology," *IEEE Transactions on Components and Packaging Technologies*, vol. 24, no. 4, pp. 698-704, 2001.
- [18] B. Ozmat, C. Korman and R. Fillion, "An advanced approach to power module packaging," in *International Workshop on Integrated Power Packaging*, Waltham, 2000.
- [19] J. Yin, J. van Wyk, W. Odendaal and Z. Liang, "Design and optimization of embedded power chip modules for double-sided cooling," in *Conference Record of the 2004 IEEE Industry Applications Conference, 2004. 39th IAS Annual Meeting*, Seattle, 2004.
- [20] K. J. Kelly, T. Abraham, K. Bennion, D. Bharathan, S. Narumanchi and M. O'Keefe, "Assessment of Thermal Control Technologies for Cooling Electric Vehicle Power Electronics," in *23rd International Electric Vehicle Symposium*, Anaheim, 2007.
- [21] Z. Libing, L. Zhuming, W. Chunlei and H. Li, "Design, Packaging and Test of A Planar Double-Sided Cooling IGBT Power Module," in *18th International Conference on Electronic Packaging Technology*, Harbin, 2017.
- [22] M. Chinthavali, T. LM, H. Zhang, H. JH, F. Barlow and B. Ozpineci, "High Power SiC Modules for HEVs and PHEVs," in *The 2010 International Power Electronics Conference- ECCE ASIA*, Sapporo, 2010.
- [23] T. A. Burrell, C. L. Coomer, S. L. Campbell, A. A. Wereszczak, J. P. Cunningham, L. D. Marlino, L. E. Seiber and H. T. Lin, "Evaluation of the 2010 Toyota Prius Hybrid Synergy Drive System," Oak Ridge National Laboratory, Oak Ridge, 2011.
- [24] T. A. Burrell, C. L. Coomer, S. L. Campbell, A. A. Wereszczak, J. P. Cunningham, L. D. Marlino, L. E. Seiber and H. T. Lin, "Evaluation of the 2008 Lexus LS 600H Hybrid

- Synergy Drive System," Oak Ridge National Laboratory, Oak Ridge, 2009.
- [25] Y. Sato, S. Ishikawa, T. Okubo, M. Abe and K. Tamai, "Development of High Response Motor and Inverter System for the Nissan LEAF Electric Vehicle," in *SAE 2011 World Congress & Exhibition*, 2011.
- [26] G. Moreno, K. Bennion, C. King and S. Narumanchi, "Evaluation of Performance and Opportunitites for Improvements in Automotive Power Electronics Systems," in *15th IEEE Intersociety Conference on Thermal and Thermomechanical Phenomena in Electronic Systems (ITherm)*, Las Vegas, 2016.
- [27] M. Anwar, S. M. N. Hasan, M. Teimor, M. Korich and M. B. Hayes, "Development of a Power Dense and Environmentally Robust Traction Power Inverter for the Second-Generation Chevrolet VOLT Extended-Range EV," in *IEEE Energy Conversion Congress and Exposition (ECCE)*, Montreal, 2015.
- [28] Z. X. Gong and A. S. Mujumdar, "A new solar receiver thermal store for space-based activities using multiple composite phase change materials," *ASME Journal of Solar Energy Engineering*, vol. 117, pp. 215-220, 1995.
- [29] Z. X. Gong and A. S. Mujumdar, "Cyclic heat transfer in a novel storage unit of multiple phase change materials," *Applied Thermal Engineering*, vol. 16, no. 10, pp. 807-815, 1996.
- [30] Z. X. Gong and A. S. Mujumdar, "Thermodynamic optimization of the thermal process in energy storage using multiple phase change materials," *Applied Thermal Engineering*, vol. 17, no. 11, pp. 1067-1083, 1997.
- [31] T. Oya, T. Nomura, N. Okinaka and T. Akiyama, "Phase change composite based on porous nickel and erythritol," *Applied Thermal Engineering*, vol. 40, pp. 373-377, 2012.

- [32] P. J. Shamberger and T. S. Fisher, "Cooling power and characteristic times of composite heatsinks and insulants," *International Journal of Heat and Mass Transfer*, vol. 117, pp. 1205-1215, 2018.
- [33] L. Boteler and S. Miner, "Power packaging thermal and stress model for quick parametric analyses," in *Proceedings of the ASME 2017 International Technical Conference and Exhibition on Packaging and Integration of Electronic and Photonic Microsystems*, San Francisco, 2017.
- [34] L. Boteler and S. Miner, "Comparison of Thermal and Stress Analysis Results for a High Voltage Module Using FEA and a Quick Parametric Analysis Tool," in *Proceedings of the ASME 2018 International Technical Conference and Exhibition on Packaging and Integration of Electronic and Photonic Microsystems*, San Francisco, 2018.
- [35] M. Deckard, P. Shamberger, M. Fish, M. Berman, J. Wang and L. Boteler, "Convergence and Validation in ParaPower: A Design Tool for Phase Change Materials in Electronics Packaging," in *2019 18th IEEE Intersociety Conference on Thermal and Thermomechanical Phenomena in Electronic Systems (ITherm)*, Las Vegas, 2019.
- [36] Environmental Protection Agency, "Vehicle and Fuel Emissions Testing," Environmental Protection Agency, 31 January 2017. [Online]. Available: <https://www.epa.gov/vehicle-and-fuel-emissions-testing/dynamometer-drive-schedules>. [Accessed 18 January 2020].
- [37] M. Ehsani, Y. Gao, S. E. Gay and A. Emadi, *Modern Electric, Hybrid Electric, and Fuel Cell Vehicles: Fundamentals, Theory, and Design*, Boca Raton: CRC Press, 2005.
- [38] Car and Driver, "Drag Queens: Aerodynamics Compared," Hearst Digital Media, 6 June 2014. [Online]. Available: <https://www.caranddriver.com/features/a15108689/drag-queens->

- aerodynamics-compared-comparison-test/. [Accessed 21 May 2020].
- [39] A. K. Agarwal, "An overview of SiC power devices," in *2010 International Conference on Power, Control and Embedded Systems*, Allahabad, 2010.
- [40] T. J. Lu, "Thermal management of high power electronics with phase change cooling," *International Journal of Heat and Mass Transfer*, vol. 43, pp. 2245-2256, 2000.
- [41] Z. Sarkany, W. He and M. Rencz, "Temperature change induced degradation of SiC MOSFET devices," in *2016 15th IEEE Intersociety Conference on Thermal and Thermomechanical Phenomena in Electronic Systems (ITherm)*, Las Vegas, 2016.
- [42] Mouser Electronics, "Mouser Electronics," Mouser Electronics, 2021. [Online]. Available: https://www.mouser.com/Wolfspeed-Cree/Semiconductors/Discrete-Semiconductors/Transistors/MOSFET/_/N-ax1sf?P=1yhq405&Keyword=SiC&FS=True. [Accessed 26 January 2021].
- [43] Alibaba, "Price of Silicon Nitride Powder," Alibaba, 2021. [Online]. Available: <https://www.alibaba.com/showroom/price-of-silicon-nitride-powder.html>. [Accessed 26 January 2021].
- [44] showtheplanet inc, "Daily Metal Prices," showtheplanet inc, 18 December 2020. [Online]. Available: <https://www.dailymetalprice.com/metalpricecharts.php?c=cu&u=kg&d=2400>. [Accessed 18 December 2020].
- [45] M. Lapedus, "SiC Demand Growing Faster Than Supply," *Semiconductor Engineering*, 23 May 2019. [Online]. Available: <https://semiengineering.com/sic-demand-growing-faster-than-supply/>. [Accessed 31 May 2021].
- [46] C. Buttay, J. Rashid, C. Johnson, P. Ireland, F. Udrea, G. Amaratunga and R. Malhan,

- "High Performance Cooling System for Automotive Inverters," in *2007 European Conference on Power Electronics and Applications*, Aalborg, 2007.
- [47] M. Marz, A. Schletz, B. Eckardt, S. Egelkraut and H. Rauh, "Power Electronics System Integration for Electric and Hybrid Vehicles," in *2010 6th International Conference on Integrated Power Electronics Systems*, Nuremberg, 2010.
- [48] H. Zhang, S. S. Ang, H. A. Mantooth and K. S, "A High Temperature, Double-sided Cooling SiC Power Electronics Module," in *2013 IEEE Energy Conversion Congress and Exposition*, Denver, 2013.
- [49] C. Chan and K. Chau, "An overview of power electronics in electric vehicles," *IEEE Transactions on Industrial Electronics*, vol. 44, no. 1, pp. 3-13, 1997.
- [50] N. Nozawa, T. Maekawa, S. Nozawa and K. Asakura, "Development of Power Control Unit for Compact-Class Vehicle," *SAE International Journal of Passenger Cars - Electronic and Electrical Systems*, vol. 2, no. 1, pp. 276-382, 2009.

APPENDIX A RESULTS

A.1. Single-Sided Package US06 Results: Sections 4.1.1 and 4.2

This chapter contains the full cycle US06 results for all single-sided configurations models. Full cycle melt fraction results for each PCM modeled are also provided for all applicable configurations.

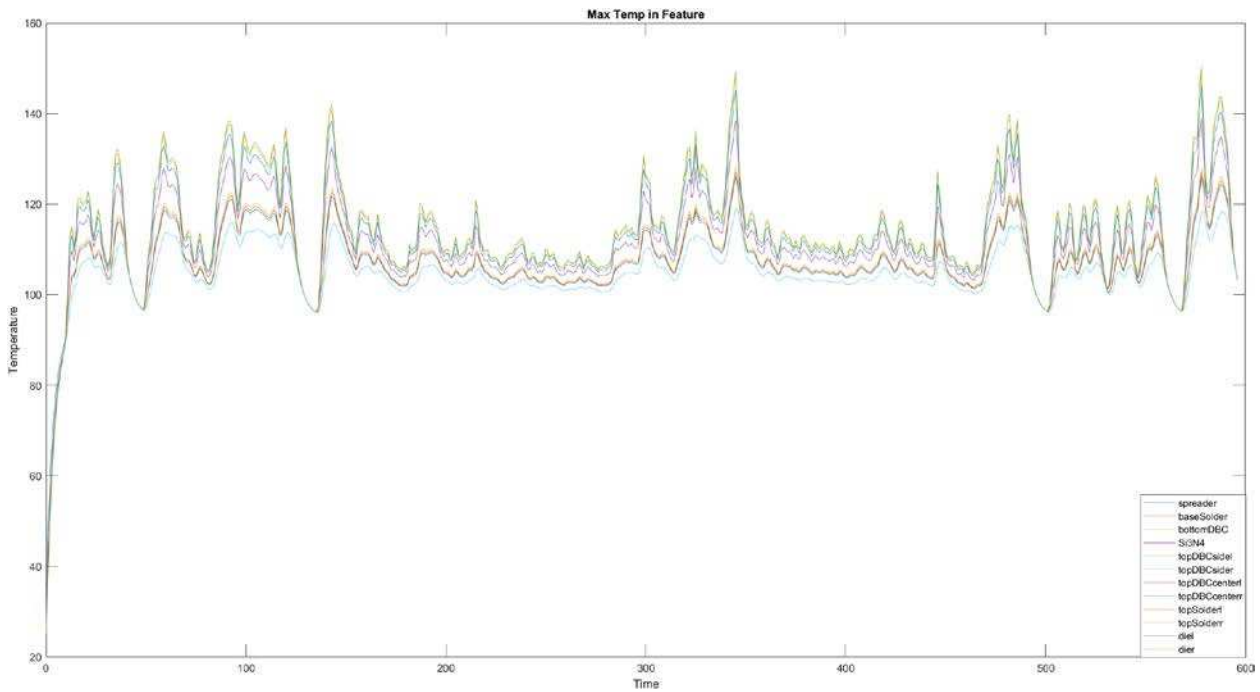


Figure A-1. Temperature profile in single-sided package with 24 die and no PCM over full US06 cycle

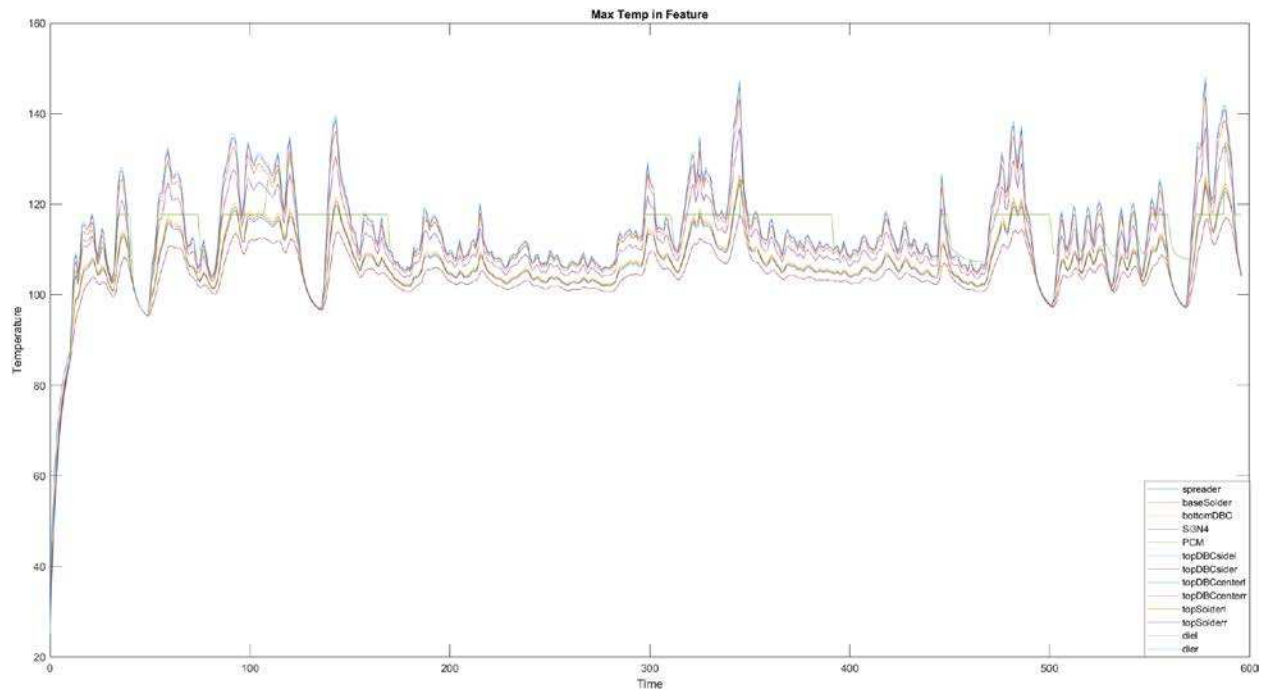


Figure A-2. Temperature profile in single-sided package with 24 die and erythritol

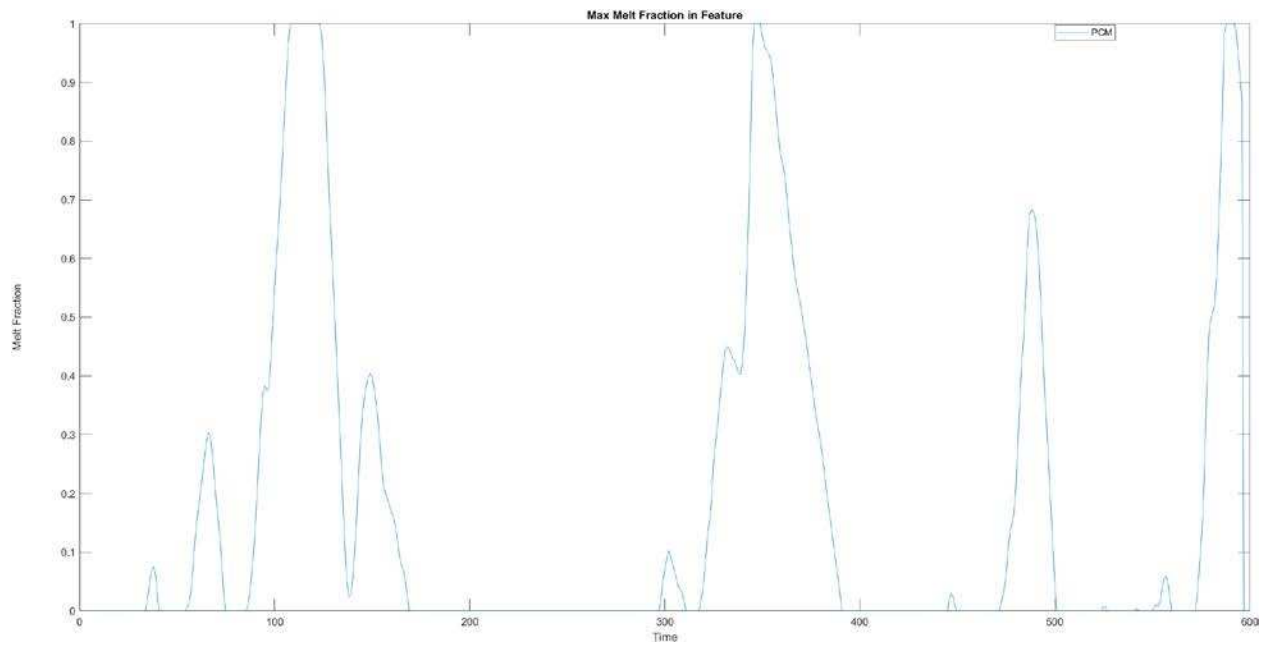


Figure A-3. Erythritol melt fraction in single-sided package with 24 die over full US06 cycle

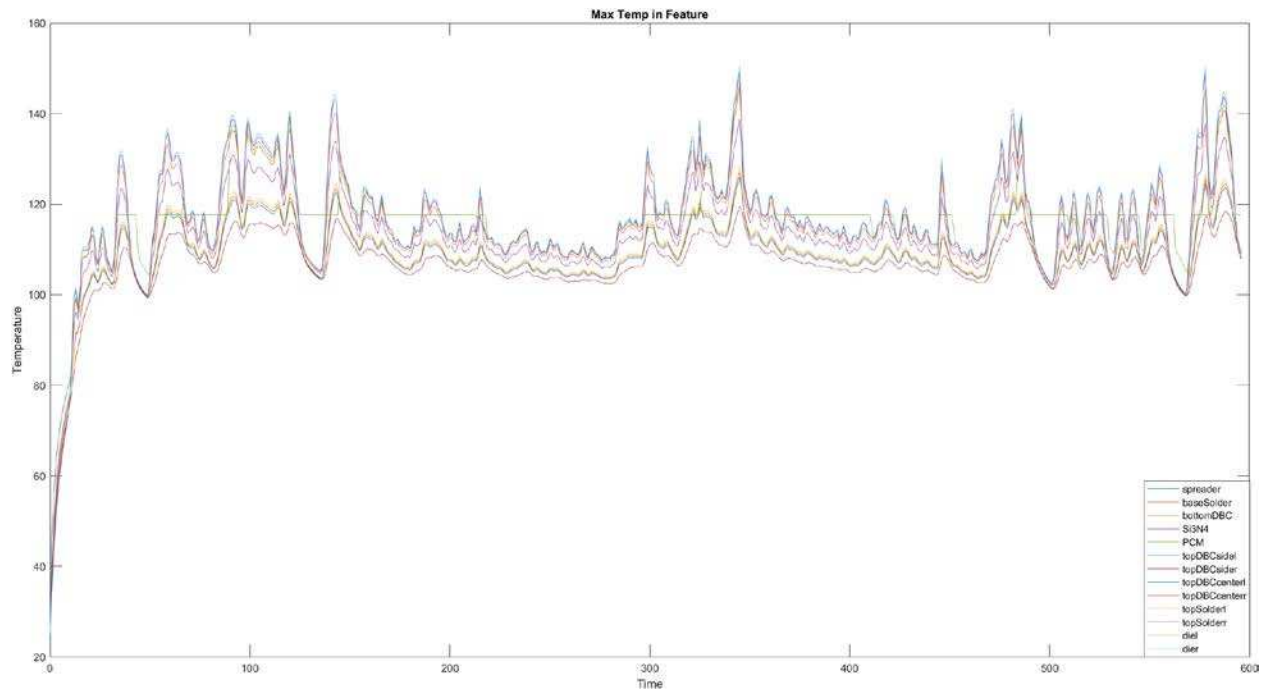


Figure A-4. Temperature profile in single-sided package with 20 die and erythritol-nickel

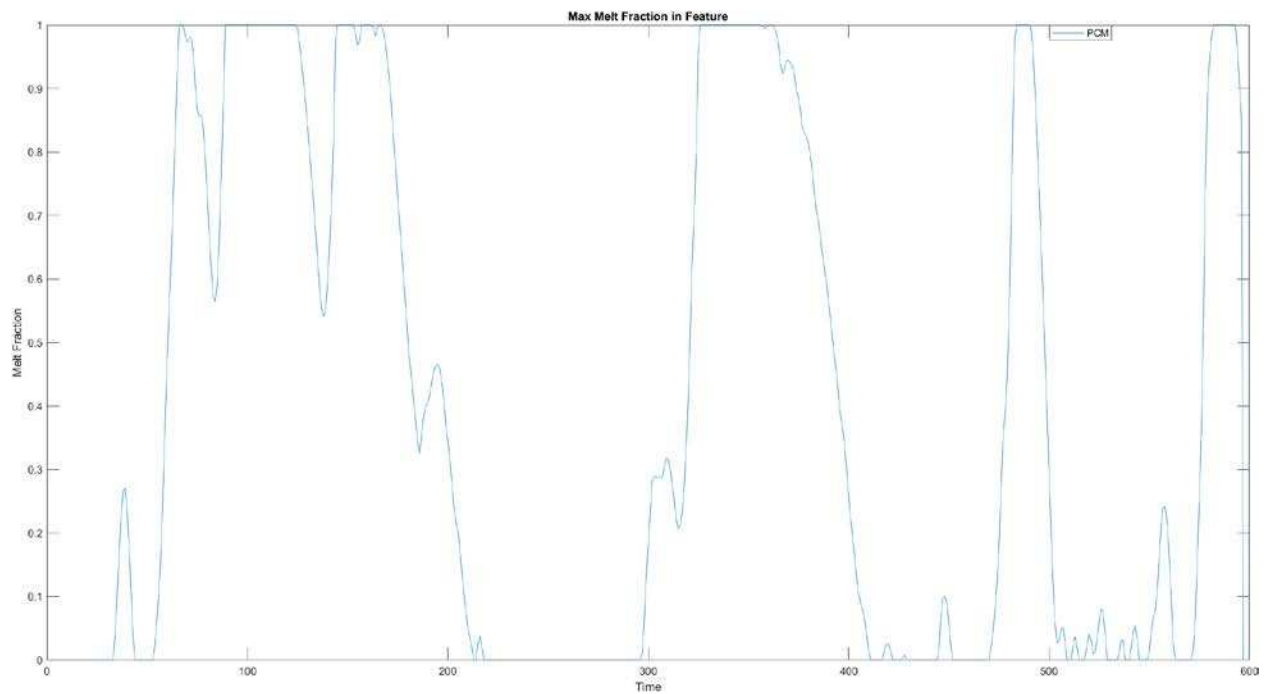


Figure A-5. Erythritol-nickel melt fraction in single-sided package with 20 die over full US06 cycle

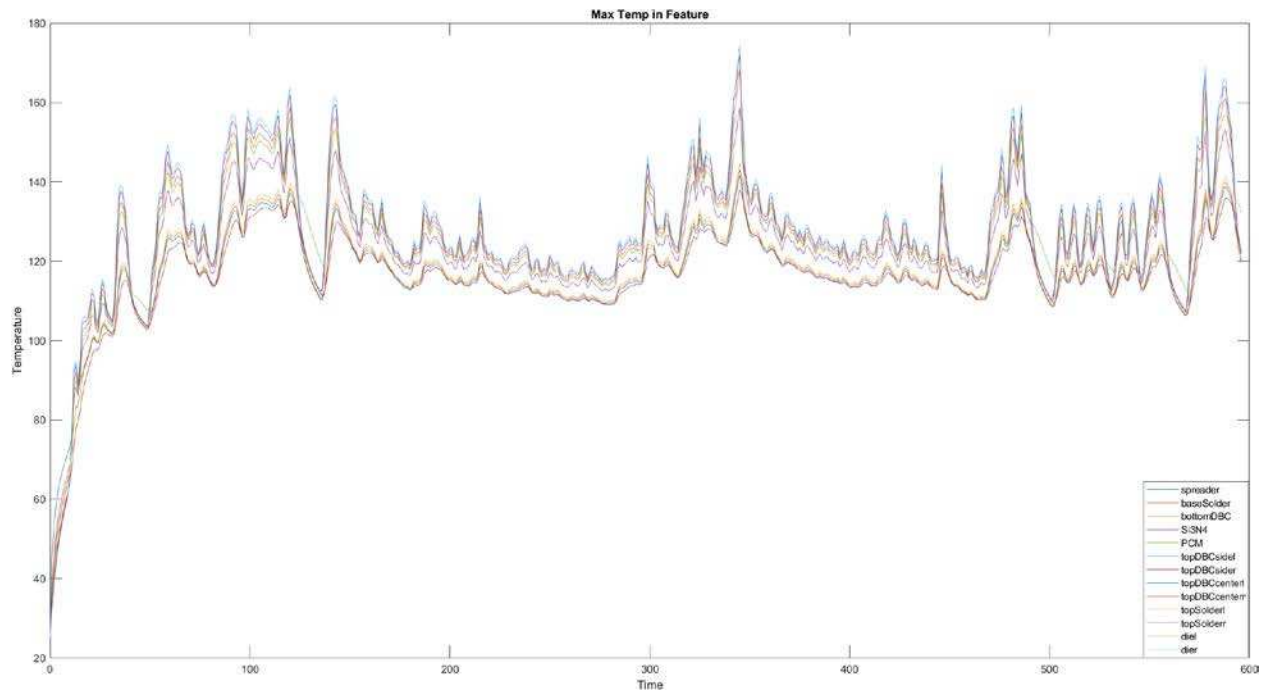


Figure A-6. Temperature profile in single-sided package with 12 die and indium

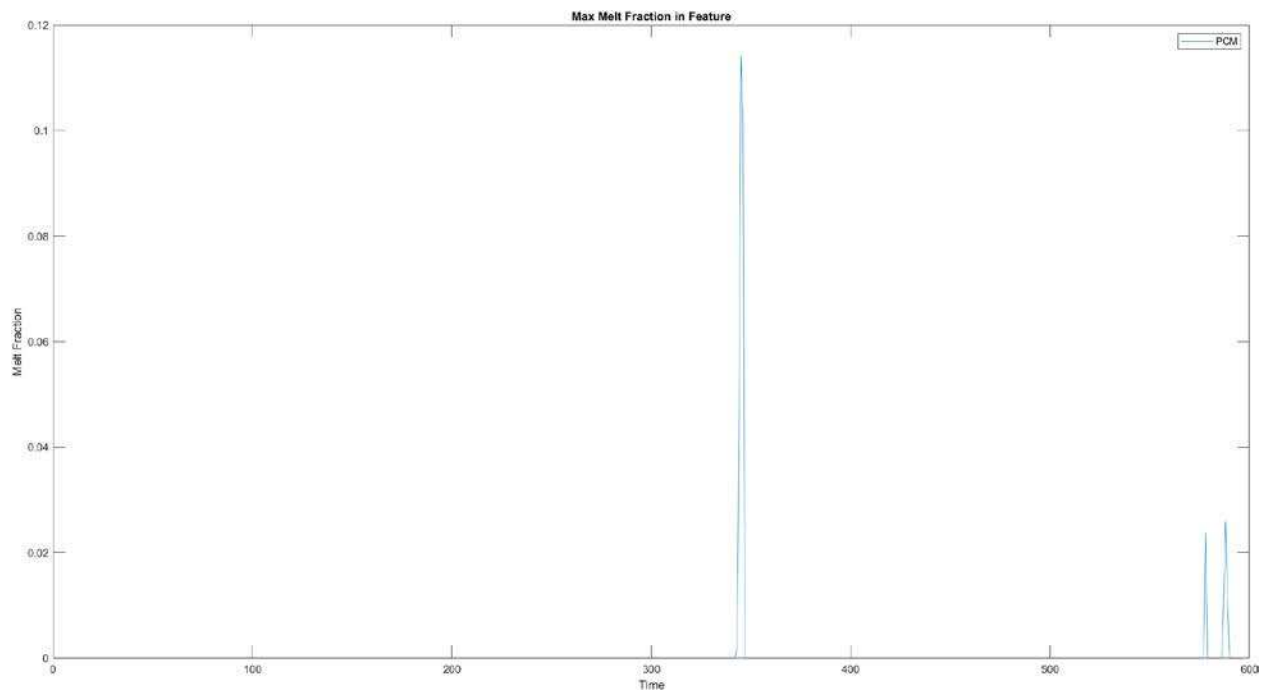


Figure A-7. Indium melt fraction in single-sided package with 12 die over full US06 cycle

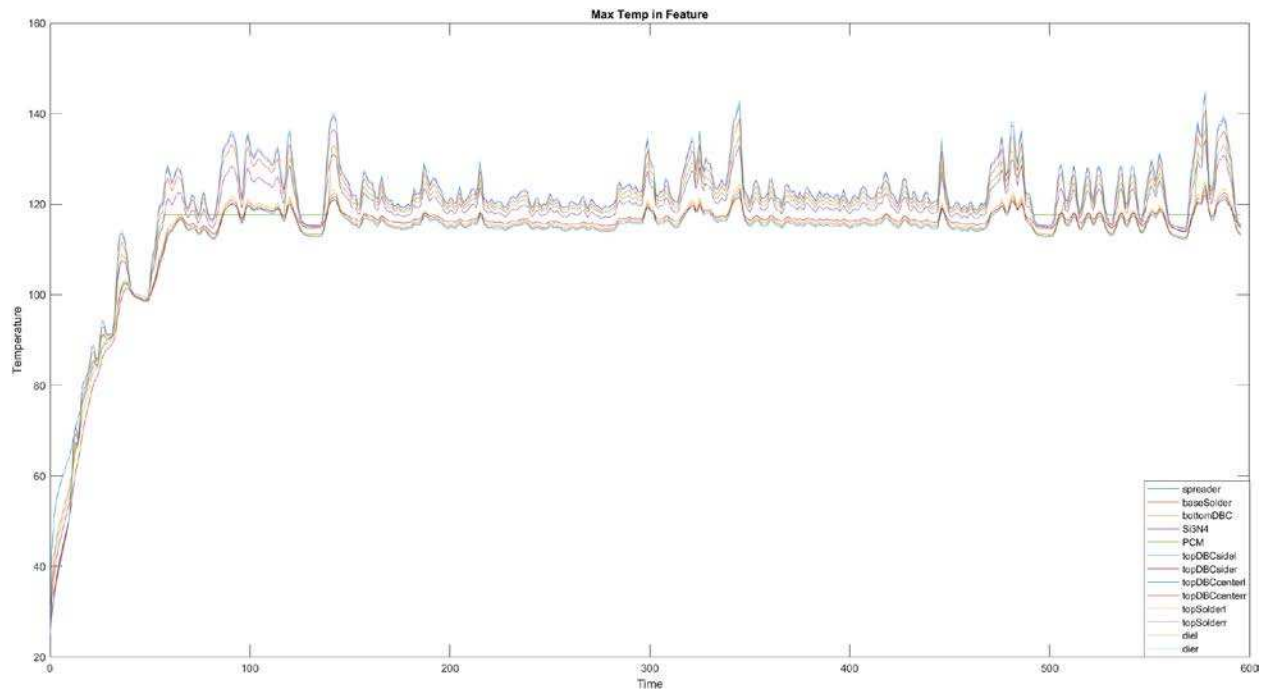


Figure A-8. Temperature profile in single-sided package with 12 die and erythritol-copper

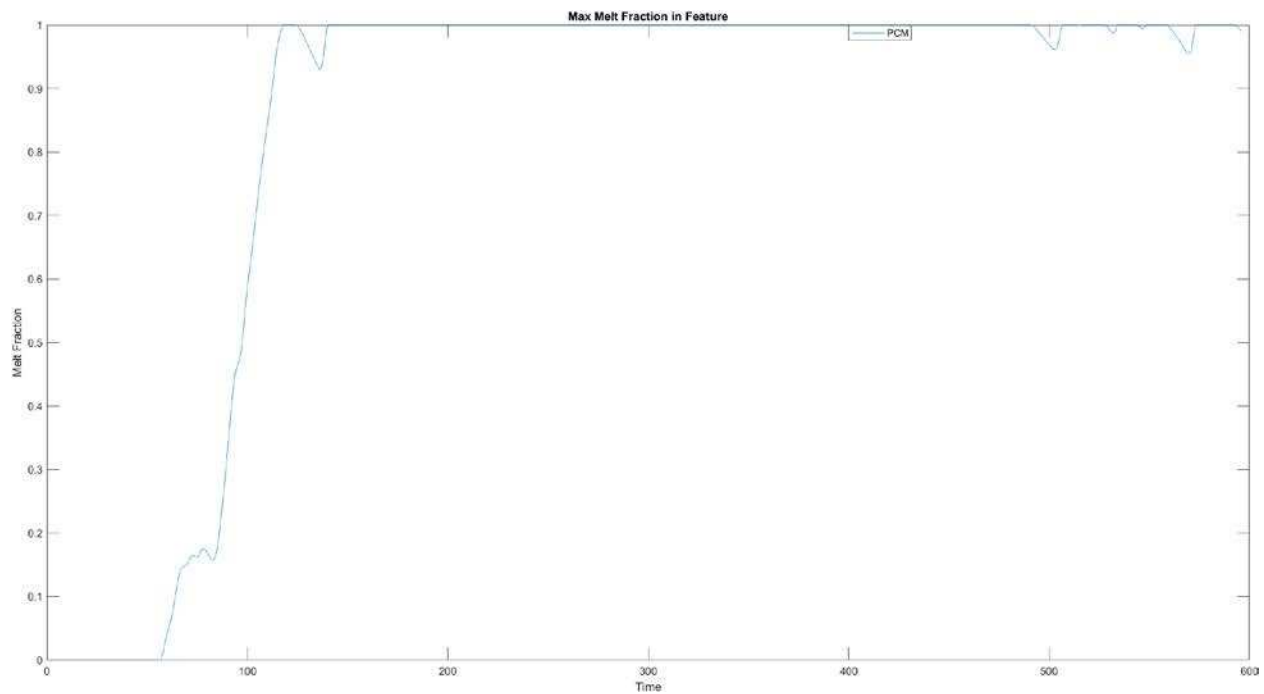


Figure A-9. Erythritol-copper melt fraction in single-sided package with 12 die over full US06 cycle

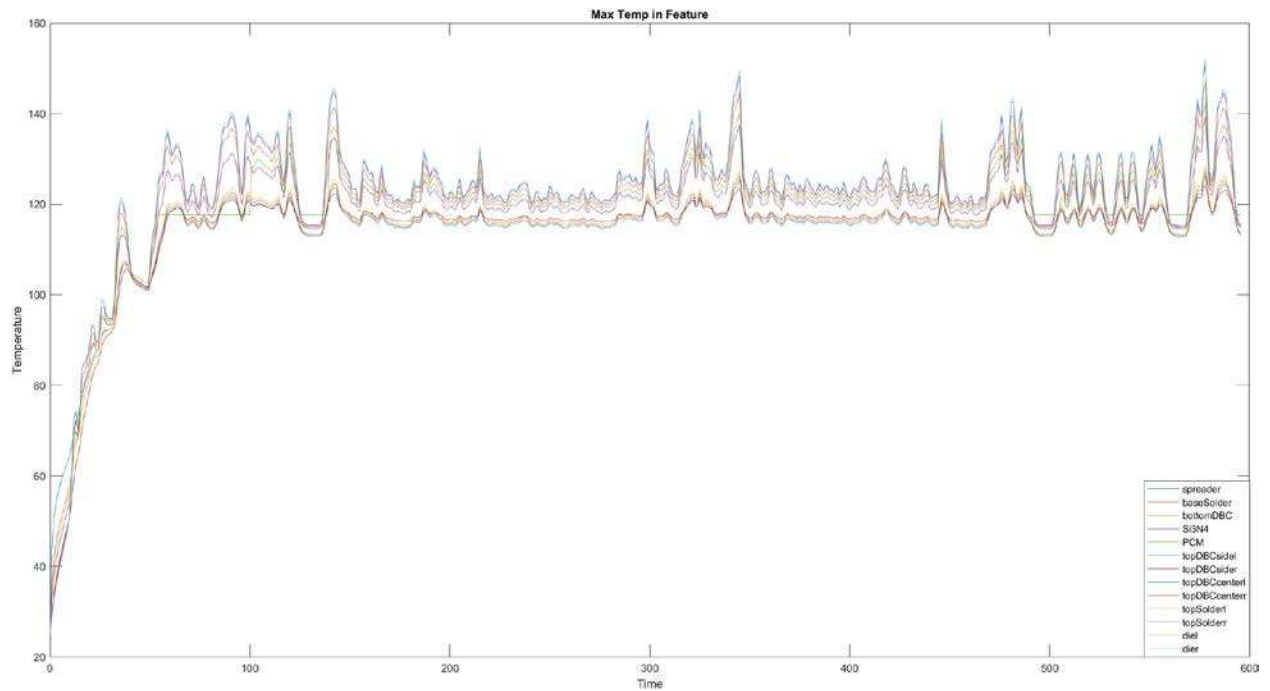


Figure A-10. Temperature profile in single-sided package with 10 die and erythritol-copper

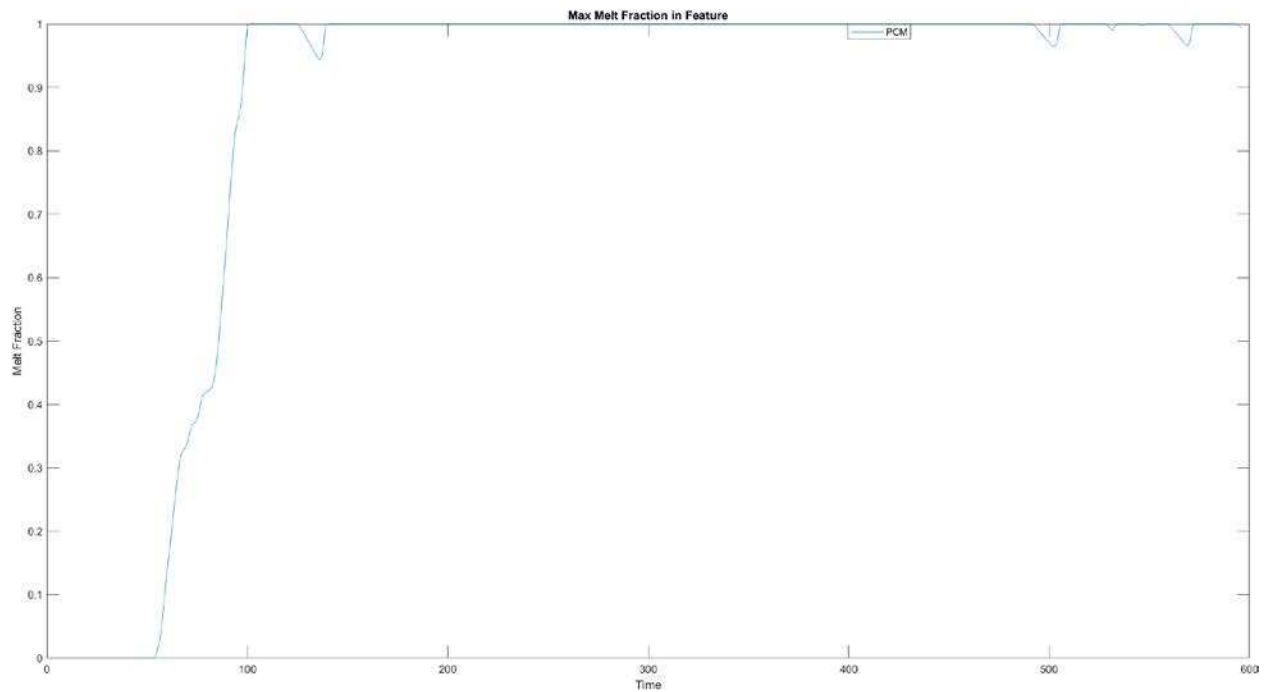


Figure A-11. Erythritol-copper melt fraction in single-sided package with 10 die over full US06 cycle

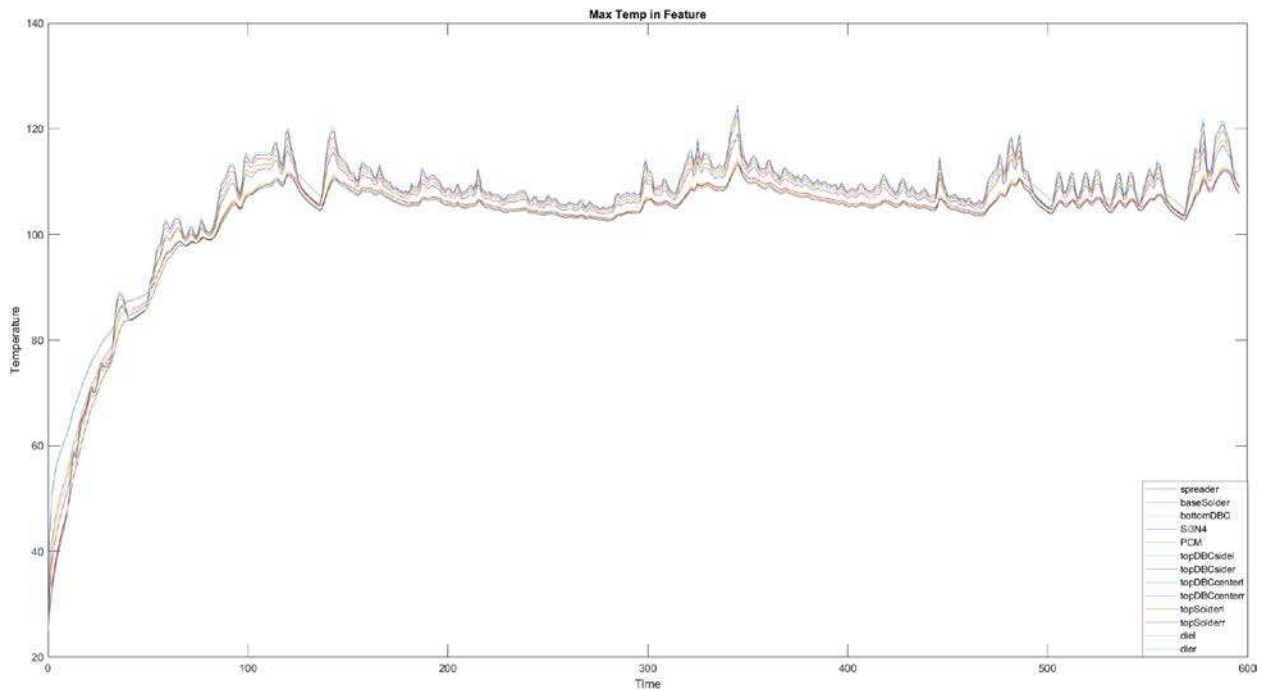


Figure A-12. Temperature profile in single-sided package with 24 die and erythritol-copper

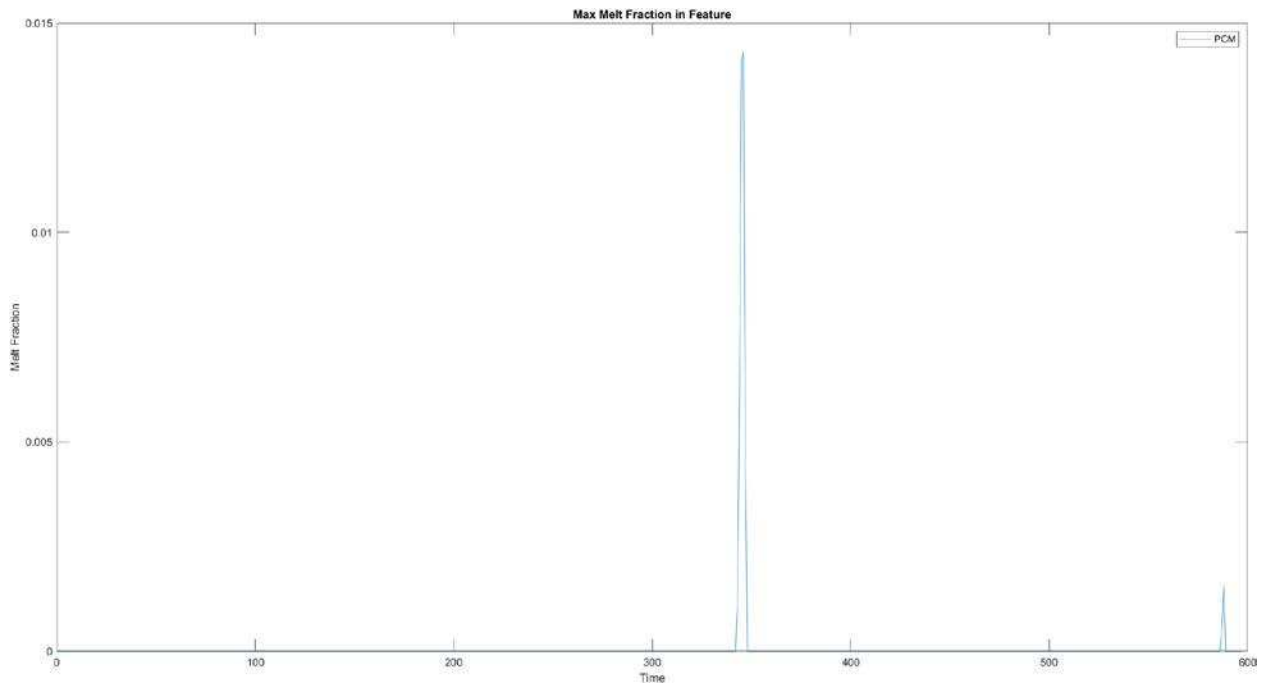


Figure A-13. Erythritol-copper melt fraction in single-sided package with 24 die over full US06 cycle

A.2. Dual-Sided Package US06 Results: Sections 4.1.2 and 4.2

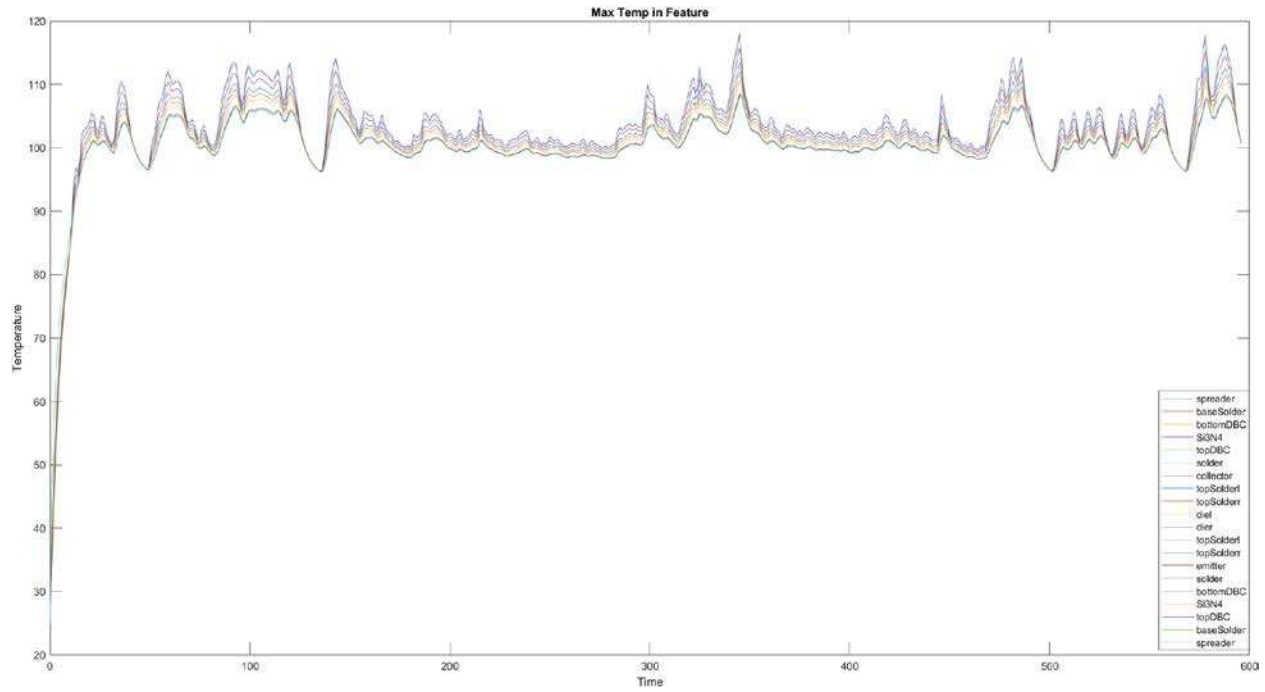


Figure A-14. Temperature profile in dual-sided package with 24 die and no PCM

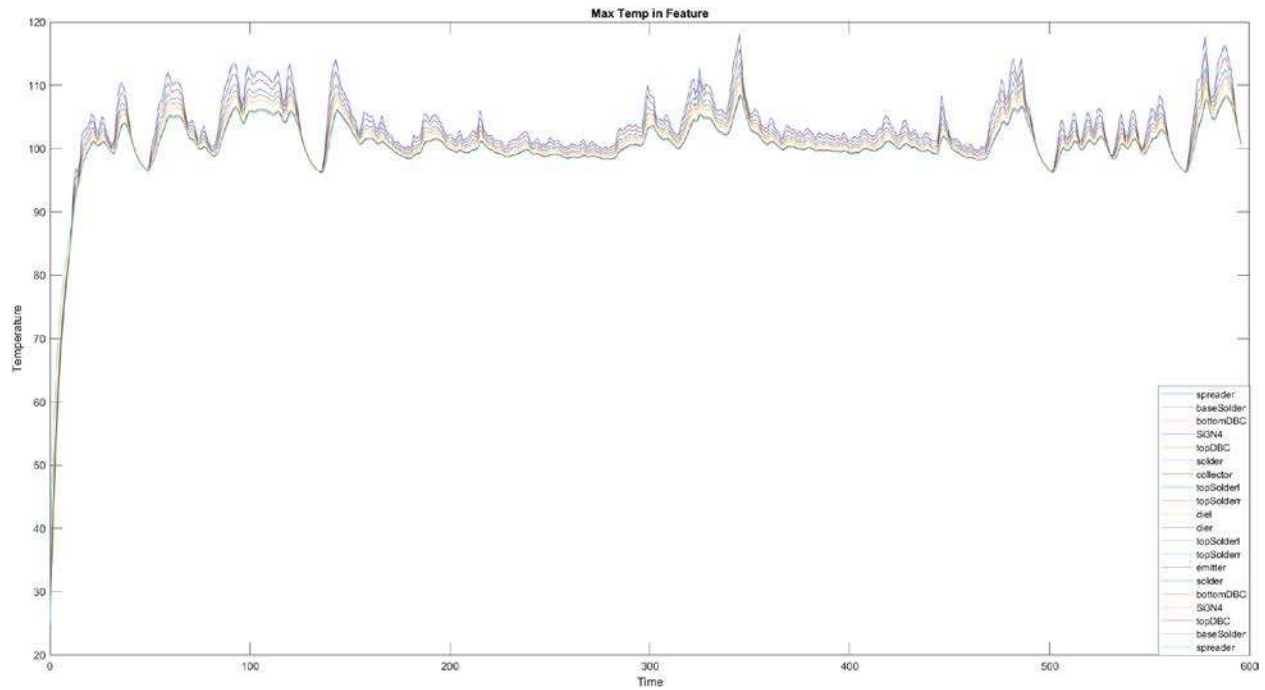


Figure A-15. Temperature profile in dual-sided package with 10 die and no PCM

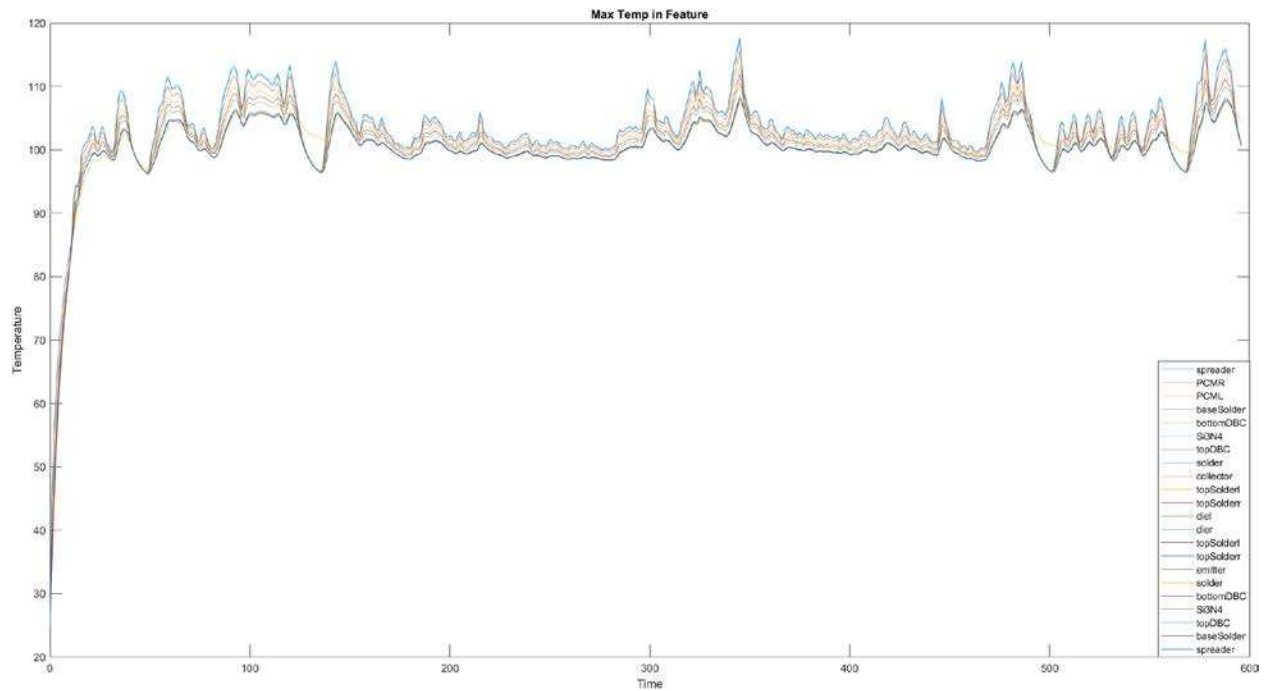


Figure A-16. Temperature profile in dual-sided package with 24 die and erythritol in the periphery over full US06 cycle

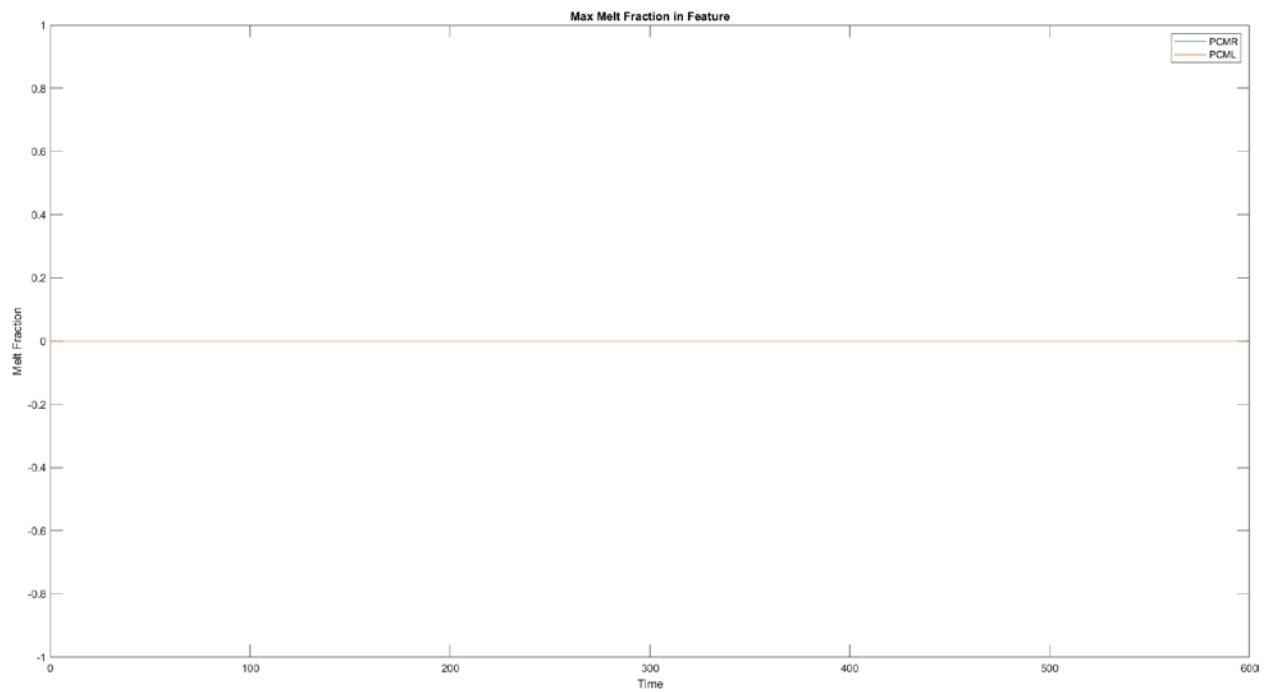


Figure A-17. Erythritol melt fraction in periphery of dual-sided package with 24 die over full US06 cycle

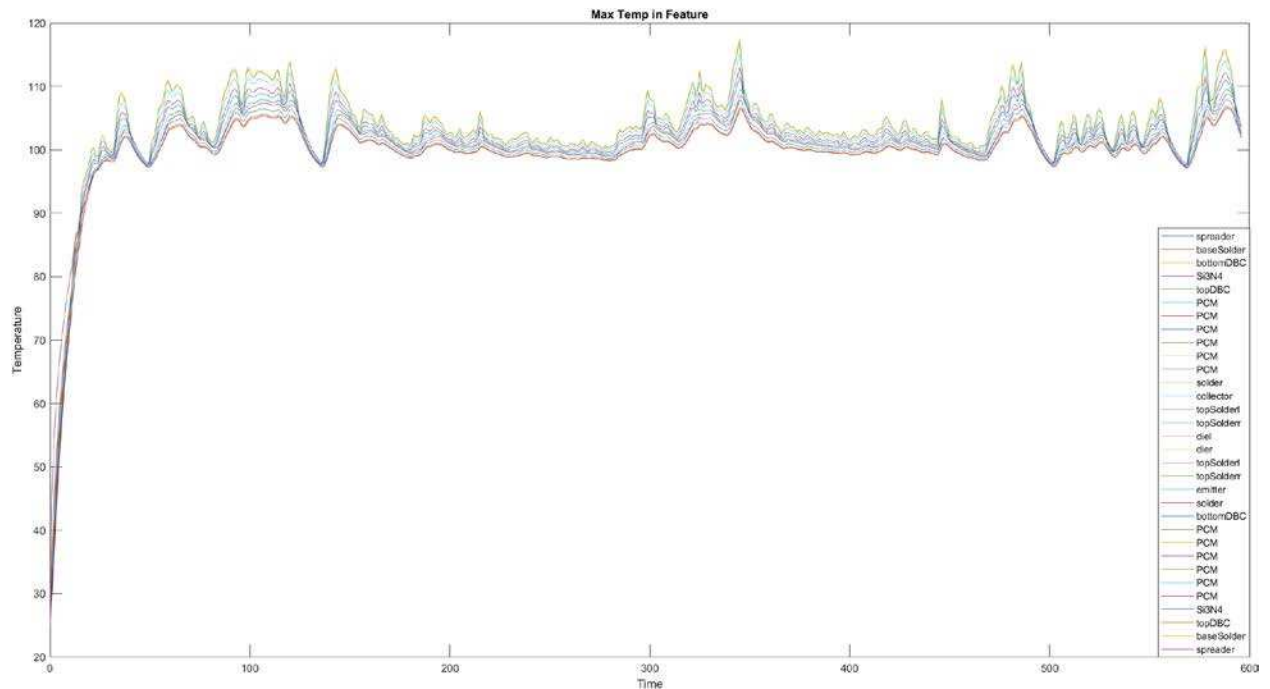


Figure A-20. Temperature profile in dual-sided package with 24 die and erythritol in the DBC over full US06 cycle

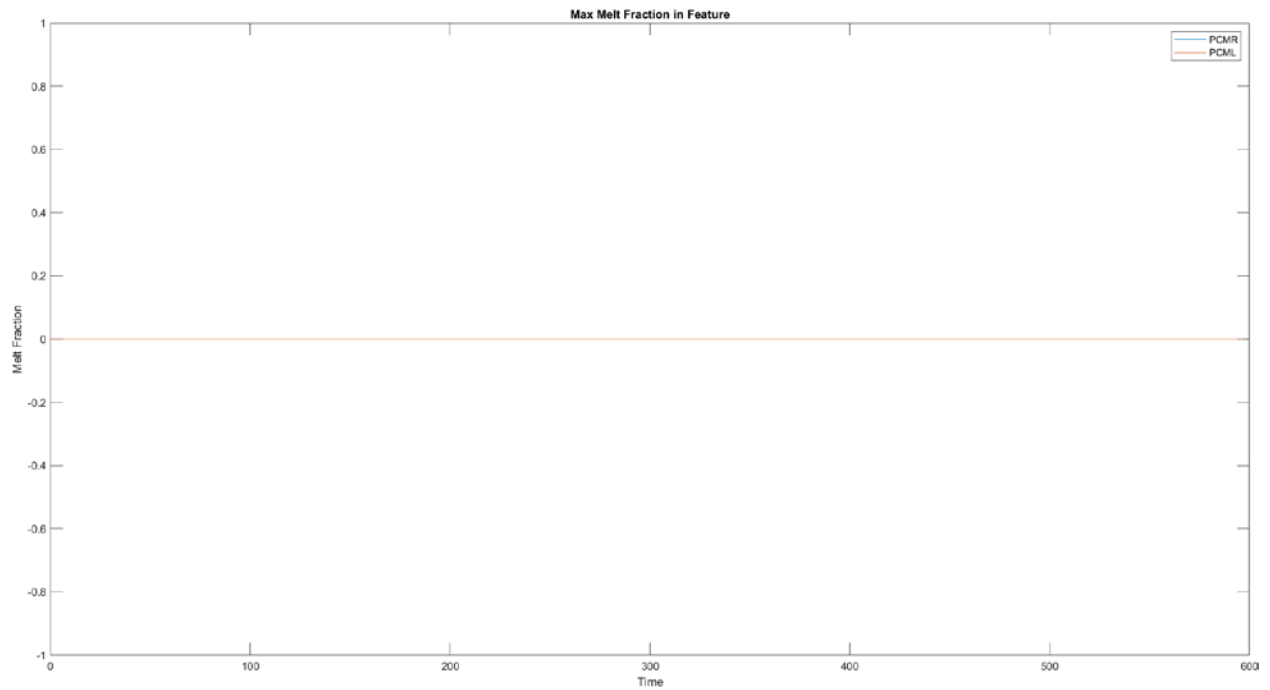


Figure A-21. Erythritol melt fraction in DBC of dual-sided package with 24 die over full US06 cycle

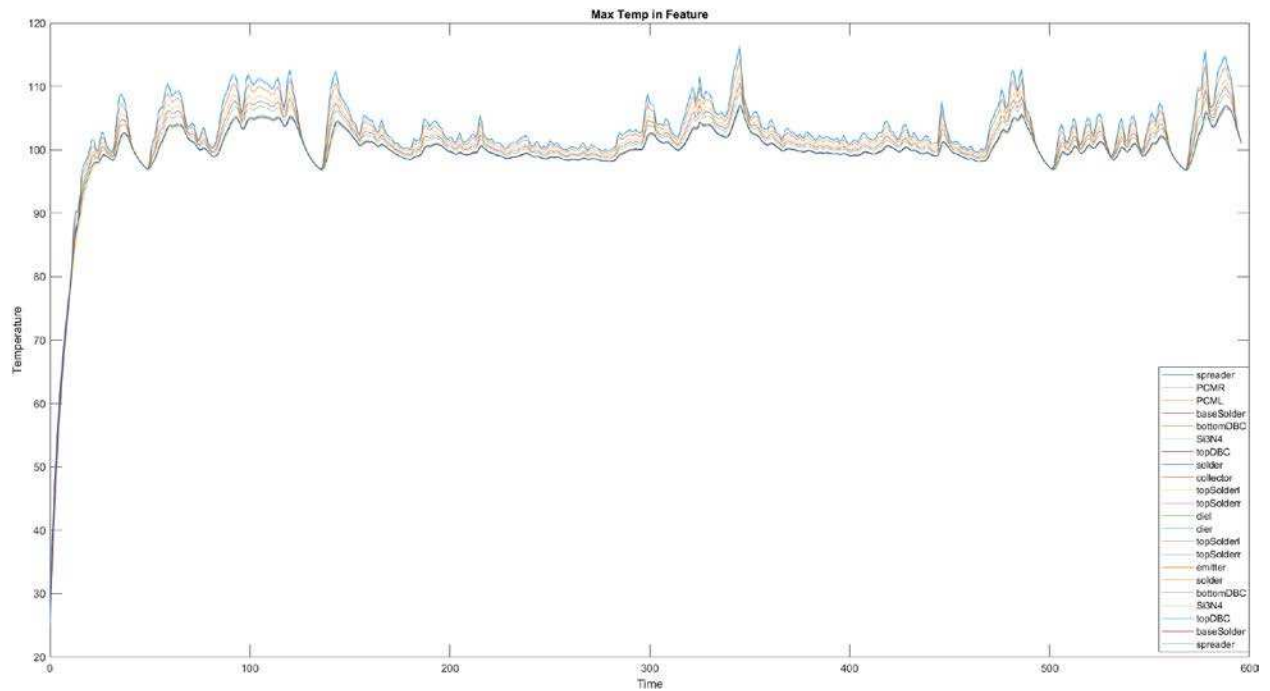


Figure A-22. Temperature profile in dual-sided package with 24 die and erythritol-copper in the periphery over full US06 cycle

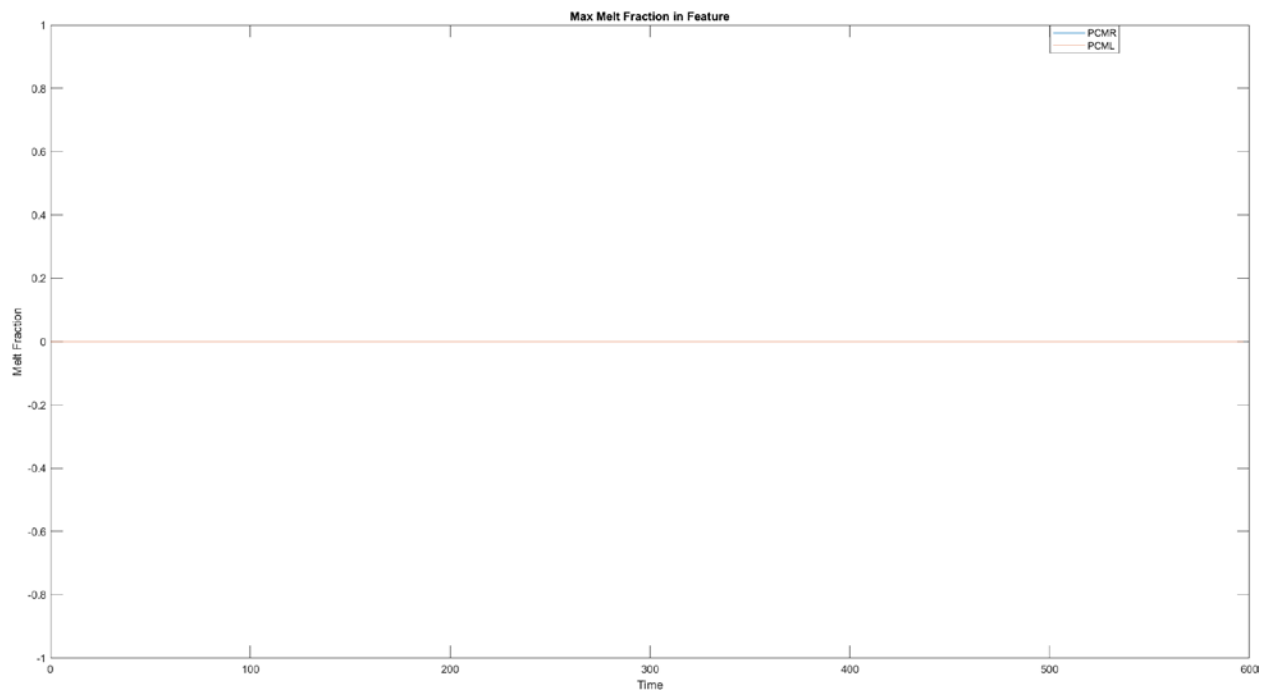


Figure A-23. Erythritol-copper melt fraction in periphery of dual-sided package with 24 die over full US06 cycle

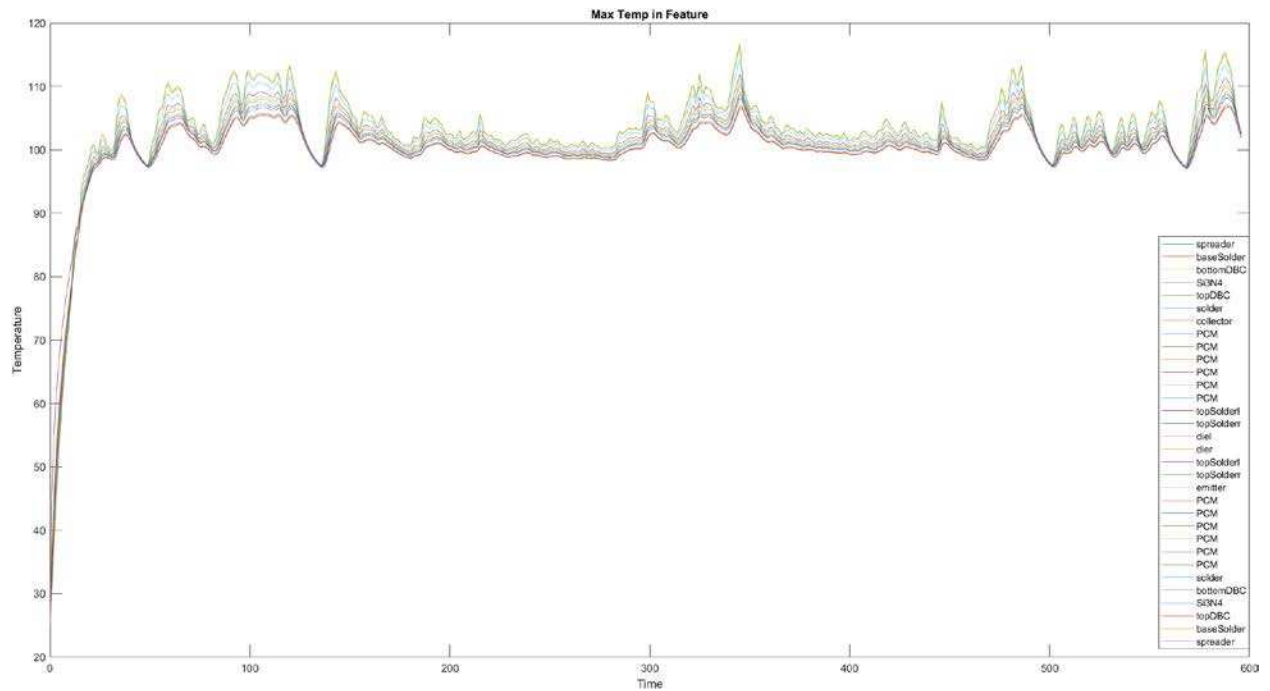


Figure A-24. Temperature profile in dual-sided package with 24 die and erythritol-copper in the emitter and collector over full US06 cycle

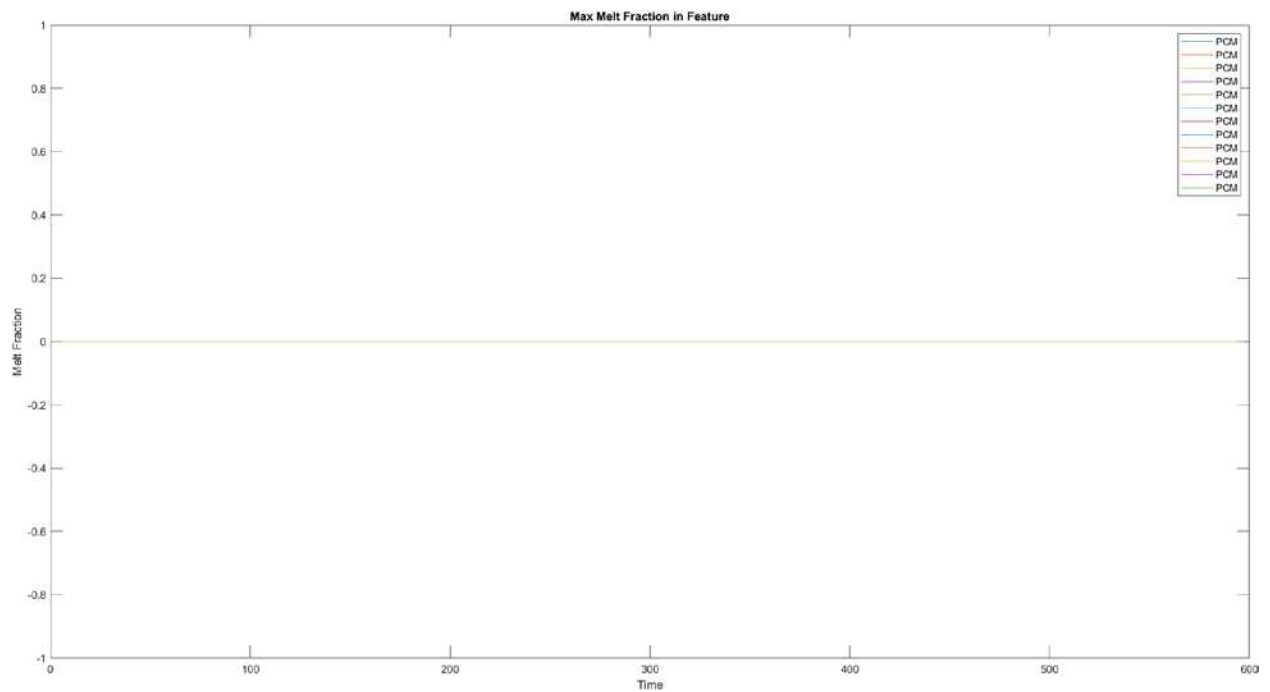


Figure A-25. Erythritol-copper melt fraction in emitter and collector of dual-sided package with 24 die over full US06 cycle

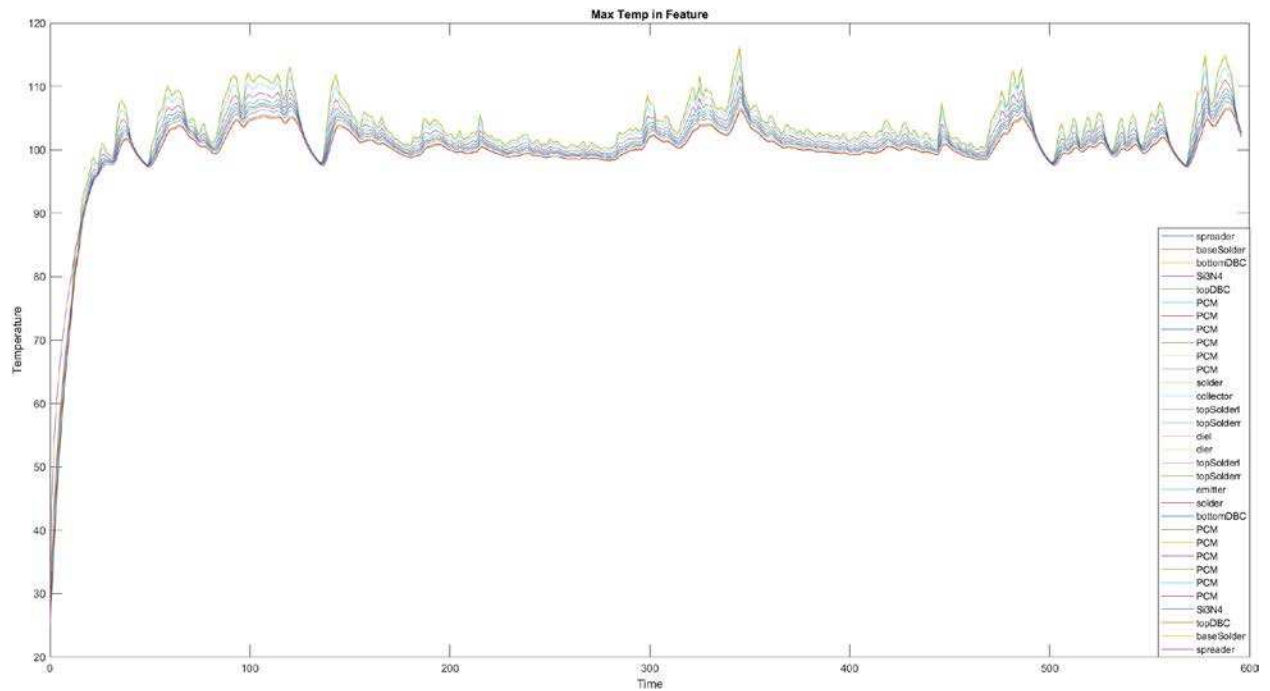


Figure A-26. Temperature profile in dual-sided package with 24 die and erythritol-copper in the DBC over full US06 cycle

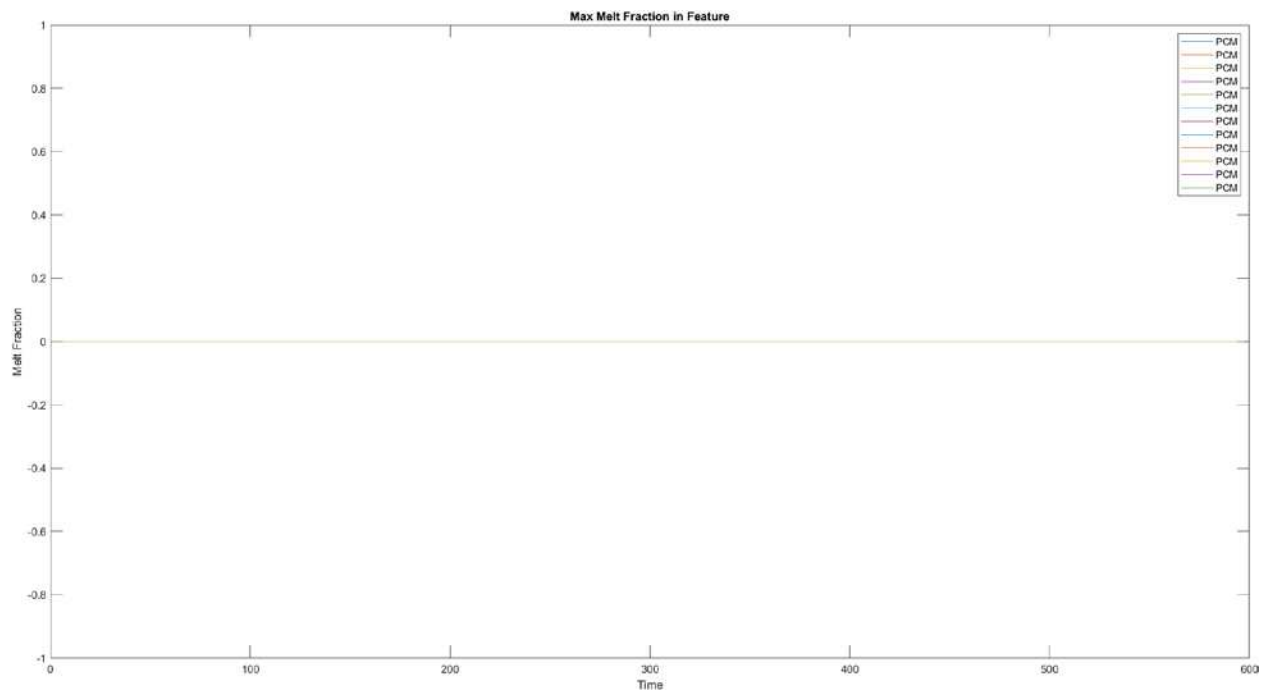


Figure A-27. Erythritol-copper melt fraction in DBC of dual-sided package with 24 die over full US06 cycle

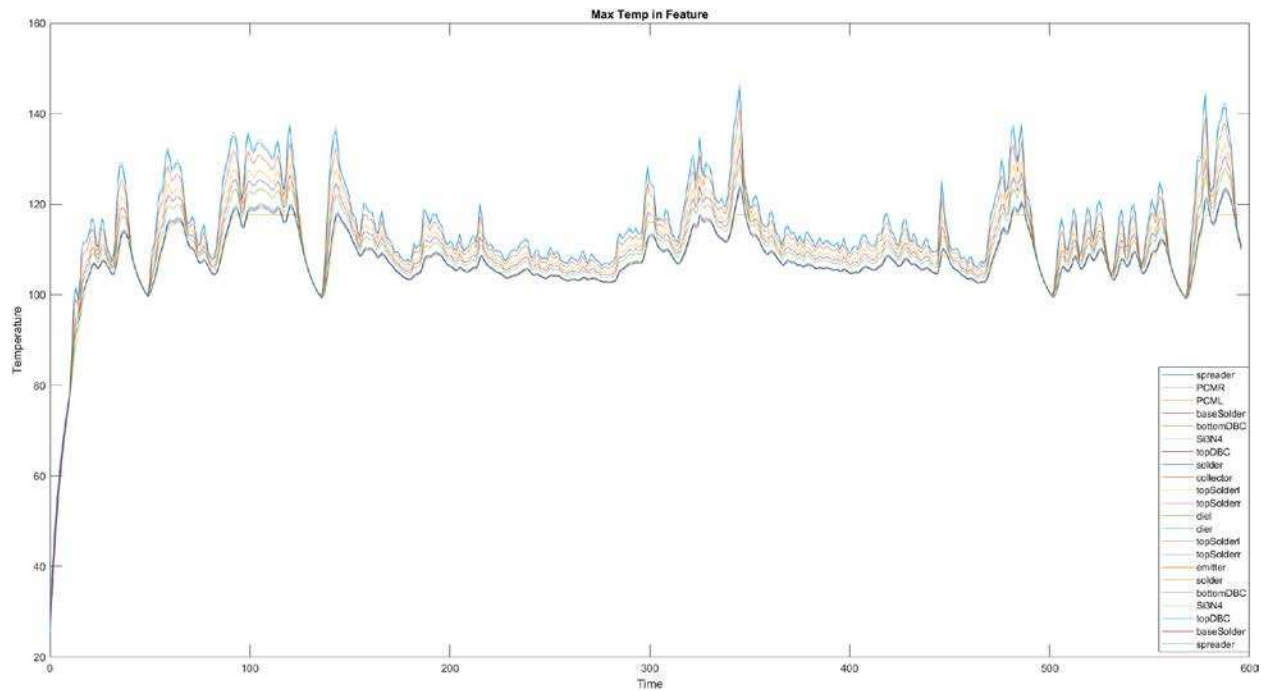


Figure A-28. Temperature profile in dual-sided package with 10 die and erythritol-copper in the periphery over full US06 cycle

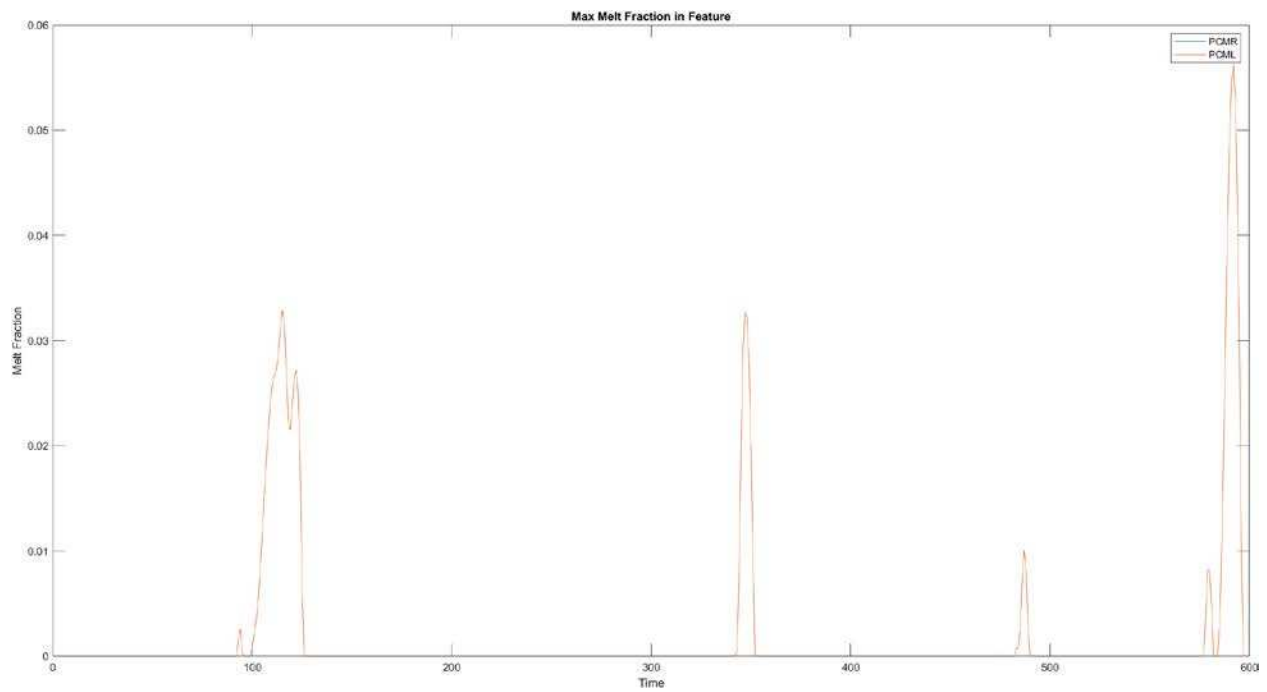


Figure A-29. Erythritol-copper melt fraction in periphery of dual-sided package with 10 die over full US06 cycle

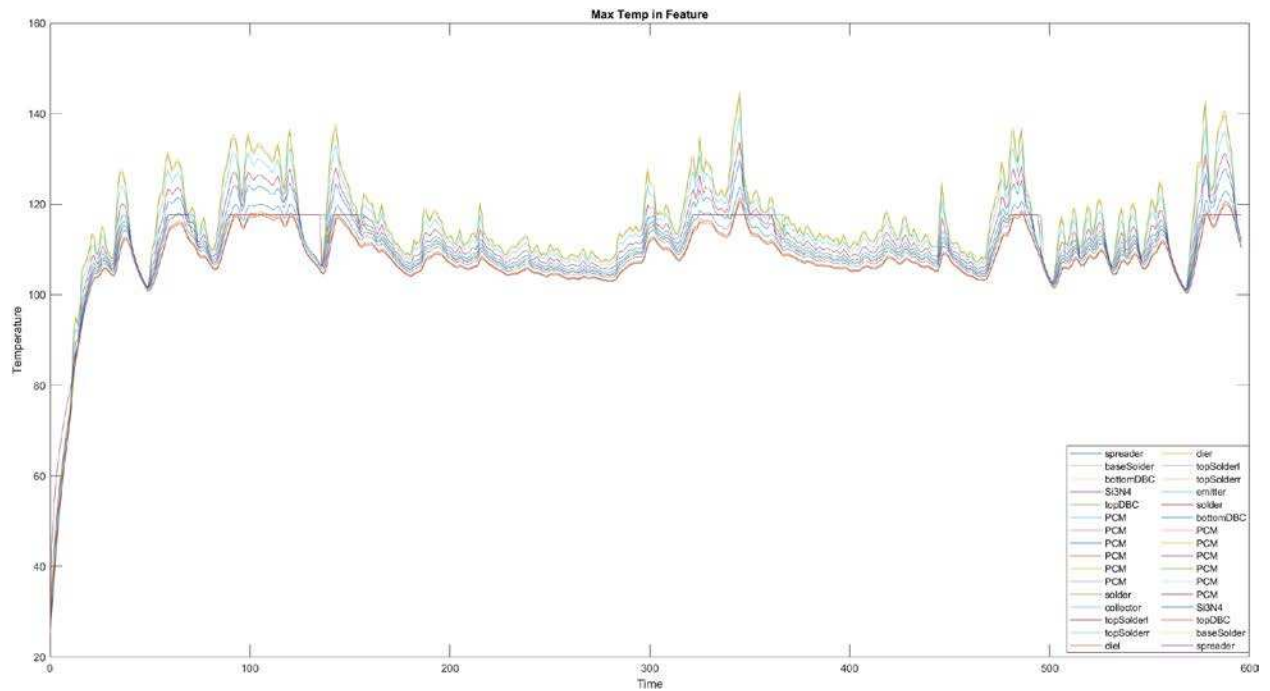


Figure A-32. Temperature profile in dual-sided package with 10 die and erythritol-copper in the DBC over full US06 cycle

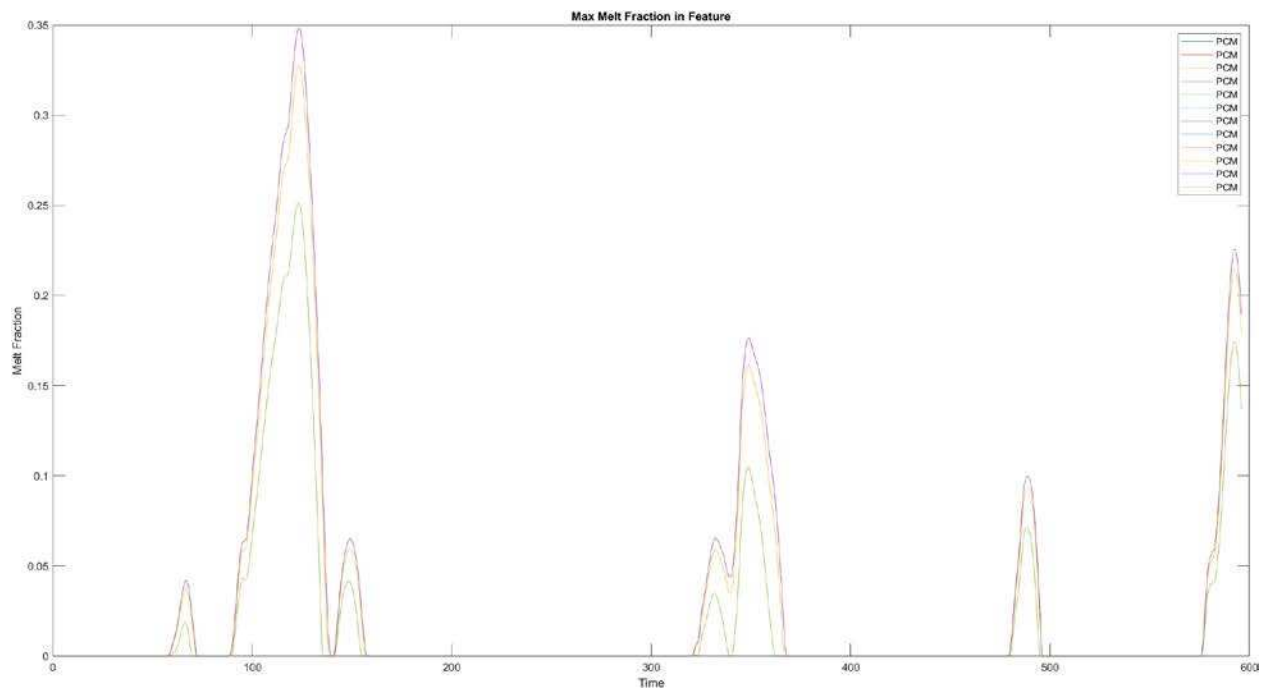


Figure A-33. Erythritol-copper melt fraction in DBC of dual-sided package with 10 die over full US06 cycle

A.3. Urban Results for Single and Dual-Sided Packages: Section 4.3

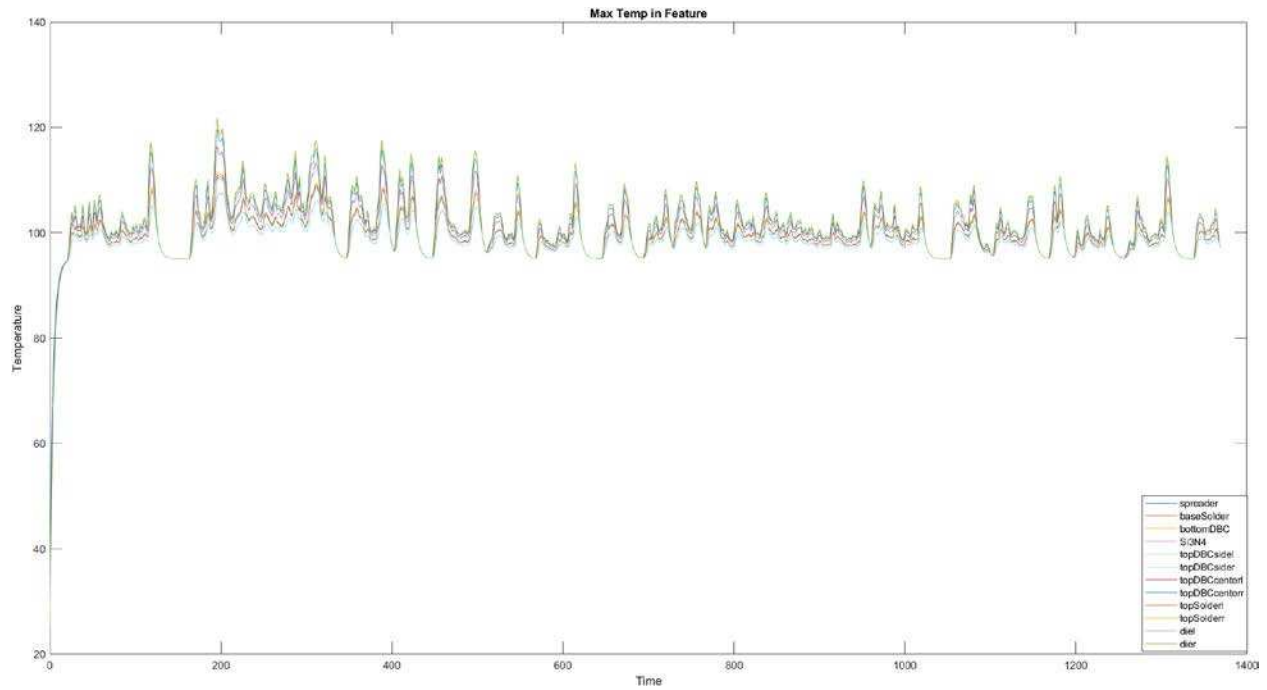


Figure A-34. Temperature profile in single-sided package with 24 die and no PCM over full urban cycle

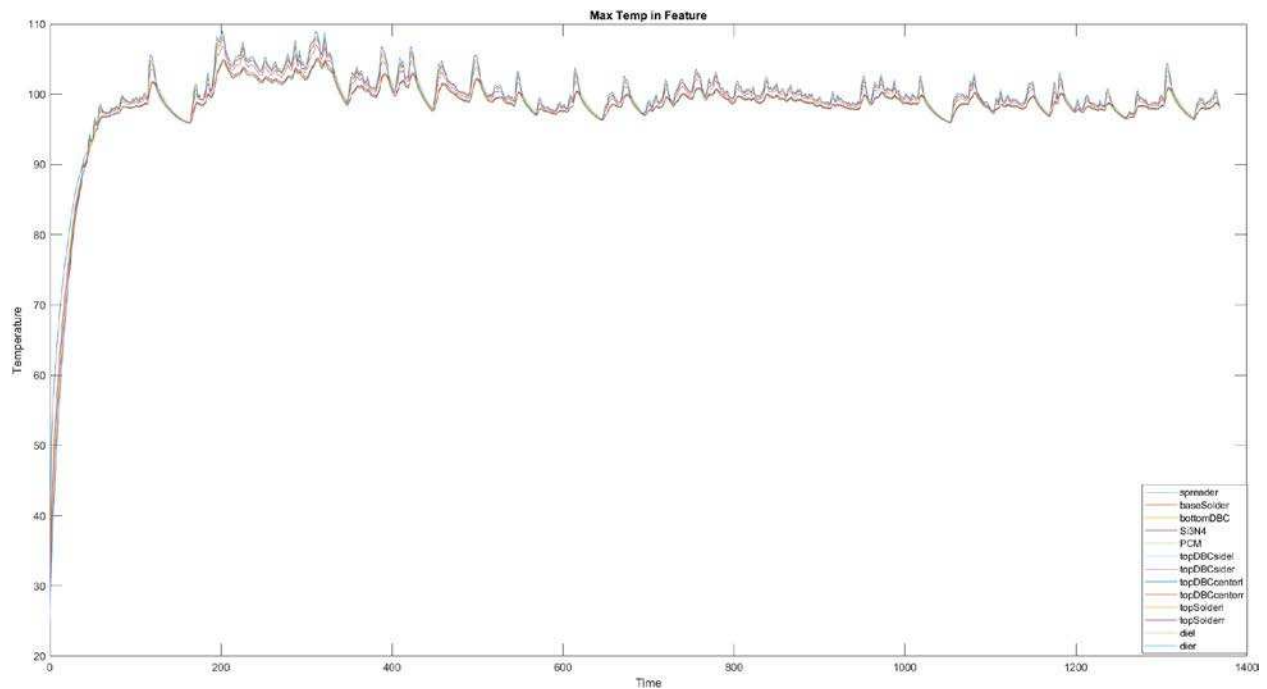


Figure A-35. Temperature profile in single-sided package with 24 die and erythritol-copper

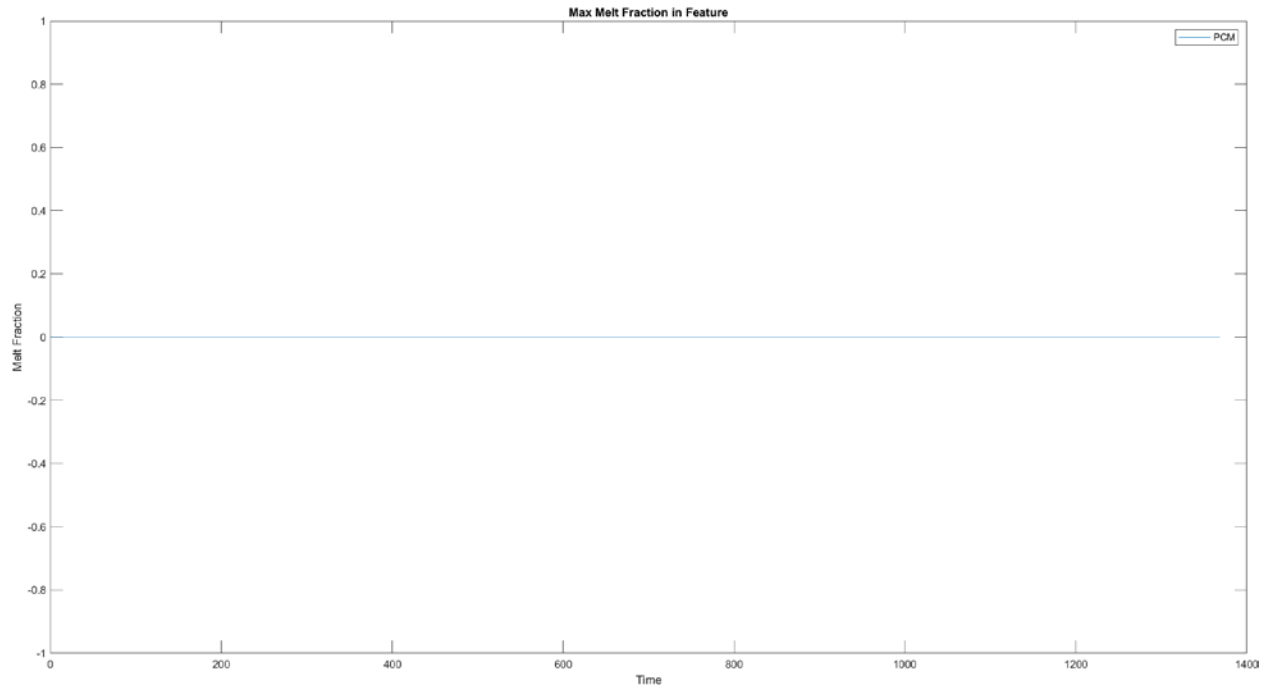


Figure A-36. Erythritol-copper melt fraction in single-sided package with 24 die over full urban cycle

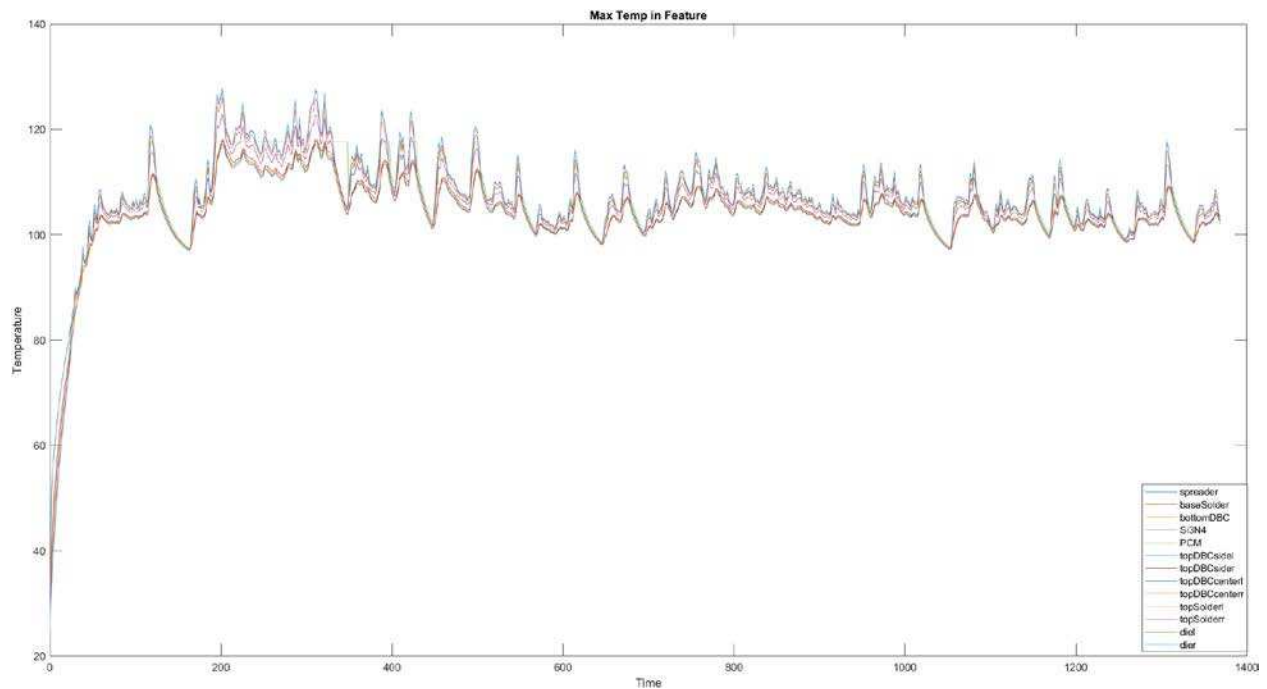


Figure A-37. Temperature profile in single-sided package with 10 die and erythritol-copper

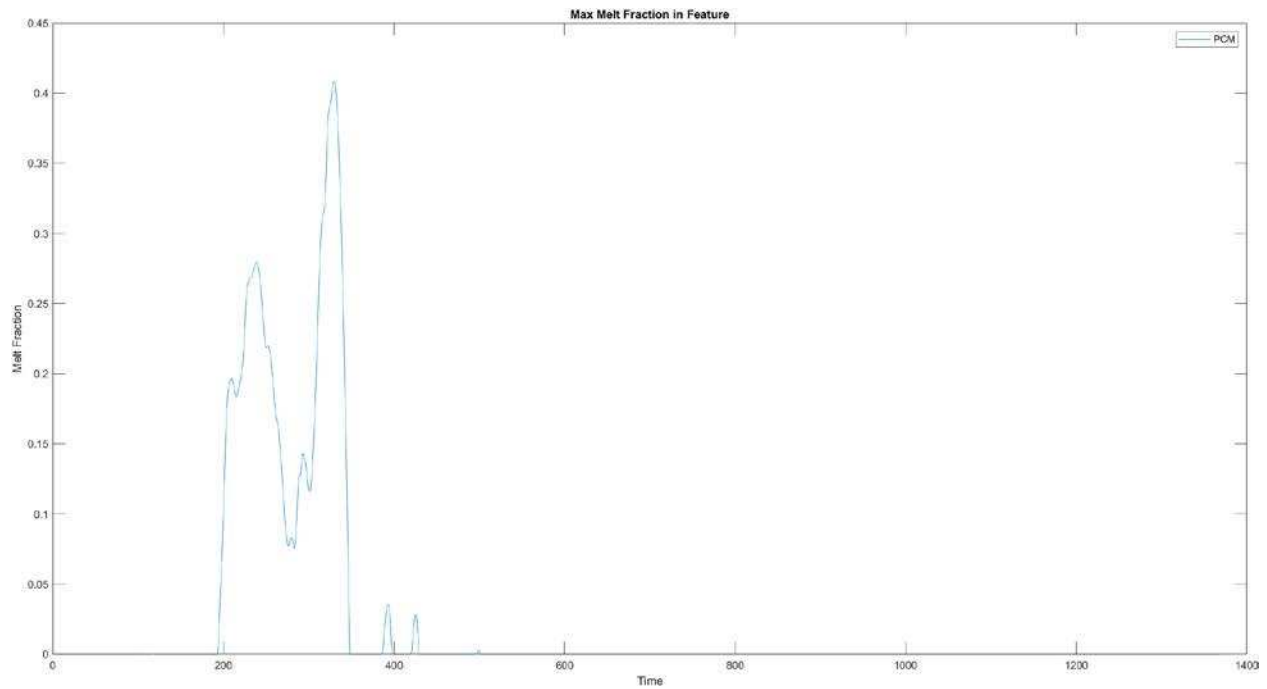


Figure A-38. Erythritol-copper melt fraction in single-sided package with 10 die over full urban cycle

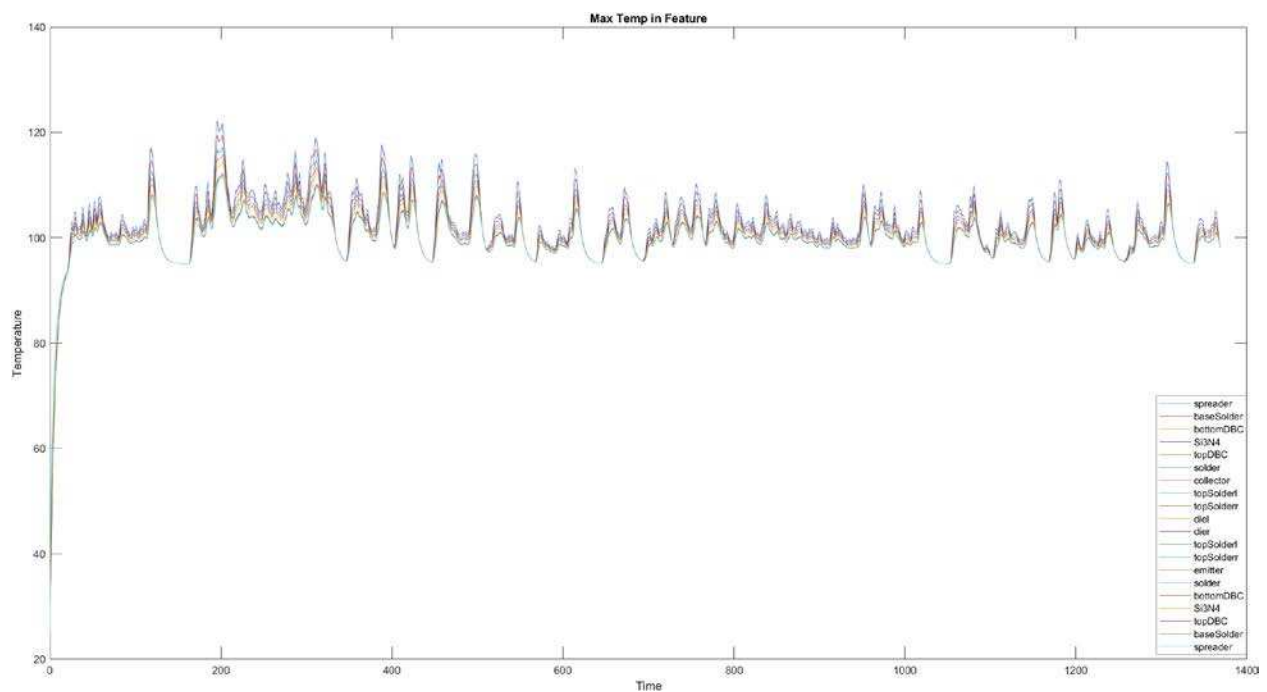


Figure A-39. Temperature profile in dual-sided package with 10 die and no PCM

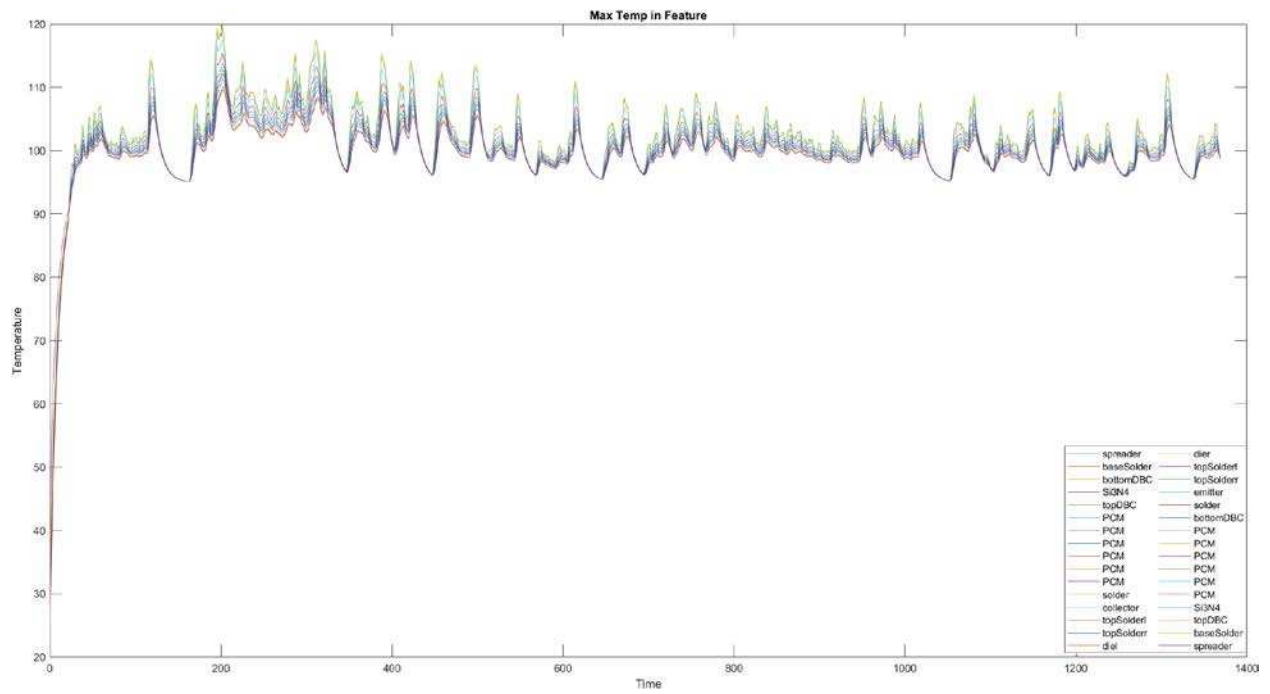


Figure A-40. Temperature profile in dual-sided package with 10 die and erythritol-copper in the DBC over full urban cycle

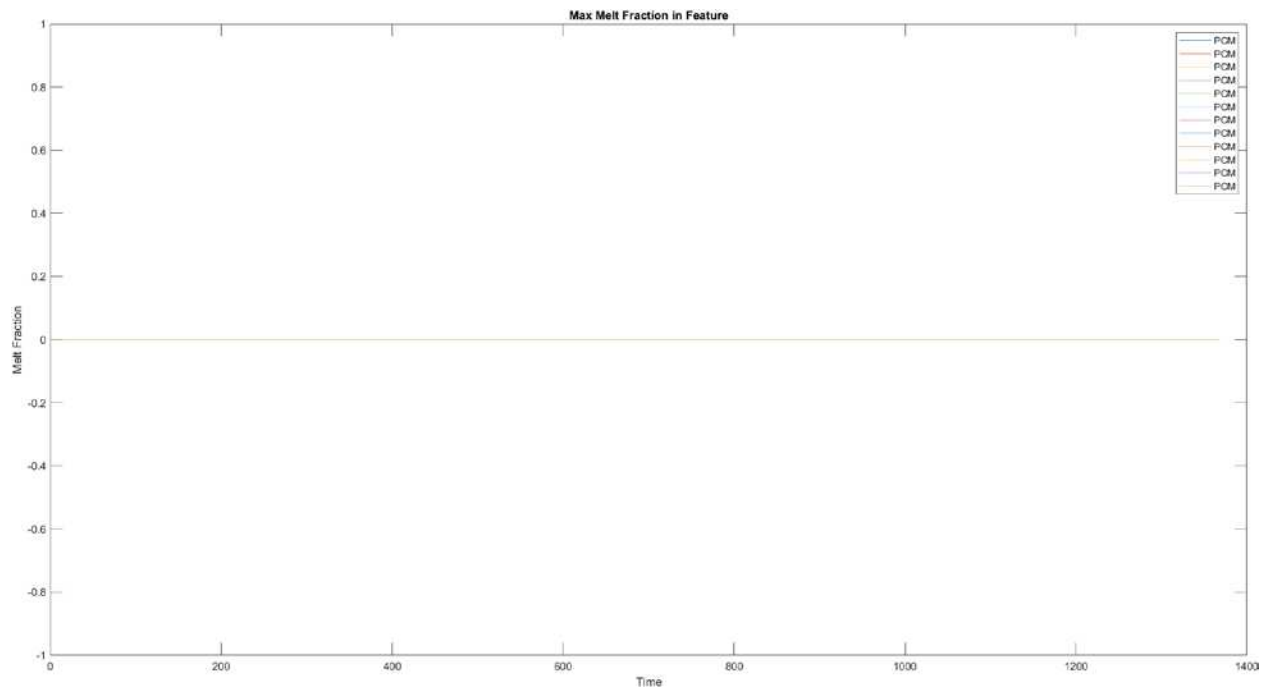


Figure A-41. Erythritol-copper melt fraction in DBC of dual-sided package with 10 die over full urban cycle

APPENDIX B HAND CALCULATIONS

The overall heat transfer coefficient used in this study was solved for in EES using Churchill correlations. Tables B-1 shows the results from the calculations. Table B-2 shows sample power calculations from a high and low acceleration, as well as a high and low deceleration, representing the power experienced by PE during US06 drive cycle.

Table B-1. Churchill correlation and overall heat transfer coefficient hand calculations

Parameter	Equation	EES Value	Hand Calculation Value	Units
Inputs	$\mu = 7.528 \times 10^{-4} \text{ kg m}^{-1} \text{ s}^{-1}$ $\rho = 1015 \text{ kg m}^{-3}$ $\rho_v = 28.84 \text{ kg m}^{-3}$ $C = 50\%$ $k = 4343 \times 10^{-4} \text{ W m}^{-1} \text{ K}^{-1}$ $D_h = 2.0 \times 10^{-3} \text{ m}$ $\dot{m} = 1.135 \times 10^{-3} \text{ kg s}^{-1}$ $P_r = 6.295$ $T = 95 \text{ C}$ $Nu_i = 5.33$ $Nu_o = 6.3$			
u	$\frac{\dot{m}}{\rho A_c}$	0.2795	0.2796	m s^{-1}
Re	$\frac{\rho D_h u}{\mu}$	753.8	753.9	-
A	$\left(2.2088 + 2.457 \ln \frac{42.683}{Re^{0.9}}\right)^{16}$	1.325e+8	1.325e+8	-
B	$\left(\frac{37530}{Re}\right)^{16}$	1.424e+27	1.424e+27	-
f	$8 \left[\left(\frac{8}{Re}\right)^{12} + \frac{1}{(A+B)^{1.5}} \right]^{\frac{1}{12}}$	0.0849	0.0849	-
Nu_i	$Nu_o + \frac{0.079 Re Pr \sqrt{f}}{(1 + Pr^{0.8})^{\frac{5}{6}}}$	33.27	33.27	-
Nu	$Nu_i^{10} + \left[\frac{\exp \frac{2200 - Re}{365}}{Nu_i^2} + \left[\frac{1}{Nu_o + \frac{0.079 Re Pr \sqrt{f}}{(1 + Pr^{0.8})^{\frac{5}{6}}}} \right]^{2.5 \cdot 0.1} \right]$	5.33	5.33	-

Table B-1. (cont.) Churchill correlation and overall heat transfer coefficient hand calculations

Parameter	Equation	EES Value	Hand Calculation Value	Units
h	$\frac{Nu k}{D_h}$	1165	1164.87	W m ⁻² K ⁻¹
L_c	$h + \frac{t}{2}$	2.5e-3	2.5e-3	-
A_f	$2L_c L$	1.2e-3	1.2e-3	-
A_b	$w_b L - NtL$	6.96e-3	6.96e-3	-
A_t	$NA_f + A_b$	2.376e-2	2.376e-2	-
m	$\sqrt{2 \frac{h_f}{k_w L_c}}$	62.31	62.31	m ⁻¹
η_f	$\frac{\tanh(mL_c)}{mL_c}$	0.992	0.992	-
η_o	$1 - \frac{A_f}{A_t} * (1 - \eta_f)$	0.9996	0.9996	-
U	$\eta_o h_f \frac{A_t}{A_b}$	3898	3898	W m ⁻² K ⁻¹

Table B-2. Representative Power Calculation

Parameter	Equation	Hand Calculation Value	Units
Inputs	$m=1600 \text{ kg}$ $c_R=0.015$ $c_D=0.3$ $\rho=1.225 \text{ kg m}^{-3}$ $g=9.81 \text{ m s}^{-2}$ $accel_{high}=2.079 \text{ m s}^{-2}$ $accel_{low}=0.0224 \text{ m s}^{-2}$ $decel_{high}=1.721 \text{ m s}^{-2}$ $decel_{low}=0.2012 \text{ m s}^{-2}$ $V_{a,high}=22.17 \text{ m s}^{-1}$ $V_{a,low}=31.97 \text{ m s}^{-1}$ $V_{d,high}=21.28 \text{ m s}^{-1}$ $V_{d,low}=30.47 \text{ m s}^{-1}$		
P	$maV + c_RmgV + \frac{1}{2}\rho c_D A V^3$	-	-
$P(t=575s)$	$m(accel_{high}) V_{a,high} + c_Rmg V_{a,high} + \frac{1}{2}\rho c_D A V_{a,high}^3$	80.1	kW
$P(t=400s)$	$m(accel_{low}) V_{a,low} + c_Rmg V_{a,low} + \frac{1}{2}\rho c_D A V_{a,low}^3$	12.15	kW
$P(t=480s)$	$m(decel_{high}) V_{d,high} + c_Rmg V_{d,high} + \frac{1}{2}\rho c_D A V_{d,high}^3$	64.6	kW
$P(t=250s)$	$m(decel_{low}) V_{d,low} + c_Rmg V_{d,low} + \frac{1}{2}\rho c_D A V_{d,low}^3$	20	kW

APPENDIX C PARAPOWVER

C.1. ParaPower

This chapter describes the use of ParaPower and the methods used in the current study. Details provided will cover: opening the ParaPower GUI, creating geometries, assigning materials to the geometry, creating materials, assigning boundary conditions, and applying functions to geometry layers.

C.1.1 Opening ParaPower

Begin by opening MATLAB and navigate to ARL_ParaPower in directory and add to path (folders and subfolders). Type “ParaPowerGUI_V2” into command line and press enter (Figure C-1).

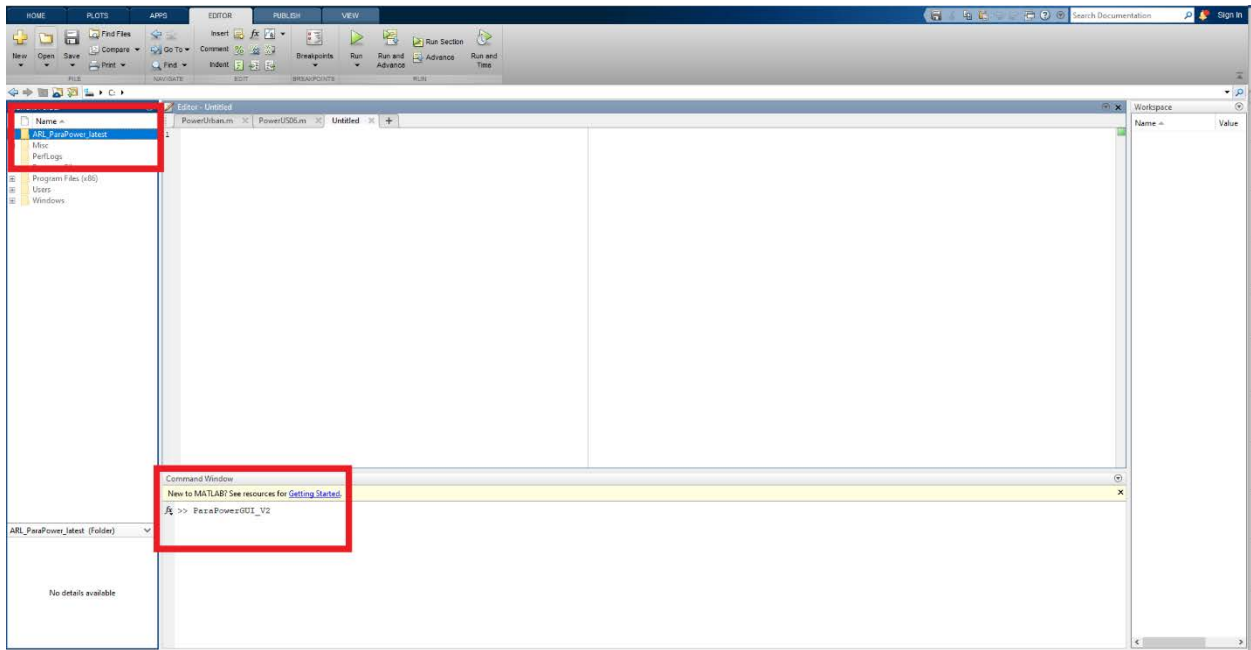


Figure C-1. MATLAB home screen with ParaPower folder and subfolders added to MATLAB path and command to open GUI in Command Window

C.1.2 ParaPower GUI

ParaPower can most simply be run via the GUI. The GUI contains 7 labeled sections

(Environmental Parameters, Transient/Stress Conditions, Define Features, Analysis, Geometry Visualization, Detailed Visual Results, and Run Solver) that allow for user input (Figure C-2).

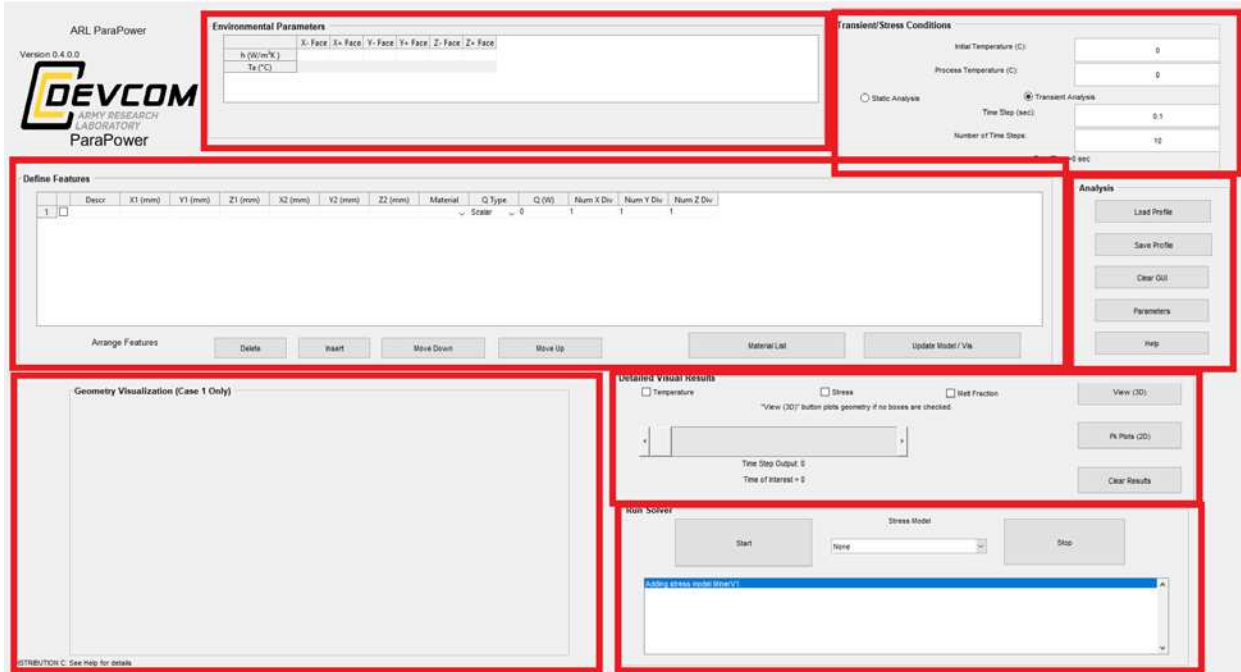


Figure C-2. Blank ParaPower GUI with 7 user interface sections boxed in red

In the Define Features section, users can define geometries, assign materials to the different geometry layers, and apply scalar heat loads or heat load functions. Figure C-3 shows the features defined to create layers 3 through 12 (cold plate and solder not shown) of the single-sided package without PCM. Also shown in the bottom right of the figure is the power function applied to simulate the heat load experienced by the US06 drive cycle. This power function calls a code from MATLAB that can be found in Appendix D.

Define Features											
		Descr	X1 (mm)	Y1 (mm)	Z1 (mm)	X2 (mm)	Y2 (mm)	Z2 (mm)	Material	Q Type	Q (W)
3	<input type="checkbox"/>	bottomDBC	-wdbcbase	tbaseplate+t...	0	wdbcbase	tbaseplate+t...	depth	Cu	Scalar	0
4	<input type="checkbox"/>	SI3N4	-wSI3N4	tbaseplate+t...	0	wSI3N4	tbaseplate+t...	depth	SI3N4	Scalar	0
5	<input type="checkbox"/>	topDBCsidel	-sidedbcdfc	tbaseplate+t...	0	-sidedbcdfc...	tbaseplate+t...	depth	Cu	Scalar	0
6	<input type="checkbox"/>	topDBCsider	sidedbcdfc	tbaseplate+t...	0	sidedbcdfc+	tbaseplate+t...	depth	Cu	Scalar	0
7	<input type="checkbox"/>	topDBCcenterl	-centerbcdfc	tbaseplate+t...	0	-centerbcdcf...	tbaseplate+t...	depth	Cu	Scalar	0
8	<input type="checkbox"/>	topDBCcenterr	centerbcdfc	tbaseplate+t...	0	centerbcdcf...	tbaseplate+t...	depth	Cu	Scalar	0
9	<input type="checkbox"/>	topSolderl	-diedfc	tbaseplate+t...	diedfe	-diedfc-wdie	tbaseplate+t...	diedfe+wdie	Pb_63Sn	Scalar	0
10	<input type="checkbox"/>	topSolderr	diedfc	tbaseplate+t...	diedfe	diedfc+wdie	tbaseplate+t...	diedfe+wdie	Pb_63Sn	Scalar	0
11	<input type="checkbox"/>	dier	-diedfc	tbaseplate+t...	diedfe	-diedfc-wdie	tbaseplate+t...	diedfe+wdie	SiC	Function(t)	PowerUS06(t)
12	<input type="checkbox"/>	dier	diedfc	tbaseplate+t...	diedfe	diedfc+wdie	tbaseplate+t...	diedfe+wdie	SiC	Function(t)	PowerUS06(t)

Figure C-3. Features define for use in current study

The Analysis section allows the user to load an existing profile, save the current profile, clear all work from the GUI, set parameters, open a help dialog (Figure C-4). The Parameters

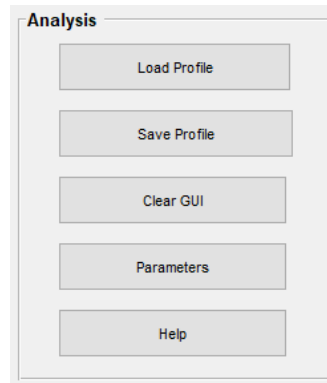


Figure C-4. Analysis section of GUI

option allows users to name and assign values to parameters (single or parametric). Figure C-5 shows named parameters with the values assigned. These parameters were assigned to the different axes and used to construct the geometry in the Define Features section of the GUI.

Parameter Name	Value
<input type="checkbox"/> tbaseplate	2
<input type="checkbox"/> wbaseplate	21.5
<input type="checkbox"/> tsolderbase	.2
<input type="checkbox"/> tsoldertop	.05
<input type="checkbox"/> wdbcbase	16.5
<input type="checkbox"/> tdbc	1.25
<input type="checkbox"/> wdbctopside	4
<input type="checkbox"/> wdbctopcenter	8
<input type="checkbox"/> tSi3N4	1.5
<input type="checkbox"/> wSi3N4	17.5
<input type="checkbox"/> tdie	.250
<input type="checkbox"/> wdie	5
<input type="checkbox"/> depth	20
<input type="checkbox"/> sidedbcdfc	12.5
<input type="checkbox"/> centerbcdfc	2
<input type="checkbox"/> diedfc	3.5
<input type="checkbox"/> diedfe	7.5

Figure C-5. Parameters used to construct single-sided package

Once a geometry has been constructed users can assign materials to the constructed layers by navigating to the material options through the Material List button in Define Features. ParaPower contains a library of materials and material properties relevant for thermal modeling. Users can also insert new materials and material properties (Figure C-6).

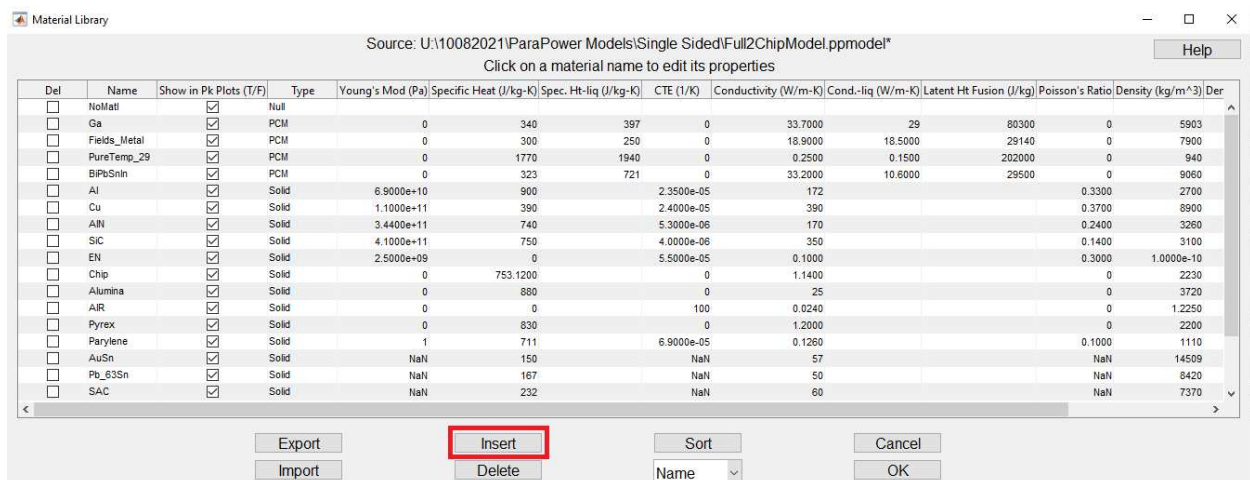


Figure C-6. Materials list with library of materials (and their properties) with option for users to insert materials

Geometry Visualization allows the user to see a visual representation of the geometry created, with color representation of the materials assigned to the geometry layers (Figure C-7).

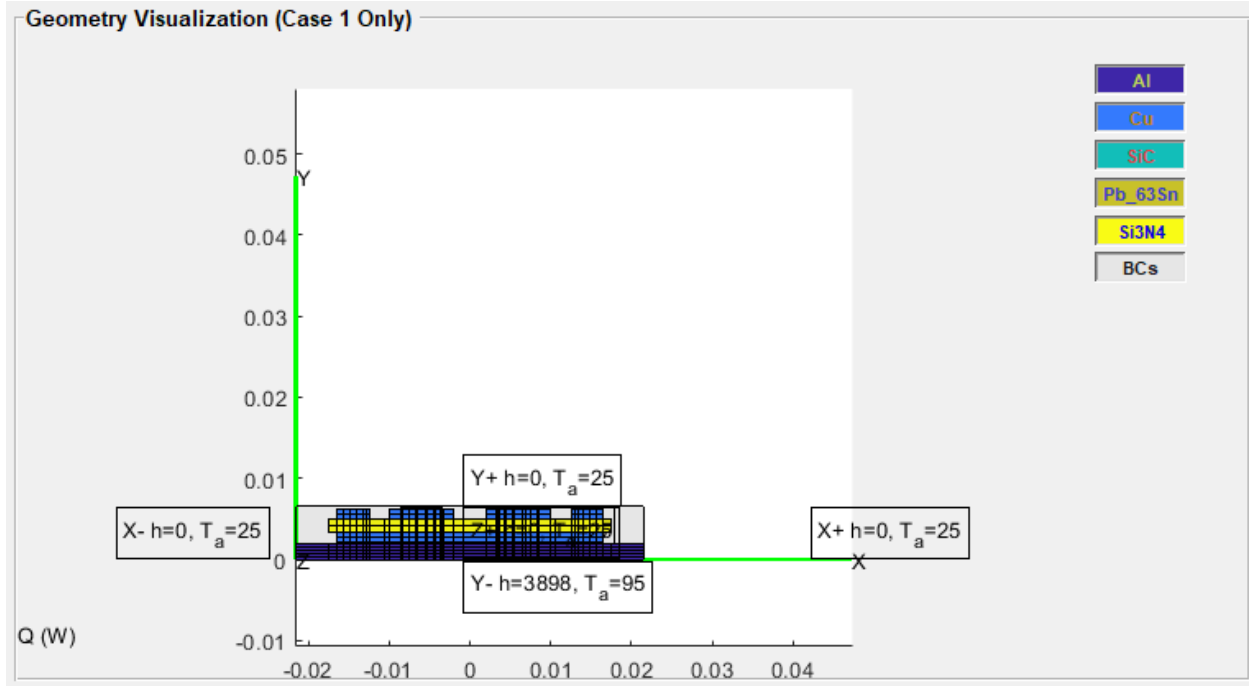


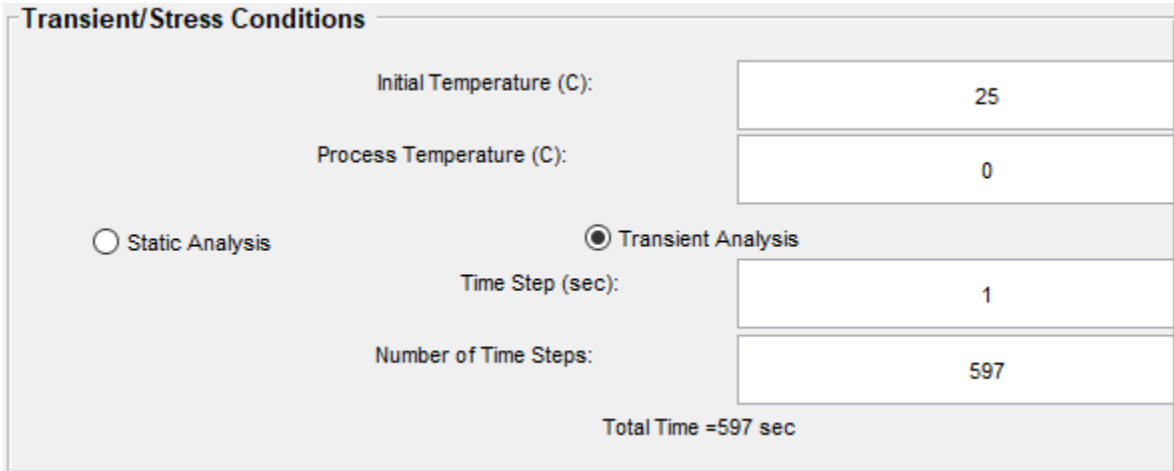
Figure C-7. Geometry visualization including materials assigned to geometry layers (single-sided package shown)

With the geometry created and materials assigned to geometry layers, users can apply external convective boundary conditions. Parameters defined and used in the current study are shown in Figure C-8.

Environmental Parameters						
	X- Face	X+ Face	Y- Face	Y+ Face	Z- Face	Z+ Face
h (W/m ² K)	0	0	3898	0	0	0
T _a (°C)	25	25	95	25	25	25

Figure C-8. Environmental Parameters used in current study

Initial conditions, analysis type, and time information is set in the Transient/Stress Conditions section of the GUI (Figure C-9). Time steps use in this study were 1 second and the number of time steps set according to the length of the drive cycle being used to provide the heat load (the US06 drive cycle was 597s), and the initial condition was assumed to be 25°C for ambient conditions.



Transient/Stress Conditions	
Initial Temperature (C):	25
Process Temperature (C):	0
<input type="radio"/> Static Analysis	<input checked="" type="radio"/> Transient Analysis
Time Step (sec):	1
Number of Time Steps:	597
Total Time =597 sec	

Figure C-9. Initial conditions, time steps, and length of analysis used in current study

To run the solver, click the Start button in the Run Solver section of the GUI (Figure C-10). An approximate run time for the simulations will be given and results will appear in a separate window once the simulation is complete. Detailed 3D results can also be viewed using the options in Detailed Visual Results.

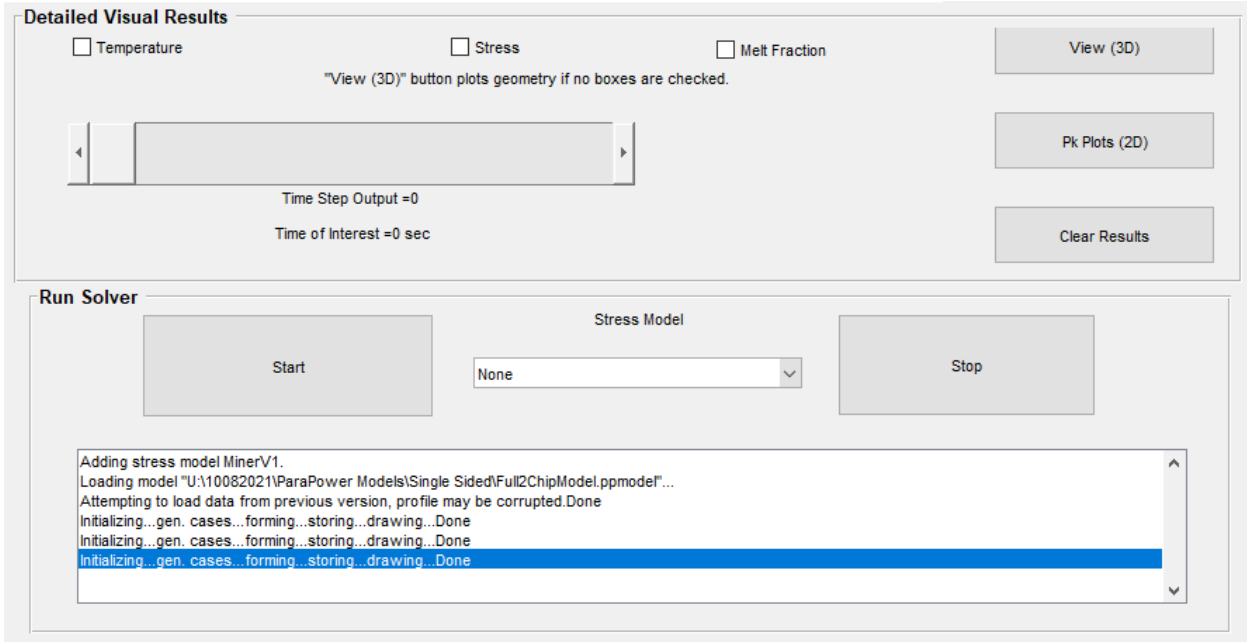


Figure C- 10. Run Solver and Detailed Visual Results sections of the GUI

APPENDIX D MATLAB CODE

This chapter provides the MATLAB functions used by ParaPower create the simulated heat loads of both the US06 and urban drive cycles. The EPA drive cycle files were downloaded from the EPA website cited in Section 3.2. Velocity values from the files were converted from miles per hour to meters per second for use in the MATLAB functions shown below.

D.1. US06 Power Function

```
function [out_power] = PowerUS06(time)
%Custom UDF for testing in ParaPower GUI
% Storing diff(L4_mph -> m/s)
load 'AccelUS06.mat' 'AccelUS06';
load 'US06Vms.mat' 'Speedms';

if isnumeric(time)

    %check unit conversions
    a=interp1([1:length(AccelUS06)]-1,AccelUS06,time);           %sets place holder for Accel
    V=interp1([1:length(Speedms)]-1,Speedms,time);             %sets place holder for Vel
    rho=1.225;          %air density
    m=1600;            %mass of vehicle
    cr=0.015;          %coefficient of rolling resistance
    cd=0.3;            %coefficient of drag resistance
    g=9.81;           %gravity
    area=0.58;         %drag area
    efficiency=.98;    %efficiency of pe
    N=24;              %number of pe
    out_power=((1-efficiency)*abs(m*a.*V + cr*m*g*V + 0.5*rho*cd*area*V.^3))/N;

elseif isSymType(time,'variable')
    out_power=@(time)PowerUS06(time);
end

end
```

D.2. Urban Power Function

```
function [out_power] = PowerUrban(time)
%Custom UDF for testing in ParaPower GUI
% Storing diff(L4_mph -> m/s)
load 'AccelUrban.mat' 'AccelUrban';
load 'DCUrbanVms.mat' 'Speedms';

if isnumeric(time)

    %check unit conversions
    a=interp1([1:length(AccelUrban)]-1,AccelUrban,time);           %sets place holder for Accel
    V=interp1([1:length(Speedms)]-1,Speedms,time);               %sets place holder for Vel
    rho=1.225;           %air density
    m=1600;             %mass of vehicle
    cr=0.015;           %coefficient of rolling resistance
    cd=0.3;             %coefficient of drag resistance
    g=9.81;            %gravity
    area=0.58;          %drag area
    efficiency=.98;     %efficiency of pe
    N=24;              %number of pe
    out_power=((1-efficiency)*abs(m*a.*V + cr*m*g*V + 0.5*rho*cd*area*V.^3))/N;

elseif isSymType(time,'variable')
    out_power=@(time)PowerUrban(time);
end

end
```